Chapter 6
Results and Discussion

6 Results and Discussion

6.1 Experimental design

The experimental design employed was Box Behnken design using Minitab Software 17. Box Behnken design and Response Surface Methodology (RSM) help analyse the influence of individual variables and the effect of interactions between independent variables on the characteristics of response. A total of 15 experimental trails were run in a randomized manner (Table 3). The observed responses were simultaneously fitted to linear and quadratic models with the application of statistical tools like ANOVA to predict the best-fit model along with the generation of three-dimensional response surface plots, contour plot and polynomial regression equations to predict the correlation of variables with the formulation properties. Based on the optimal prediction, batches were prepared, and various response parameters were estimated. The quantitative values of resultant responses were compared with predicted values for the determination of percentage prediction error.

Table 3: Box-Behnken design table with the response value

Batch	PLGA cocn(%w/v)	Pluronics F-127 (%w/v)	Rotation speed (RPM)	Porosity (%)	% Drug Loading
1	12.5	1	1500	57.50	12.40
2	5.0	5	1000	62.07	10.86
3	5.0	3	500	55.30	8.09
4	12.5	5	1500	60.50	8.40
5	12.5	5	500	82.07	12.26
6	12.5	3	1000	53.30	6.09
7	5.0	3	1500	72.54	10.21
8	5.0	1	1000	80.24	11.02
9	12.5	3	1000	70.14	10.02
10	12.5	3	1000	92.11	8.60
11	20.0	5	1000	70.40	7.25
12	20.0	3	500	68.50	8.10
13	12.5	1	500	91.04	6.40
14	20.0	3	1500	60.22	6.10
15	20.0	1	1000	61.50	6.50

The main effect plot for mean shown in figure 13 (a) demonstrates that non-horizontal line to the x-axis for PLGA and Pluronics F127 (independent variables) indicating the mean of response is different across all factor levels. The greater the magnitude of the main effect, the steeper is the slope. Additionally, the main effect plot of the rotation speed shows horizontal line at the low and medium level (500-1000 RPM), indicating a similar effect at both the factor levels, but the increased slope of the line from 1000-1500 RPM shows the increment in the magnitude of the main effect. The slopes of lines usually help to analyse the relative magnitude of the factor on the response.

Furthermore, the delta value is the difference between the maximum and minimum mean response values for each factor identified by the Minitab. Ranks are designated in the Minitab according to obtained delta values; highest delta value is ranked as 1, with rank 2 being the second-highest, and so on, and indicate the relative influence of each factor on the response [231]. Delta value for response of mean shows that Pluronics F127 (Delta 9.26, Rank=1) has the highest effect on the slopes, followed by PLGA (Delta 7.99, Rank = 2), and lastly, the Rotation speed (Delta 3.32, Rank = 3) as shown in table 13 (a).

The signal-to-noise ratio (S/N ratio) identifies control factors that minimize the change due to noise. Similarly, in the main effect graph of the signal-to-noise ratio (S/N ratio), PLGA (Delta 0.8003, Rank = 1) has the most significant effect on the S/N ratio, followed by Pluronics F127 (Delta 0.5477, Rank = 2), then followed by Rotation speed (Delta 0.1883, Rank = 3) as shown in table 4 (b).

In contrast, minimization of the standard deviation and maximization of the S/N ratio and their slopes led to a fitted experimental design model. PLGA (Delta 11.35, Rank = 1) has the most significant effect on the standard deviations, followed by Pluronics F127 (Delta 8.41, Rank = 2), then followed by Rotation speed (Delta 4.20, Rank = 3) as shown in table 13 (c).

Table 4: Response table determines delta value of (a) means, (b) S/N ratio and (c) Standard deviation

	(a) Response Table for Means			(b) Response Table for Signal to Noise Ratios			(c) Response Table for Standard Deviations		
Level	**PLGA**	**Pluronics F127**	**Rotation speed**	**PLGA**	**Pluronics F127**	**Rotation speed**	**PLGA**	**Pluronics F127**	**Rotation speed**
1	34.37	36.93	36.76	0.1353	-0.1119	-0.2768	33.83	37.60	38.07
2	37.10	43.09	37.00	-0.665	-0.3147	-0.3445	39.86	44.84	38.52
3	42.36	33.82	40.08	-0.556	-0.6596	-0.4650	45.18	36.43	42.27
Delta	7.99	9.26	3.32	0.8003	0.5477	0.1883	11.35	8.41	4.20
Rank	**2**	**1**	**3**	**2**	**1**	**3**	**2**	**1**	**3**

The main effect plots of PLGA, Pluronics F127 and Rotation speed for the mean of % drug loading are non-linear, indicating an increase in PLGA concentration is associated with a decrease in % drug loading. In contrast, a hyperbolic curve was observed for the effect of Pluronics F-127 on % drug loading showing a dual effect figure 14. A similar effect of the rotation speed was observed on % drug loading. There was a slight decrease in loading with an increase in rotation speed followed by an increase in loading at 1500 rpm, as shown in figure 14 (a).

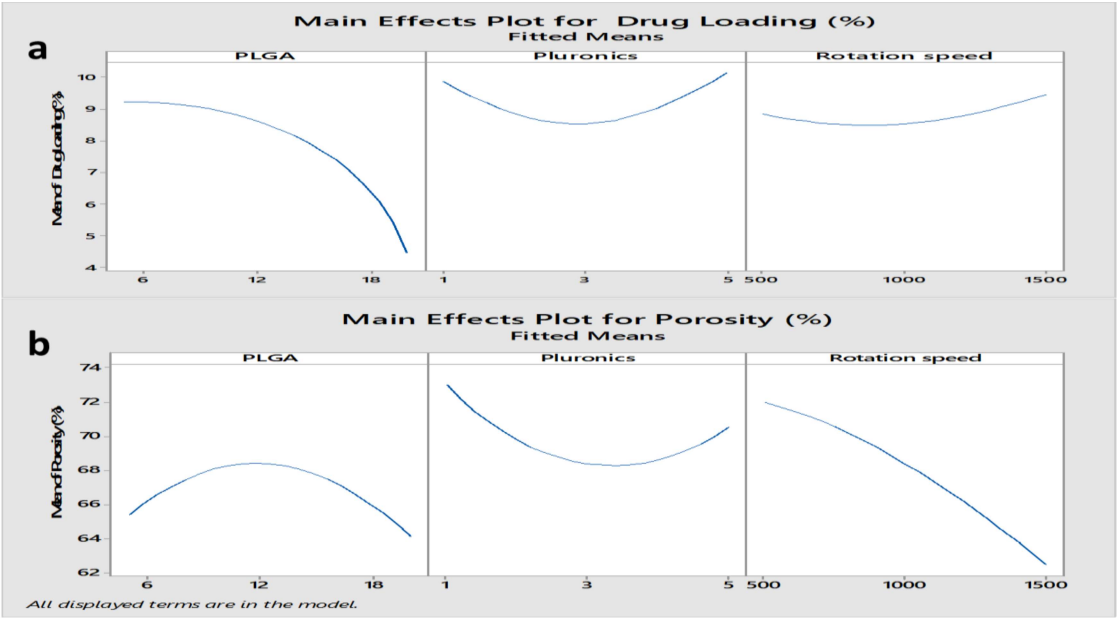

Figure 14: Main effect plot for (a) % drug loading with fitted means of PLGA, Pluronics F127 and Rotation speed (b) % porosity with fitted means of PLGA, Pluronics F127 and Rotation speed.

The main effect plot of porosity has been shown in figure 14 (b). A nonlinear hyperbolic correlation was observed between % porosity and PLGA concentration. A similar correlation was observed between mean porosity and concentration of pluronics F-127. An inverse correlation was observed between the rotation speed and the porosity (Figure 14 (b)).

The interaction between various factors is represented in the interaction plots, wherein the combined influence of factor level on the response is recorded. The level of each factor is represented on the horizontal axis, and the interaction plots are indicated by different coloured lines and symbols.

Interaction plots are used to understand the alteration in the behaviour of one variable with change in the value of another. Interaction effects are analysed in regression analysis, DOE (Design of Experiments) and ANOVA (Analysis of variance). The interaction plot mainly represents the relationship between one categorical factor along with continuous responses to the second categorical factor. The non-interaction and interaction between two factors are indicated by parallel and intersecting (non-parallel lines) respectively, as shown in the interaction plot [232].

The values on the y-axis of the interaction plot are of the dependent variables, and those on the x-axis represent independent variable. In the interaction diagram for drug loading (%), as shown in figure 5, minor interaction is observed between rotational speed and PLGA. However, in the interaction plot for porosity (%), considerable interaction was observed between Pluronic F127

and PLGA, rotation speed and PLGA, rotation speed and Pluronic F127 as indicated by nonparallel lines (figure 15 (a-b)). In addition to the interaction plot, the linear analysis of the model was done to determine if the interaction was significant.

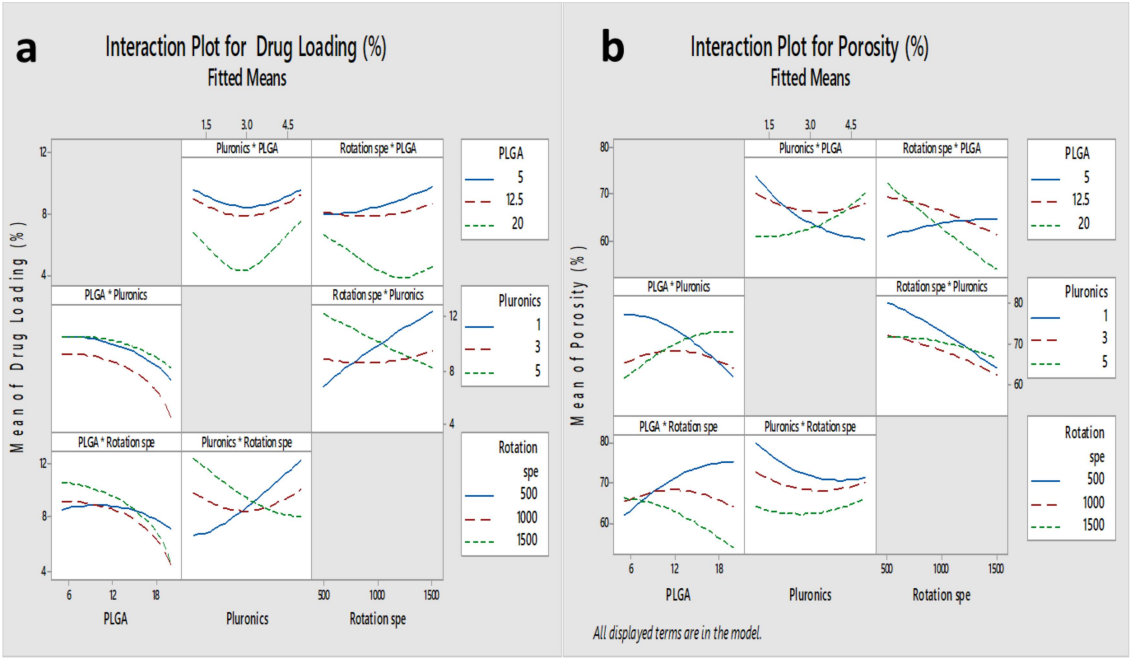

Figure 15: Interaction plot for (a) % drug loading with fitted means of PLGA, Pluronics F127 and Rotation speed (b) % porosity with fitted means of PLGA, Pluronics and Rotation speed.

6.1.1 Statistical analysis of experiments

The resulting design was statistically analysed using ANOVA, and the quadratic model was found to be significant ($p < 0.05$). The relationship between the dependent variable (porosity and drug loading) and the independent variable (PLGA (% w/w), Pluronics F127 (% w/w), rotational speed (RPM)) has been described in terms of the regression equations (12 and 13). The table 6 summarize the result and statistical parameters obtained for each response.

6.1.2 Effect on Porosity (%) and Drug loading

The polynomial equations 12 and 13 show quadratic relationship with more than one-factor combination representing interaction among variables, and the regression equations indicate that models obtained are significant ($p < 0.05$). In the experimental model, PLGA concentration, Pluronics F127 concentration and rotation speed directly correlate with drug loading (%) as indicated by the positive values of the coefficient. In contrast, the Pluronics F127 exhibits a positive relation with porosity (%).

$$Porosity = -0.0141 + 0.000477X_1 + 0.00285X_2 - 0.00004X_3 + 0.000014X_{1\,2} + 0.000170X_{2\,2} - 0.000X_{3\,2} + 0.000095X_1X_2 - 0.0X_1X_3 - 0.0000001X_2X_3 \ldots\ldots\ldots\ldots \text{eq } 12$$

$$Drug\ loading = 2.42 + 0.263X_1 + 0.62X_2 + 0.00801X_3 + 0.0095X_{1\,2} + 0.301X_{2\,2} + 0.000002X_{3\,2} - 0.0152X_1X_2 - 0.000275X_1X_3 - 0.002465X_2X_3 \quad \ldots\ldots 13$$

In the equations, positive sign represents a favourable effect, and a negative sign indicates detrimental effect. In polynomial equation 12, an increase in the value of X_1 and X_2 will contribute to increase in porosity, while increase in X_3 will result in decrease in porosity. As can be seen in polynomial equation 13, increase in the value of factors X_1, X_2 and X_3 will increase the drug loading of nanoscaffolds. Pluronic F-127 (X_2), also known as Poloxamer 407, is used as non-ionic surfactant which acts as surface stabilizer by imparting surface stability. With a decrease in the concentration of Pluronic F-127 mean pore size of nanoscaffolds increases due to reduced interfacial stability leading to coalescence of pores. Similarly, the increased concentration of PLGA (X_1), rotation speed (X_3) and Pluronic F-127 (X_2) positively affect drug loading. Higher PLGA concentration forms a viscous layer which prevents leaching of drug / drug diffusion into the aqueous phase, resulting in higher drug loading.

Further, the % drug loading in NPs is affected by drug-polymer interaction and miscibility of drug in the polymeric solution. % drug loading efficiency in NPs will increase with increase in pluronic F-127 and PLGA concentration as indicated by positive value of coefficient in polynomial equation [233]. Memantine being a hydrophobic drug gets entrapped inside the PLGA nanoscaffolds and pluronic-F127 stabilizes the nanoparticles by diffusing out the water molecules forming a polymer rich coacervate during the process of preparation of nanoscaffolds which favor high loading efficiency of drug inside nanoscaffolds. Moreover, the LA:GA ratio (50:50-100:0) can also impact the loading of drug content within the nanoscaffolds due to hydrophobic interaction between Memantine and PLGA [234]. In this study, 1:1 ratio of PLGA (50:50) and PLGA (75:25) were used to get the desired formulation with high drug encapsulation and controlled drug release characteristics.

6.1.3 Prediction of optimized formulation

For the preparation of the optimal batch, the concentration of PLGA, Pluronic F127 and rotation speed were determined and based on the R^2 value of optimal batch significance of the fitted model was determined. The correlation coefficient (R^2) indicates the correlation between the experimental data and the predicted data, while the adjusted R^2 and the predicted R^2 indicate the model significance [235]. The correlation coefficient (R^2), adjusted R^2 and predicted R^2 of the model for the porosity and drug loading were 0.9174, 0.9160 and 0.9120, respectively (Table 5). From the analysis of the coefficients of each factor, it was found that the PLGA and Pluronic F127 had a significant effect on porosity and drug loading.

Table 5: Optimized batch characteristics with the value of correlation coefficient (adjusted and predicted)

PLGA (w/v)	Pluronic F127 (w/v)	Rotation Speed (rpm)	Porosity (%)	Drug loading)	Opt Point Fit	R^2	R^2 (adjusted)	R^2 (Predicted)
19.18	4.98	500	82.7	11.6	1.18931	0.9174	0.9160	0.9120

6.1.4 Analysis of Variance

The two-way analysis of variance (ANOVA) is used to determine whether the mean of dependent variable is the same in two or more unrelated groups of independent variables. Data of Analysis of Variables with the statistical significance values (regression coefficient with effect, standard error coefficient (coef SE), T-value and P-value) of the two-way ANOVA, has been shown in table 6. The statistical significance of the bi-directional ANOVA was determined by analysis of "P-Value" and the level of significance ($p < 0.05$), which confirmed that the model generated is statistically significant ($P = 0.049$ and $F = 4.80$). The entire model was found to be significant (F value = 4.80; $p < 0.05$) because the Fischer variance ratio (F) of 4.80 was greater than $F = 4.772$ (significance level: $a = 0.05$) indicating highly significant data as mentioned in table 6 [236]. There is a statistically significant difference within each group of the independent variable at each of the levels. The results obtained from analysis of variance and regression coefficient terms indicated that individual effect of PLGA and interactive effect of Pluronics F-127 and rotation speed had a significant effect on response as represented by P value (< 0.05) (Table 6).

Table 6: Analysis of variance with degree of freedom (DF), an adjusted sum of square (Adj SS), Adjusted mean of square (Adj MS), F-value and P-value of the experimental model

Source	DF	Adj SS	Adj MS	F-Value	T- Value	P-Value
Model	9	84.1726	9.3525	4.80	3.50	0.049*
Linear	3	21.4347	7.1449	3.67	3.22	0.098
A-PLGA	1	20.1727	20.1727	10.35	0.024*	0.024*
B-Pluronics F127	1	0.2567	0.2567	0.13	0.731	0.731
C-Rotation Speed	1	1.0054	1.0054	0.52	0.505	0.505
Square	3	15.8176	5.2725	2.71	-	0.156
A^2	1	2.5607	2.5607	1.31	-1.15	0.304
B^2	1	10.9573	10.9573	5.62	2.37	0.064
C^2	1	1.6863	1.6863	0.87	0.93	0.395
2-Way Interaction	3	46.9203	15.6401	8.03	-	0.023*
A*B	1	0.1384	0.1384	0.07	0.27	0.801
A*C	1	3.6283	3.6283	1.86	-1.36	0.231
B*C	1	43.1536	43.1536	22.15	-4.71	0.005*
Error	5	9.7433	1.9487	-	-	-
Lack-of-Fit	3	3.4681	1.1560	0.37	-	0.788
Pure Error	2	6.2751	3.1376	-	-	-
Total	14	93.9159	-	-	-	-

* Significant effect of factor on response.

6.1.5 Response Surface methodology

6.1.5.1 Contour plots

A contour plot is a 2D view that connects all points with the same response to create a continuous response boundary. Contour plots help to understand the desired response values and operating conditions. The contour plot can be represented mathematically as z = f (x,y) indicating variation in z-axis value (Response variables) with variation in x and y-axis value (independent variables and are used as predictors) in a 2-dimensional plane. The contour lines represent z value which is known as iso-lines. In the current work, the contour plot was used to correlate the effect of independent variable pairs such as Pluronics F127 and PLGA, Rotation speed and Pluronics, Rotation speed and PLGA, Pluronics F127 and PLGA. The value of drug loading and porosity (dependent variable) can be determined by the crosshairs flag mentioned at the right corner (Figure 16 (a-c)).

The contour plot analysis of drug loading vs PLGA and Pluronics F127, PLGA and rotation speed, and Pluronics F127 and rotation speed at hold value of 1000 rpm rotation speed, 3% w/v Pluronics F127 and 12.5%w/v PLGA respectively (Figure 16 (a-c)) shows that the PLGA concentration (5-13.36 % w/v) along with Pluronics F-127 concentration (4.84-5 % w/v) and rotation speed (500-797 rpm) could produce drug loading greater than 10%.

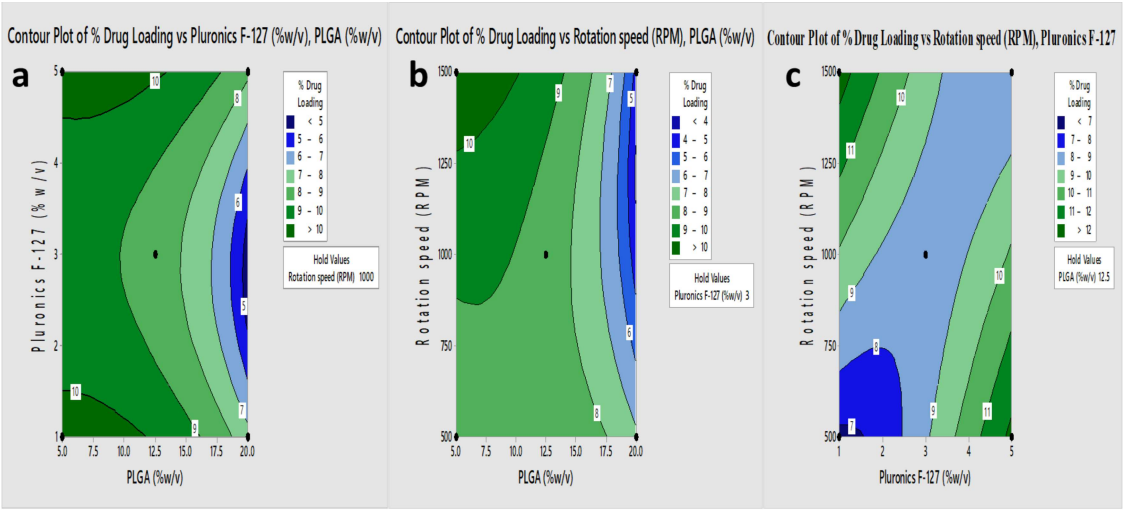

Figure 16: Contour plot of (a) % Drug loading (Y_1) vs PLGA(X_1) and Pluronics F127(X_2) at rotation speed 1000 rpm as holding value (b) % Drug loading (Y_1) vs PLGA(X_1) and Rotation speed (X_3) at Pluronics F127 3%w/v as holding value (c) % Drug loading (Y_1) vs PLGA(X_1) and Pluronics F127(X_2) at rotation speed 1000 rpm as holding value.

Similarly, the contour plot analysis of porosity vs PLGA and Pluronics F127, PLGA and rotation speed, and Pluronics F127 and rotation speed at hold value 1000 rpm rotation speed, 3% w/v Pluronics F127 and 12.5%w/v PLGA respectively (Figure 17 (a-c)) shows that the

variation of PLGA concentration ranging from 17.5 – 20% w/v along with Pluronics F-127 concentration ranging from (4.8-5% w/v) and Rotation speed (500-734 rpm) can produce a formulation with porosity greater than 75%. Further, it also clarifies that maximal response can be obtained at higher concentrations of PLGA and Pluronics F127 at lower rotation speed.

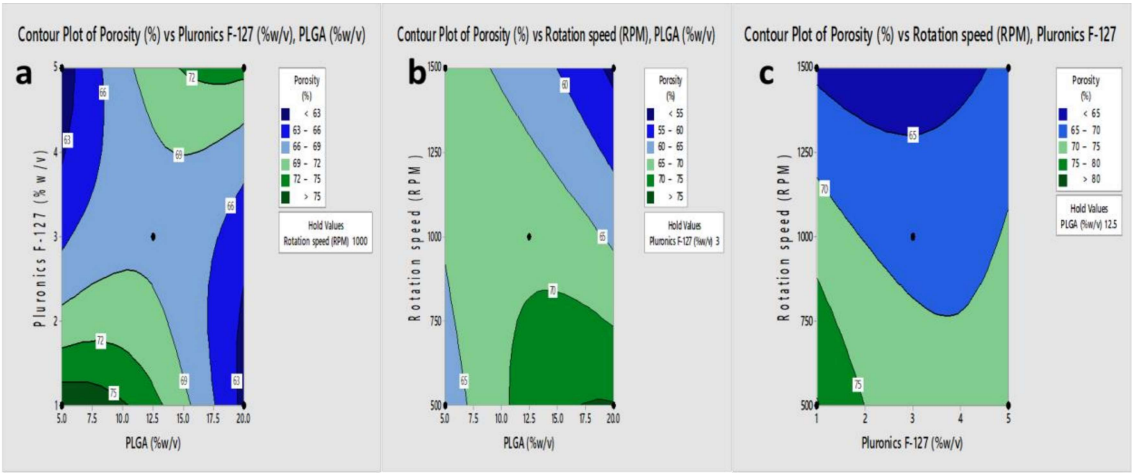

Figure 17: Contour plot of (a) % Porosity (Y_2) vs PLGA(X_1) and Pluronics F127(X_2) at rotation speed 1000 rpm as holding value (b) % Porosity (Y_2) vs Rotation speed and PLGA (X_1) at Pluronics F127(X_2) 3%w/v as holding value (c) Contour plot of Porosity (Y_2) vs Pluronics F127(X_2) and rotation speed 1000 rpm by keeping 12.5% w/v PLGA(X_1) as holding value.

6.1.5.2 3D Surface Plot

Surface plots are 3D data plots that show the functional relationship between a named dependent variable (Y) and two independent variables (X and Z). A two-dimensional X and Z grid is built that is in the equal data range. The Y value is the calculated average of all data values for each grid point and is plotted on the 3D surface. These plots are helpful for regression analysis to visualize the relationship between the dependent variable and independent variables. The surface plot generated between independent variable pairs such as Pluronics and PLGA, Rotation speed and Pluronics F127, Rotation speed and PLGA, Pluronics and PLGA at X-Z axis, and drug loading and Porosity as a dependent variable at Y-axis have been shown in figure 18 (a-c) and 19 (a-c).

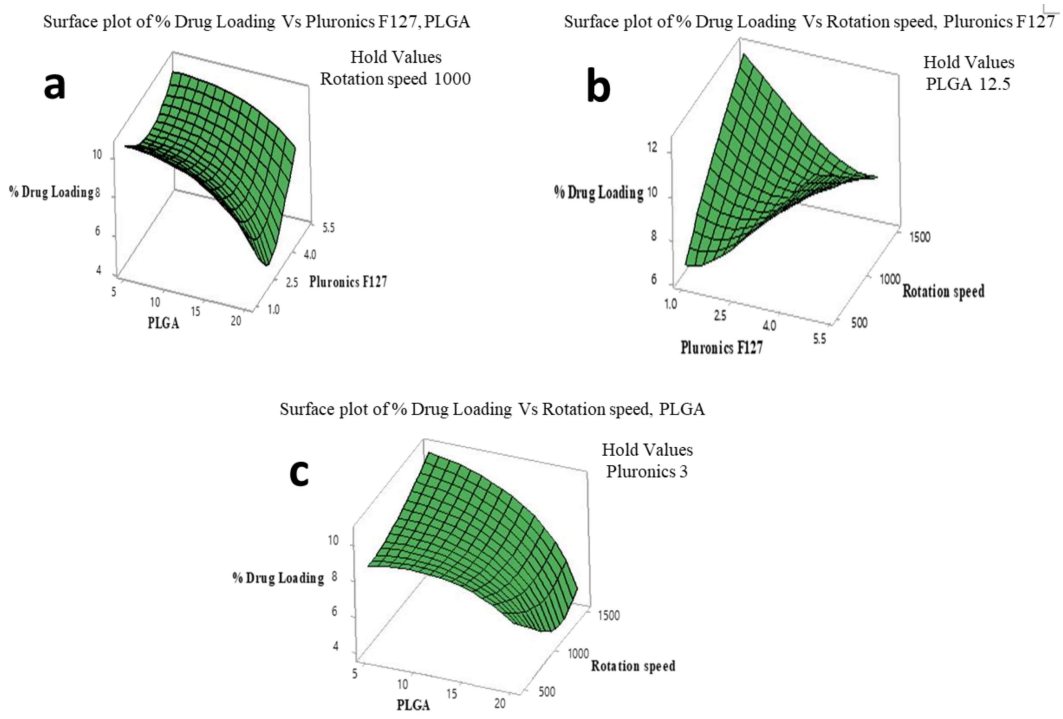

Figure 18: Surface plot of % Drug Loading (Y_1) (a) vs PLGA (X_1) vs Pluronics F127 (X_2) at constant Rotation speed (X_3) of 1000rpm taken as holding value (b) PLGA (X_1) vs Rotation speed (X_3) at 3% w/v Pluronics F127 (X_2) (taken as holding value) (c) Pluronics F127 (X_2) vs Rotation speed (X_3) at 12.5% w/v PLGA (X_1) taken as holding value.

The effects of factors on the responses further can be explained by these plots. In figure 18 (a), response surface plot shows the effects of X_1, X_2 on the drug loading (%), keeping value of X_3 constant at 1000 rpm. It can be seen that at high X_1 concentrations (17.7 %) and X_2 from 4 % to 5.5 %, significantly high % drug loading can be obtained.

Figure 18 (b) shows the effect of X_1 and X_3 on the drug loading (%), keeping X_2 (3%) constant. It can be deduced from the graph that at higher PLGA concentration (up to 19.8 %) and rotation speed (up to 1500) drug loading improves (up to 11.66%).

Similarly, the effect of X_2 and X_3 on the drug loading (%), keeping X_1 (12.5 %) a constant can be inferred from the plot wherein with an increase in X_3 from 500 to 1000 rpm increase in drug loading is possible (figure 18 (c)).

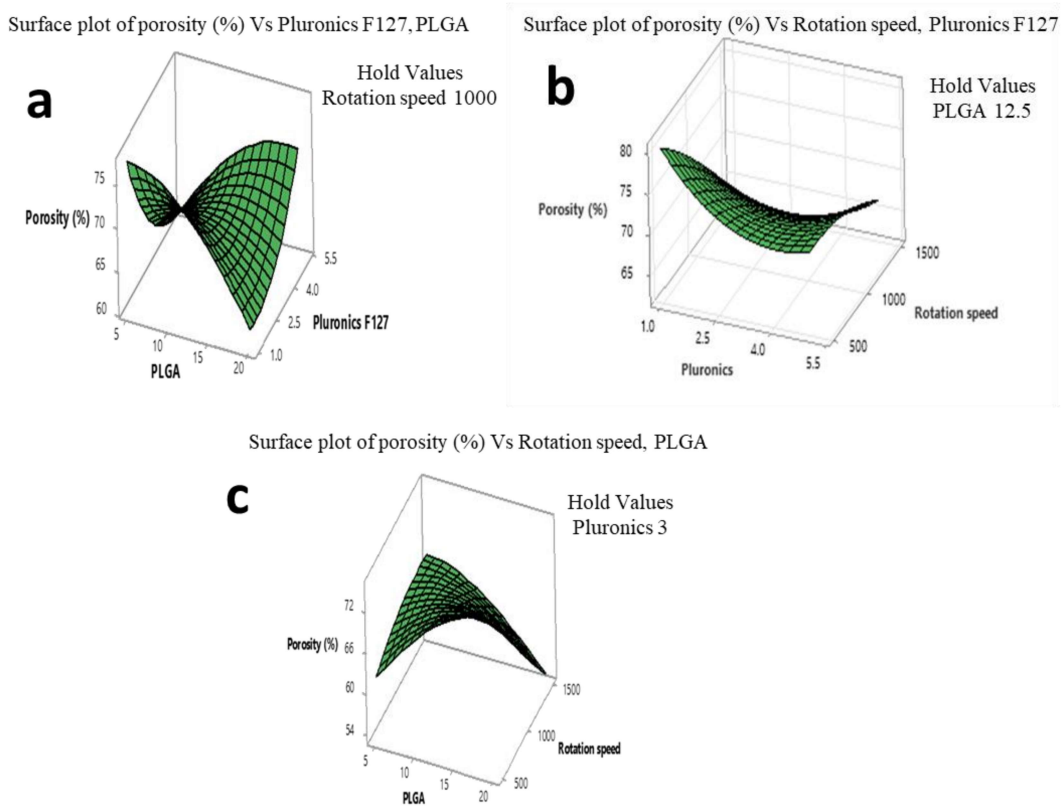

Figure 19: Surface plot % Porosity (Y_2) (a) PLGA(X_1) vs Pluronics F127 (X_2) at 1000 rpm Rotation speed (X_3) taken as holding value (b) Pluronics F127 (X_2) vs Rotation speed (X_3) at 12.5% w/v PLGA (X_1) taken as holding value (c) PLGA (X_1) and Rotation speed (X_3) at 3% w/v Pluronic-F127 (X_2) taken as holding value.

Moreover, the response surface plot for Porosity shows the effects of X_1, X_2 on the Porosity (%), keeping X_3 constant at 1000 rpm, and increasing X_1 up to 20% and X_2 up to 5.5 % can result in up to 82.62% porosity as shown in figure 19 (a). Similarly, the effect of X_2 and X_3 on Porosity (%), keeping X_1 (12.5%) constant can be described such that higher porosity can be obtained by preparing the scaffolds at higher rotation speed (figure 19 (b)). The effect of X_1 and X_3 on the Porosity (%), keeping concentration of X_2 (3%) constant can be similarly analysed from the plot that increase in X_1 (up to 20%) along with a decrease in X_3 (up to 500 rpm), can produce formulations with up to 72.16% porosity as shown in figure 19 (c).

The optimization chart is a Minitab response optimization tool that shows the impact of various experimental settings on the predictive response of a preserved model. The optimized diagram modifies the settings for variable components, process variables, and their quantities to get variable settings with optimal properties, examines the sensitivity of variables to changes in design variables, and responds and 'calculates' expected site responses for a variable of interest and searches for variable settings with higher composite desirability. The optimization of

response surface is assessed with the help of the desirability function. The predictions obtained are converted to a "d" scale ranging from d = 0 to d = 1. Zero indicates an unacceptable response, and 1 represents an entirely desirable response [231].

Table 7: Optimized Memantine loaded nanoscaffolds with predicted and experimental responses with relative errors

Parameters	Goal	Lower Limit	Upper Limit	Optimal value	Predicted value	Experimental results	Relative Errors
PLGA	Optimum	5(%w/v)	20(%w/v)	19.18	-	-	-
Pluronics F127	Optimum	1(%w/v)	5(%w/v)	4.98	-	-	-
Rotation Speed	Optimum	500 (RPM)	1500(RPM)	500	-	-	-
Porosity	Maximum	38.915(%)	96.4550	-	82.7	86.6133±0.020	+3.9
Drug Loading	Maximum	4.2750	12.4950	-	11.6	10.3112±0.012	-1.28

The optimized graph shows the effect of each factor (columns) on the response of composite desirability (rows). The vertical red line on the chart shows the current factor ratio setting. The number at the top of the column indicates the current position of the factor level (shown in red). Blue horizontal lines and numbers represent the response to the current factor level. The optimization plot shown in figure 10 shows that % drug loading is maximum at the predicted value of 19.18% w/v PLGA, and the loading increases with increase in pluronic F127 concentration (maximum at 4.98% w/v). The % drug loading decreases with an increase in rotation speed, and the maximum loading can be obtained at 500 rpm. Similarly, % porosity increases with increase in concentration of PLGA (maximum at 19.18% w/v), and that of Pluronic F127 (4.98% w/v). However, % porosity decreases with increase in rotation speed with maximal porosity obtained at 500 rpm. A higher concentration of polymer and Pluronic F127 produce polymeric phase with sufficiently higher viscosity that can entrap a considerable amount of drug. Using the predicted values of PLGA, Pluronics, and Rotation speed, the % drug loading and % porosity was predicted to be 11.66%, and 82.62 % respectively with composite desirability (d) of 0.88240 and 0.75548 respectively. The optimized formulation composition with predicted and experimental response values has been shown in table 7, indicating the relative error of porosity and drug loading as +3.9 and -1.28, respectively. The optimal desirability (D) of optimized nanoscaffold was found to be 0.8165, indicating a desirable response at the predicted value.

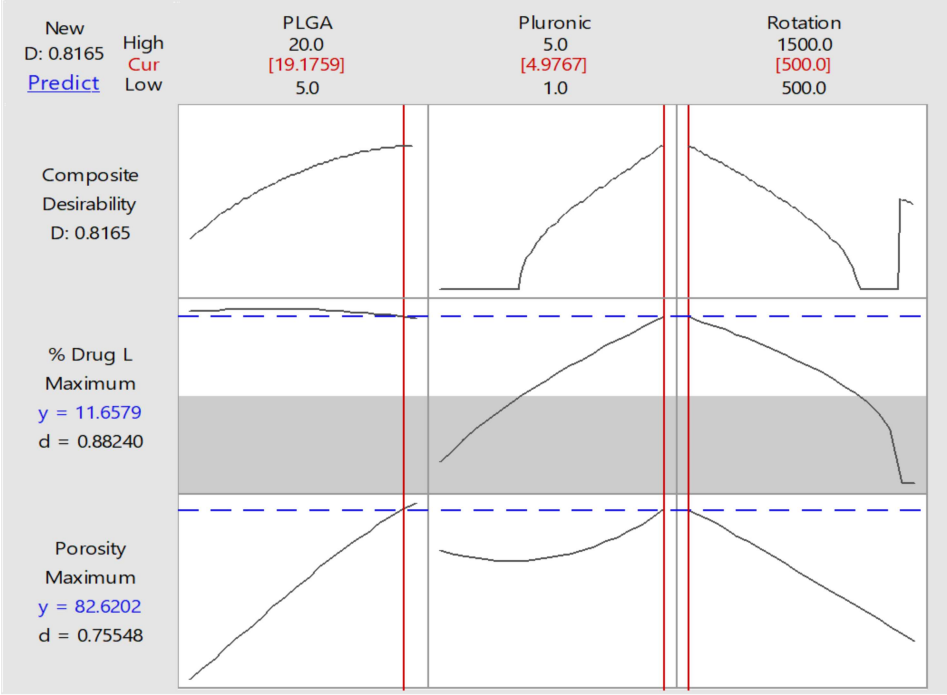

Figure 20: Optimization response at PLGA concentration (19.18% w/v), Pluronic concentration (4.98% w/v),and Rotation speed(500rpm) which predicted % drug loading at 11.66, and % porosity of 82.62 with a composite desirability (d) 0.88240 and 0.75548 respectively.

Additionally, the significant response surface analysis of porosity and drug loading based on the interactions of three variables has been mentioned in figure 20 along with the limits and effectiveness of each parameter and the optimal parameter values with the expected responses of each variable.

6.2 Characterization of Memantine loaded nanoscaffolds

6.2.1 Surface morphology (SEM)

The Scanning electron microscope (SEM) is one of the most widely used techniques for the characterization of nanomaterials and nanostructures. The signals that derive from electron-sample interactions reveal information about the sample including surface morphology (texture) of the sample. The surface morphology of prepared memantine-loaded nanoscaffolds was assessed using scanning electron microscopy (SEM) (FEI QuantaTM 200, USA) possessing a secondary electron detector at an accelerated voltage of 10 kV in the size scale of 100 nm and 200 nm (Figure 20 (a-b)). The samples were sputter-coated with aluminium pre-coated with silver glue, under vacuum, and observed in SEM. The scanning electron microscopic studies showed that nanoscaffolds exhibited spherical structures in nano-size range with porous surface characteristics as shown in figure 21 (a-b). The SEM images of memantine-loaded PLGA

nanoscaffolds displayed uniform distribution of nanoscaffolds with size in the range of 100-200 nm. The nanoscaffolds were found to be of self-assembling type arranged in a definite configuration which can support the growth and development of neurons by mimicking the extracellular matrix. The growth and development of neurons is an important aspect of the treatment of Alzheimer's disease.

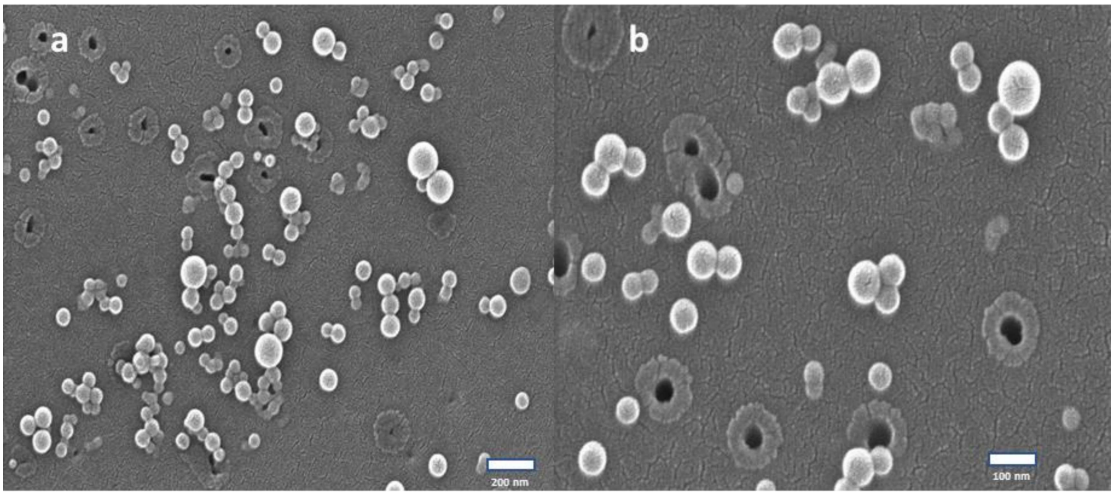

Figure 21: SEM of Memantine-loaded nanoscaffolds at scale (a) 200 nm (b) 100 nm.

Size and texture of nanoscaffolds depend on the concentration of pluronic F-127. When concentration of pluronic F-127 was increased, particle size was found to decrease. Nanoscaffolds in the size range 100-200 nm with porous texture were produced upon incorporation of 4.98% w/v of pluronic F-127, which could arrange spontaneously and self-assemble to act as extracellular matrix. It has also been helpful in improving the therapeutic efficacy of drug and for neurological disorders and targeted delivery [237]. Polymer concentration also affects the size of nanoscaffolds and it was reported that the particle size of nanostructure increased with increasing concentration of polymer [238]. The designed nanoscaffolds with optimum concentration of PLGA at 19.18% w/v exhibit smaller size with improved drug delivery, longer circulation in the blood, and low toxicity.

Zeta potential value of nanostructures was found to be 23±4.51 mV despite non-ionic PEG coating indicating stable nature of nanoscaffolds due to reduced electrostatic interactions.In buffer media pH 6.8 there is high H+ ionization as compared to hydroxyl end group ionization which reduces the net negative charge on PEG coated PLGA nanoscaffolds and potentiate positive zeta potential [239].

Research studies have shown that PEGylation increases the particle zeta potential which further facilitates cytoplasmic transport of PEGylated nanocarriers [240]. The PLGA

nanoscaffolds are relatively hydrophobic in nature [241]; and, PEG coating increases the hydrophilicity which leads to decreased van der Waals interactions between nanoparticles in the solution and hence lesser aggregation of the PEG coated PLGA Nanoscaffolds. as At higher charge differences (-30mV to +30mV) greater interparticle repulsion is observed hence, there is enhancement of colloidal stability with increasing zeta potential values [242].

6.2.2 Percentage porosity

Porosity is a measure of the percentage of empty space in nanoscaffolds that can incorporate active ingredients or cells for imparting therapeutic effect therefore; a high percentage of porosity can contain more active ingredients and provide space for the cell growth and impregnation. The predicted value of percentage porosity of the optimized formulation was 86.45%. The actual percent porosity of memantine-loaded nanoscaffolds was found to be 82.33%. The growth and development of neurons is generally based on interconnecting channels and porosity of the nanoscaffolds. Novel fabrication techniques of nanoscaffolds can selectively be designed to meet the specificity of neurodegenerative disorders. Previous research studies such as biodegradable hybrid inorganic nanoscaffolds and biodegradable poly (L-lactic acid) (PLLA) nanoscaffolds developed by *Yang L et.al.*,2018 and *Yang F et.al., 2004* respectively suggested that higher porosity (65-80%) enables greater therapeutic efficacy of the drug and stem cells accompanied by improving neuron development and signalling [243,244]. Our findings suggest that encapsulation, drug release, and pharmacological effects are directly correlated with pores and the interface between brain structures and scaffolds. Pluronics F-127 is used as a pore-forming agent that helps to maximizing porosity and increase surface area to mass ratio enhancing drug loading and regeneration potential by inducing cell adhesion, proliferation, and differentiation [245]. The above findings suggest that the memantine-loaded PLGA nanoscaffolds with porosity of 82.33% offer a promising environment similar to extracellular matrix along with higher drug incorporation and good drug release kinetic which favours neuronal cell adhesion, proliferation and differentiation for neuronal recovery of degenerated neurons in the condition of AD.

6.2.3 Entrapment Efficiency and Drug Loading

The Entrapment study indicates that approximately 90.61±0.48 % of memantine was entrapped within the nanoscaffolds. The nanoscaffolds were formulated using a mixture of 75:25/50:50 PLGA, the biodegradable polymer forms a porous structure that helps in entrapment within the nanoscaffolds. The actual drug loading content obtained was 11.66 ±0.05 %. Earlier reported studies suggested the direct correlation of entrapment efficiency to the molecular weight and

hydrophobicity of the polymer [234]. A high molecular weight polymer has the ability to restrict the escape of the encapsulated drug from within the pores and core due to its high viscosity and polymer phase ratio, resulting in high entrapment efficiency. Furthermore, the hydrophobicity of the polymer can also influence the entrapment efficiency; highly hydrophobic polymer restricts the escape of encapsulated drugs into the aqueous medium. However, a highly hydrophobic polymer affects the release kinetics of drugs. A mixture of PLGA 50:50 and PLGA 75:25 polymer has been used in this study to optimize the entrapment efficiency and drug release characteristics of nanoscaffolds. Previous research suggested that PLGA is a polymer consisting of poly lactic acid (PLA) and polyglycolic acid (PGA) copolymer, and their incorporated ratio is responsible for drug delivery and pharmacological activity [105]. The results of their study demonstrated that an increase in glycolic acid percentage accelerates polymer degradation and; preferential favours degradation of polymer PLGA 50:50 faster as compared to PLGA 75:25. Also, the greater hydrophobicity of PLGA 50:50 (PLA/PGA) than PLGA 75:25 (higher hydrophilicity) maximize the entrapment efficiency of memantine (lipophilic in nature) up to 90.61% and showed controlled drug release characteristics.

6.2.4 Biodegradation study

The effect of enzymatic degradation on nanostructured PLGA nanoscaffolds were studied by incubating PLGA nanoscaffolds for four weeks in phosphate buffer saline (pH-6.8) (PBS) and water containing lysozyme (Lz/PBS). PLGA nanoscaffold treated in Lz/PBS exhibit more irregular pore boundaries with signs of breakdown in the continuity of honey-comb-like nanostructure. After four weeks, the formation of large pores was evident on scaffolds incubated in degradation media with greater pore roughness. The weight loss of PLGA nanoscaffold from 0.578g to 0.1727 g indicated 70.24±3.45 % degradation after four weeks of incubation in Lz/PBS. The control samples incubated in PBS without lysozyme showed an approximately 32.45±2.26 % loss in weight after fourth week. As reported in literature biodegradation of PLGA occurs purely through hydrolysis. However, the PLGA polymer biodegrades into lactic and glycolic acids. Then, lactic acid and glycolic acid enters the tricarboxylic acid cycle and are subsequently eliminated from the body in form of carbon dioxide and water [105]. The toxicity of inorganic biomaterial restricts the use of gold, silver, iron, platinum for the treatment of neurodegenerative disorders like AD.

6.2.5 Swelling index and water uptake study

The swelling index of both plain nanoscaffolds and memantine-loaded nanoscaffolds was evaluated in 15 mL of pH 7.4 PBS at 37 °C. The accurately weighed dry nanoscaffolds and memantine-loaded nanoscaffolds were immersed in PBS pH 7.4. At different time intervals (1,

4, 8, 12, and 24 h), the swollen scaffold was taken out and excess water was carefully removed. It was then weighed immediately to find out the swelling index of nanoscaffolds. Three independent experiments were performed for each time point measurement. The graphical presentation of swelling index of blank nanoscaffolds and memantine-loaded nanoscaffolds at regular time intervals has been illustrated in figure 22. The swelling index of memantine-loaded nanoscaffolds (Nme) and blank nanoscaffolds (N) was calculated to be 84.87±2.12 % and 84.54 ±3.48% respectively. However, after maximum swelling at 24 h, further increase in degree of swelling was not observed with time, and water-soluble memantine also interacts with the polymeric chain through hydrogen-bond crosslinks that restricts further entry of water after maximum swelling of nanoscaffolds at 24h [246,247]. Studies suggest that the swelling index controls the release kinetics of drug by providing slow dissolution of polymer via layer-by-layer erosion over time. The swelling of polymeric PLGA molecules actually help to achieve control of drug delivery inside the brain for longer duration by following diffusion and erosion kinetics.

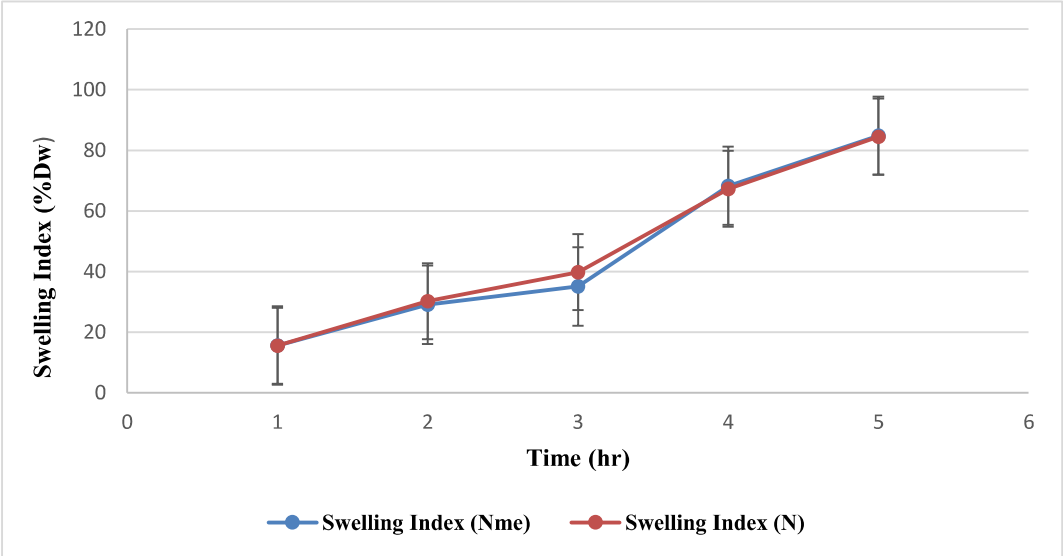

Figure 22: Swelling index of Memantine loaded PLGA nanoscaffolds.

6.3 Characterization of (PEG-MEM-PLGA) SANs

6.3.1 Drug and polymer incompatibility study (FTIR) and Thermal Characteristics (TGA and DSC)

FT-IR spectra of Memantine, PLGA, Pluronics F127 and (PEG-MEM-PLGA) SANs were recorded and shown in the figure 23 (a). The presence of characteristic peaks in the FT-IR spectra of drugs and excipients confirmed that drug and polymers are compatible with each other. The characteristic peaks of pure PLGA 50:50/75:25 due to OH stretching (3745.8 cm^{-1}), -CH (2859-3012 cm^{-1}), carbonyl -C = O stretching (1712.1 cm^{-1}) and C-O stretching (1512.2

cm^{-1}) were observed in the spectra [248]. The peaks of C–H stretching (2859 cm^{-1}), in-plane O–H bending (1345-1468 cm^{-1}) and C–O stretching (1085.73 cm^{-1}) were observed for Pluronic F127 in the spectra [249]. The characteristic FTIR peak of Polyethylene glycol due to stretching and bending vibrations were observed for C-O stretch in the region 1508.9 cm^{-1} and OH stretching vibration at 3749.6 cm^{-1} [250]. Memantine showed its characteristic peak at 1448.7 and 2892.5 cm^{-1} which corresponds to NH out of plane stretching and CH stretching respectively [251]. The FTIR spectrum of (PEG-MEM-PLGA) SANs indicates no interaction among the drug and the excipients, as all the specific peaks were present in the formulation.

Thermogravimetric analysis (TGA) was used to determine the physical properties related to temperature, heating rate and weight loss (%). TGA provides information about transitions due to changes in properties as a function of time at a constant temperature. Figure 23 (b) shows the TGA profile of the PLGA 50:50/75:25, PEG, Pluronic F-127 and (PEG-MEM-PLGA) SANs. During the thermal analysis thermal stability of PLGA 50: 50/75: 25, Pluronics F127, PEG, (PEG-MEM-PLGA) SAN was observed up to 254°C, 313°C, 245°C and 384°C respectively after which the thermogram showed an approximate weight loss of 86.2%, 89.84%, 74.17% and 33.68% respectively in the temperature range of 300-420°C. The thermogram of (PEG-MEM-PLGA) SANs exhibited higher thermal stability of nanostructure than the individual components, possibly due to its intact molecular structure and framework. The DTG plot of PLGA 50:50/75:25, PEG, and Pluronic F-127 shows the stages of weight loss observed during TGA analysis (figure 23 (c)). The melt transition of PLGA 50:50/75:25, PEG, and Pluronic F-127 occurred at 331°C, 332°C, and 393°C respectively, whereas the DTG plot of (PEG-MEM-PLGA) SANs has shown slight weight loss between 30°C to 600°C, which can be attributed to the thermal stability of nanostructures compared to polymer and excipient individually.

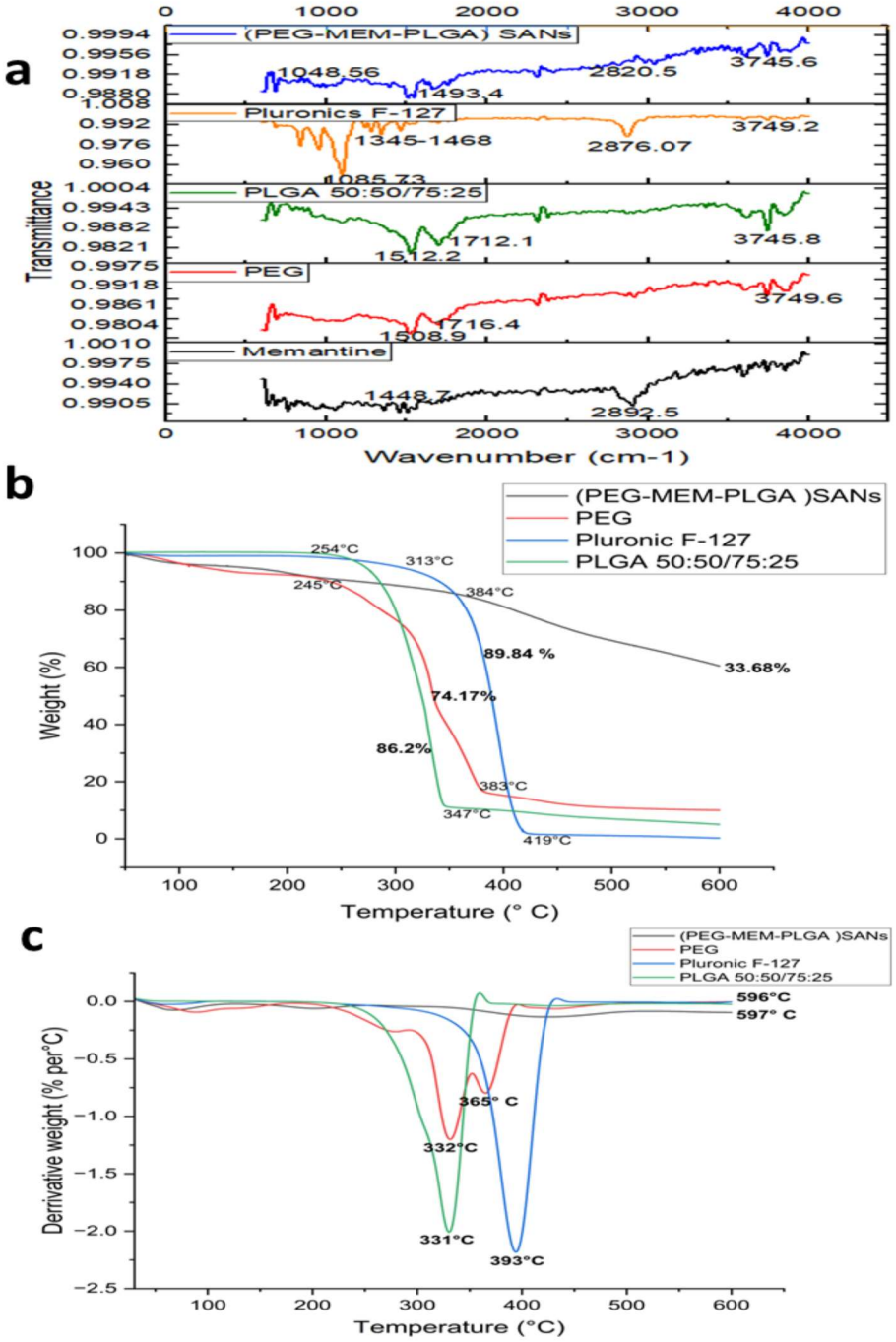

Figure 23. (a) FTIR spectrum of PLGA 50:50/75:25, Pluronics F127, PEG and (PEG-MEM-PLGA) SANs; (b-c) Thermogram (TGA/DTG) of PLGA 50:50/75:25, PEG, Pluronics F127 and (PEG-MEM-PLGA) SANs from temperature 30 °C to 600 °C.

6.3.2 Surface morphology (SEM, Particle size and Zeta potential)

The surface morphology of prepared (PEG-MEM-PLGA) SANs was assessed using scanning electron microscopy (SEM) (FEI QuantaTM 200, USA) possessing a secondary electron detector at an accelerated voltage of 10 kV at 1000, 2000 and 5000 resolution in the size scale

of 1 μm (Figure 24 (a-b)). The samples were sputter-coated with aluminium pre-coated with silver glue, under vacuum, and observed in SEM. The scanning electron microscopic studies showed that nanoscaffolds exhibited self-assembled structures in three-dimension in nano-size range as shown in figure 24 (a-b). The organization of self-assembled elongated structures is due to PLGA and Pluronic F-127. Self-assembly is a process in which nanoparticles at the nanoscale spontaneously arrange into ordered superstructures that can be exploited in various applications. This spatial arrangement of nanoscale material can influence cell adhesion, spreading, alignment, and morphology within brain. As a result, 3D spatial features of a nanoscaffolds' construct can influence the neural cell response upon encapsulation of cells within the biomaterial and further, mimic the extracellular neuronal environment.

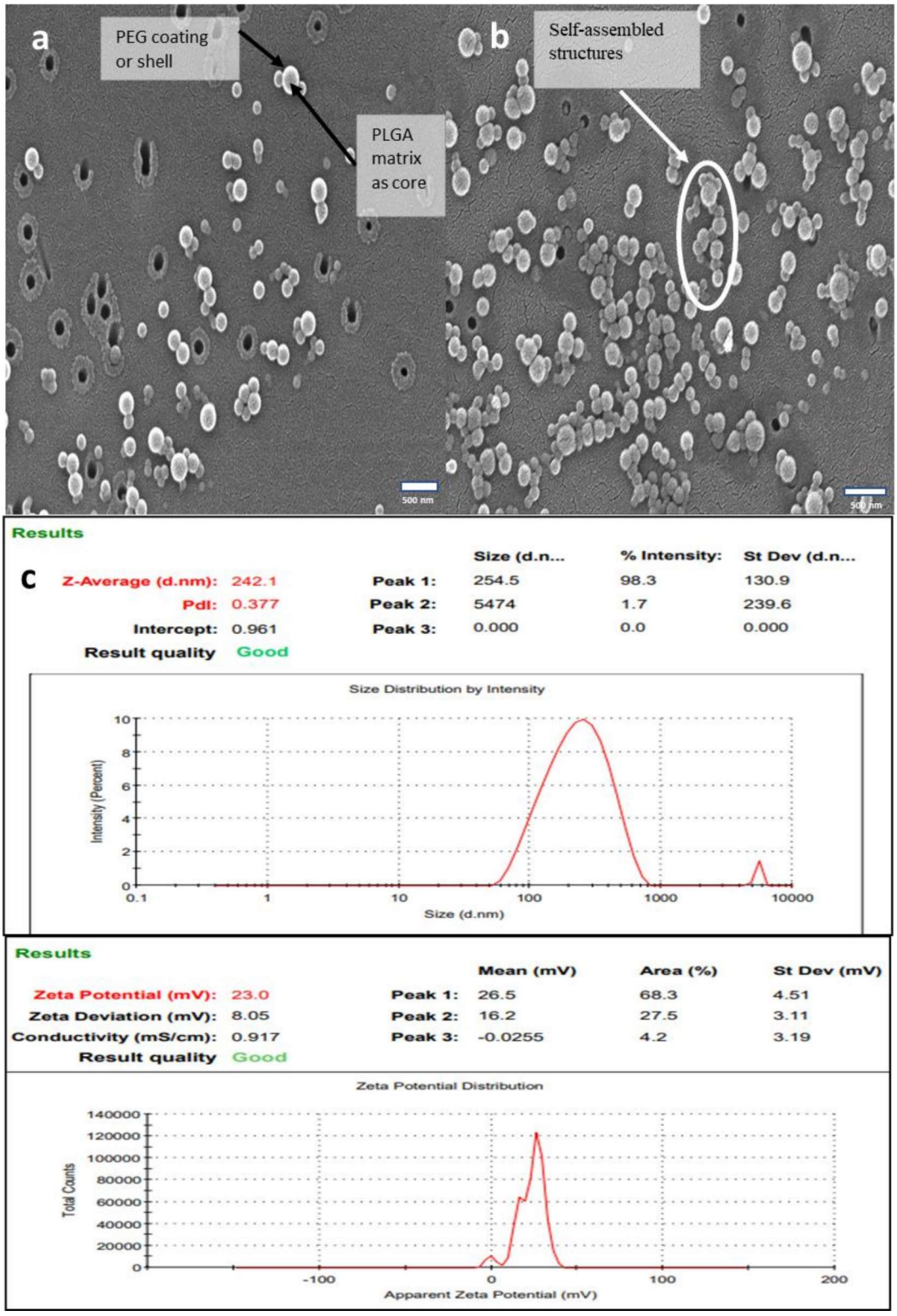

Figure 24: Scanning electron microscopy (SEM) of (PEG-MEM-PLGA) SANs at (a-b) scale 500 nm (c) showed Particle size, polydispersity index and zeta potential plot of (PEG-MEM-PLGA) SANs.

The average particle size of (PEG-MEM-PLGA) SANs obtained was 242.1±130.9 nm. The

polydispersity index (PDI) of the nanoscaffolds was 0.377 representing polydisperse nature of the scaffolds (Figure 24 (c)) [252]. Zeta potential value of nanostructures was found to be 23±4.51 mV indicating stable nature of nanoscaffolds (Figure 24 (c)).

6.3.3 Determination of porosity (%)

The percentage porosity of (PEG-MEM-PLGA) SANs was found to be 82.33±0.852 %. The porosity of self-assembled nanoscaffolds is dependent on the concentration of Pluronic F127 and PLGA that helps in creating a three-dimensional (3D) nanoarchitecture with improved drug entrapment, cell penetration, and can thus be utilised as functional tissue-engineered nanoscaffolds [253]. Pluronic F127 acts as a surface modifier and pore-forming agent. It also helps in self-assembly forming core/shell configuration [254]. PLGA are also helpful in information of pores upon adsorption of water alongwith degradation/erosion of the polymer. The pH significantly influences the formation of pores especially at around pH 5–6 [255].

6.3.4 Entrapment Efficiency

Approximately 90.61±0.48 % of memantine HCL was entrapped within (PEG-MEM-PLGA) SANs. The nanoscaffolds were formulated using mixture of 75:25/50:50 PLGA which is a biodegradable polymer and forms porous structures that help in entrapment of drug within the nanoscaffolds. Approximately, 11.66±0.05 % memantine was loaded into the nanoscaffolds. Further, the % drug loading in NPs is affected by drug-polymer interaction and drug miscibility in the organic solution. Memantine is a small molecule (MW=215.76) with high lipophilicity and exhibits high miscibility in the organic phase by virtue of efficient polymer interaction and this results in maximal entrapment within the PLGA nanoscaffolds. Moreover, the LA:GA ratio (50:50-100:0) also has an effect on drug content of nanosca ffolds due to an increase in hydrophobic interaction of Memantine and PLGA. Lactide rich PLGA copolymers are less hydrophilic, absorb less water and subsequently degrade more slowly as compared to glycolide rich PLGA polymer, and at 50:50 ratio PLGA copolymer exhibits faster degradation [105]. Whereas PLGA copolymer 75:25 is less hydrophilic and exhibit slow release of drug from the polymeric matrix. Hence, in this study, 1:1 ratio of PLGA (50:50) and PLGA (75:25) were used to get the desired formulation with high drug encapsulation and controlled drug release characteristics.

6.3.5 Biodegradation and Swelling index study

(PEG-MEM-PLGA) SANs which were incubated for four weeks in pH 1.2, 5.7, 6.8, 7.4 and water containing lysozyme (Lz/PBS) exhibited irregular pore formation due to the breakdown of polymeric matrix. After four weeks, higher pore size with increased pore irregularity was observed on incubation in degradation medium. The decrease in weight of SANs from 0.578g

to 0.1245g, 0.166g, 0.1583g, 0.1727g resulted in 78.4±4.52 %, 71.28±3.12%, 72.61±6.34%, and 70.24±2.44 % degradation after four weeks of incubation in Lz/PBS in pH 1.2, 5.7, 6.8 and 7.4 respectively as shown in figure 25 (a). Control samples incubated in lysozyme-free saline showed weight loss of approximately 32.45±2.54 % at the end of 4 weeks. From the experimental data, it can be inferred that degradation of (PEG-MEM-PLGA) SANs slowed when the pH of the media is changed from acidic to basic. Acidic conditions enhance the hydrolysis of self-assembled nanoscaffolds into lactic acid and glycolic acid.

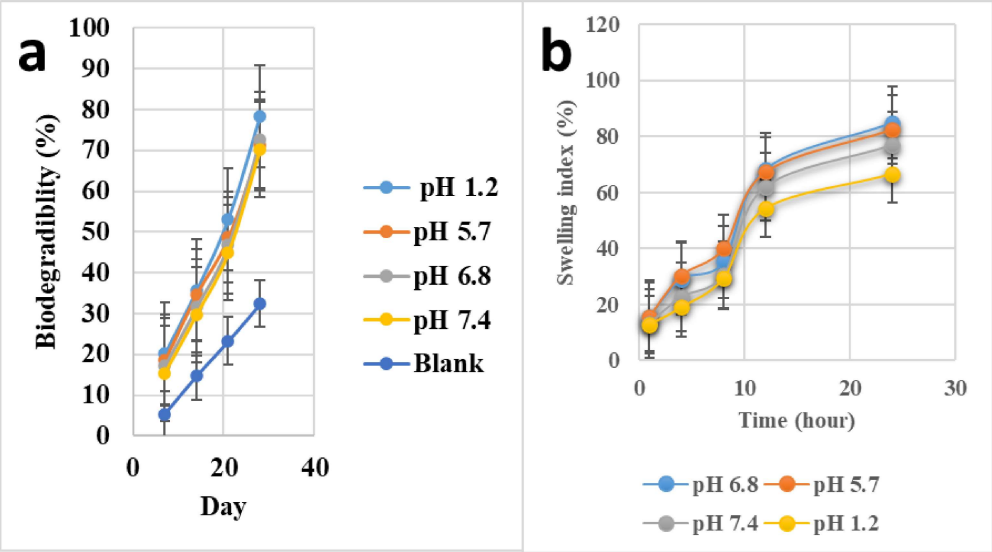

Figure 25: (a) Biodegradation of (PEG-MEM-PLGA) SANs at pH 1.2, 5.7, 6.8 and 7.4 and blank during a four-week study. (b) Swelling index of (PEG-MEM-PLGA) SANs at pH 1.2, 5.7, 6.8 and 7.4.

Accurately weighed dry (PEG-MEM-PLGA) SANs were immersed in each of 15 ml buffer of pH 1.2, 5.7, 6.8, 7.4 at 37 °C. The swollen scaffolds were taken out at different time intervals (1, 4, 8, 12 and 24 h), and excess water was carefully removed before weighing. Three independent experiments were performed for each time point measurement. The swelling index of (PEG-MEM-PLGA) SANs was calculated as 66.5 %± 0.04, 82.54%± 0.028, 84.8%± 0.051, 76.8%± 0.041 respectively at pH 1.2, 5.7, 6.8 and 7.4 has been shown in figure 25 (b). The optimal swelling capability of self-assembled nanoscaffolds was observed in the pH range of 5 to 7 and the maximum swelling index was obtained at pH 6.8. Due to the presence of PEG, which is hydrophilic, on the surface enhanced wettability of the polymeric surface was observed contributing to increase in swelling and porosity of the nanoscaffolds [256]. The remarkably high swelling of nanoscaffolds at pH 6.8, shows that pH can be used as a stimuli while development of nanocarriers for sustained/controlled/targeted delivery of drugs [257].

6.3.6 Stability Studies

The stability studies of (PEG-MEM-PLGA) SANs were performed at two different conditions: 40°C/75% RH and ambient storage conditions. The obtained entrapment efficiency and % porosity of (PEG-MEM-PLGA) SANs at 25 ± 2 °C, 60 ± 5 %RH was 90.21± 0.40 % and 81.86± 0.82 %, and at 40 ± 2°C/75 ± 5 %RH it was 85.34± 0.34 %and 76.54± 0.61 % respectively (Table 8). There was no significant change in entrapment efficiency and % porosity at 25 ± 2 °C, 60± 5 % RH and can be used suitably for storage of SANs, while a decrease in entrapment efficiency and % porosity was observed at 40°C/75% RH suggesting that high temperature induces degradation and is not suitable for long term storage.

Table 8: Accelerated stability study performed in two storage conditions

Storage conditions (Temperature and Relative humidity)	0 month		3 months	
	Entrapment Efficiency	Porosity (%)	Entrapment Efficiency	Porosity (%)
25±2 °C, 60± 5 % RH	90.61±0.48 %	82.33±0.85 %	90.21±0.40 %	81.86±0.82 %
40±2 °C, 75± 5 % RH	90.61±0.48 %	82.33±0.85 %	85.34±0.34 %	76.54±0.61 %

6.3.7 In-vitro studies

6.3.7.1 Drug Release study and Kinetic model

The release of Memantine from 10 mg (PEG-MEM-PLGA) SANs was studied in acidic buffer (pH 1.2 and 5.7) and phosphate buffer (pH 6.8 and 7.4) using *in-vitro* dialysis bag technique with the analysis being performed at a wavelength of 218 nm. Higher cumulative percent release (CPR) of (PEG-MEM-PLGA) SANs was obtained at pH 5.7 (89.52 ±5.32 %) and 6.8 (94.52±6.29 %) (Figure 26 (b)). An initial burst release of drug from the surface upon hydration, followed by diffusion of the drug from the swollen polymeric matrix with sustained release was observed. The marketed memantine HCL tablet exhibited a burst release with approximately 91.45±7.7% release up to a maximum of 24 h only. The ionic strength and buffer capacity of the dissolution media influences drug release from pH-responsive nanocarriers. In AD, the accumulation of Amyloid-β peptide (Aβ) leads to a decrease in pH of brain due to formation of endo-lysosomal vesicles. Thus, the release of drug from the matrix of (PEG-MEM-PLGA) SANs at pH (5.7 and 6.8) might be helpful maintaining higher concentration of drug at the diseased site.

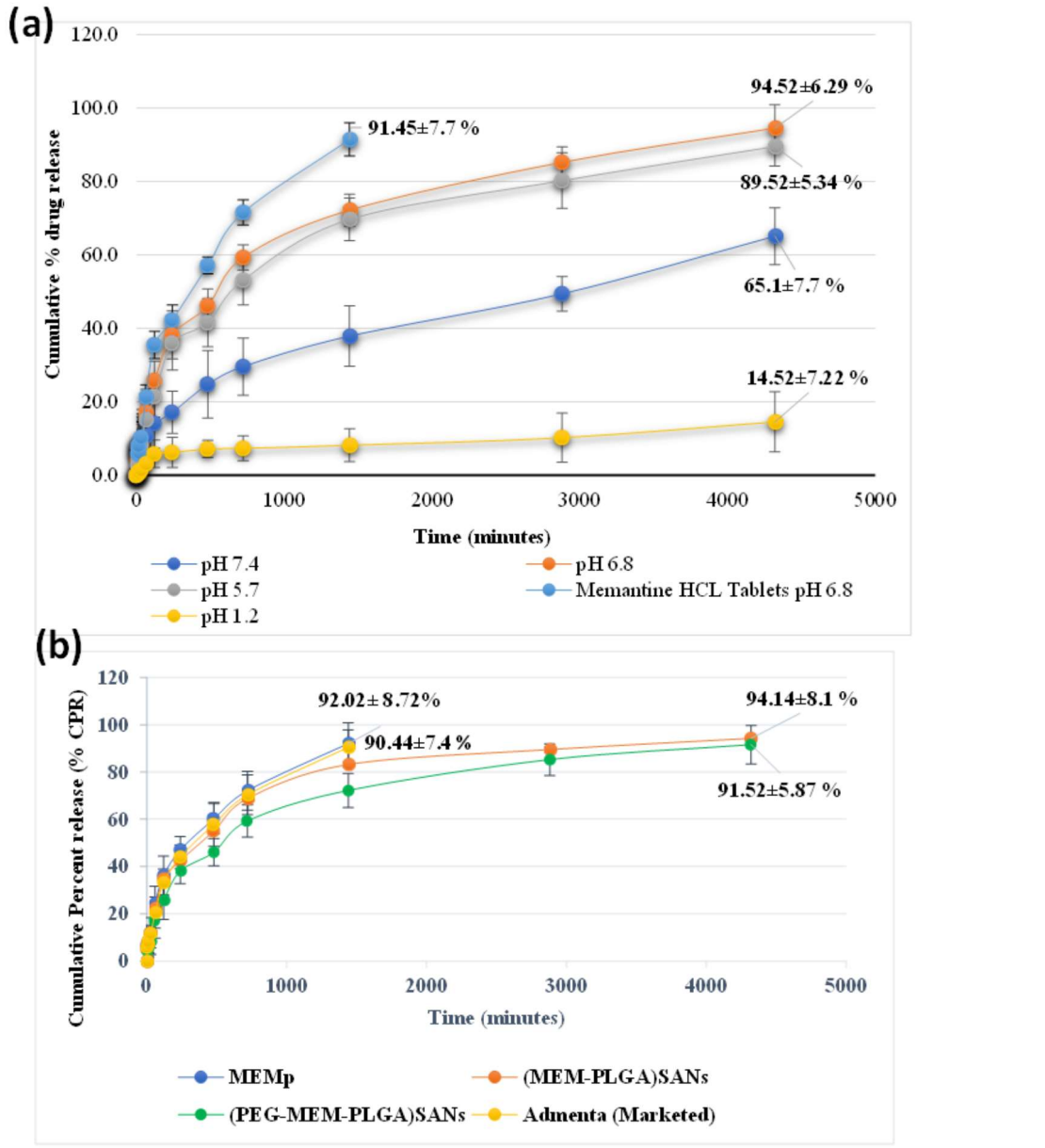

Figure 26: *In-vitro* release profile of (a) (PEG-MEM-PLGA) SANs at pH 1.2, 5.7, 6.8 and 7.4 and Memantine HCL Tablets at pH 6.8 (b) A comparative drug release profile of MEMp, (MEM-PLGA) SANs, (PEG-MEM-PLGA) SANs and Admenta (Marketed tablet) at pH 6.8.

In order to determine the drug release kinetics, the in vitro drug release data was analysed and modelled (figure 27). The drug released from (PEG-MEM-PLGA) SANs exhibited Korsmeyer-Peppas drug release kinetics with a correlation coefficient (R^2) of 0.9901 as shown in figure 27. The model can be described according to equation 14 that indicates drug release pattern from a polymeric system.

$$M_t / M_\infty = Kt^n \quad \text{.....(eq 14)}$$

Mt is the amount of drug released in time t, M∞ is the amount of drug released after time ∞, n

is the diffusional exponent or drug release exponent, Kp is the Korsmeyer release rate constant. To study release kinetics a graph is plotted between log cumulative % drug release vs. log time (log t). The release exponent or the diffusion exponent (n) was found to be lower than 0.45 which implies that the drug release from the system follows fickian law.

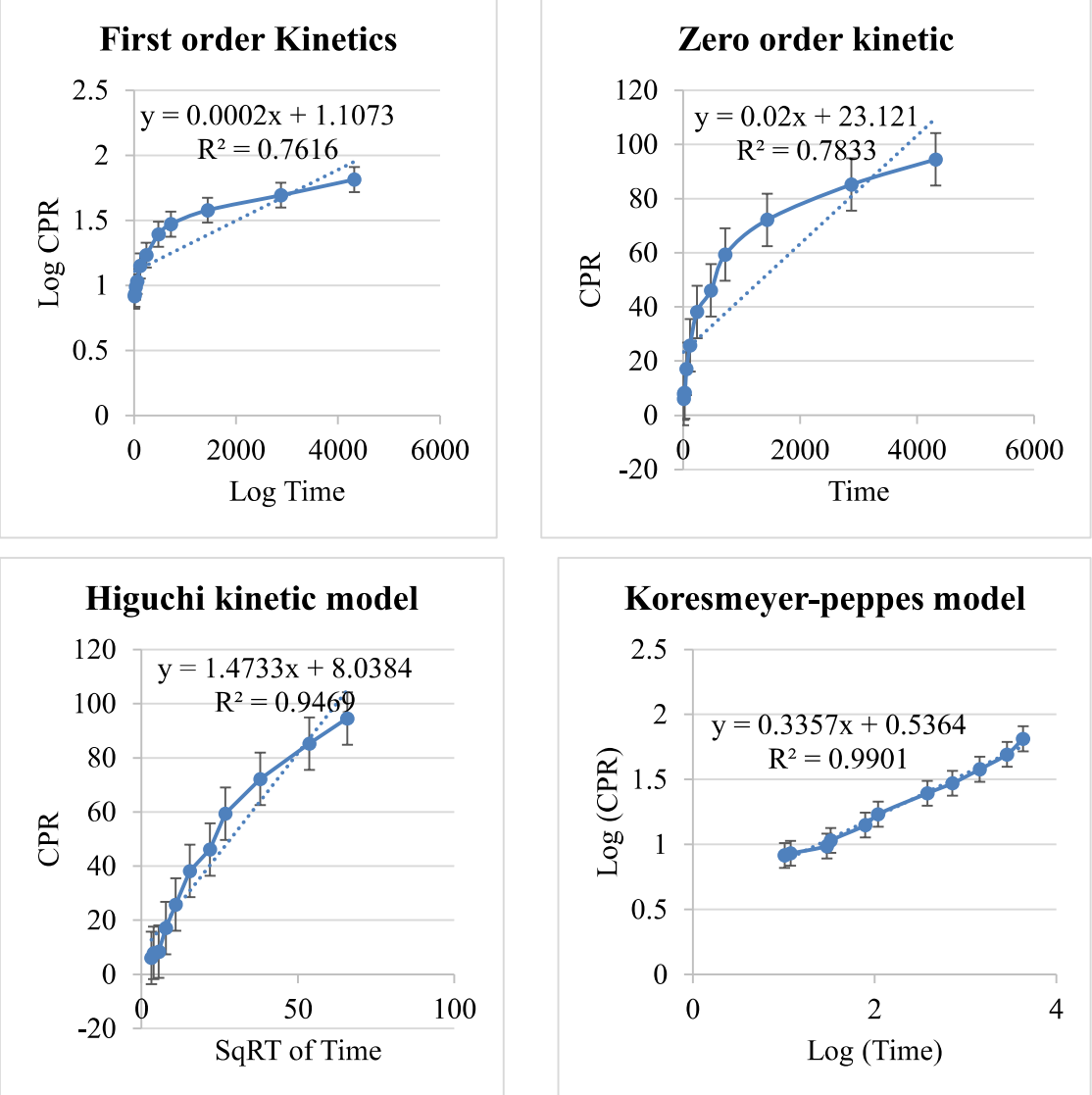

Figure 27: Drug release kinetic model of (PEG-MEM-PLGA) SANs.

6.3.7.2 Blood-brain barrier permeation assay (PAMPA-BBB)

PAMPA test is a simple approach that measures permeability across artificial membranes which helps to determine passive diffusion and transport across gastrointestinal tract, blood-brain barrier and cell membranes. Compounds can be divided into low and high permeability based on evaluated Pe value.

The permeability of drug and the carrier across blood-brain barrier (BBB) is a prerequisite for targeting AD. *In vitro* permeability (Pe) of the self-assembled nanoscaffolds and Memantine

were performed using porcine brain lipid (PBL) soaked overnight in dodecane. MEMp, (MEM-PLGA) SAN, (PEG-MEM-PLGA) SAN and Admenta (commercial memantine tablets) which exhibited Pe values of 5.6 x 10^{-6} cm/s, 11.2 x 10^{-6} cm/s, 13.7 x 10^{-6} cm/s and 8.2 x 10^{-6} cm/s respectively. According to the literature, Pe > 4.3 × 10^{-6} cm/s is indicative of a high permeability across the central nervous system, and a higher BBB permeability of (PEG-MEM-PLGA) SANs was observed as compared to MEMp, (MEM-PLGA) SANs and marketed tablet, the latter also being significantly higher in reference to the threshold value. Surface coating with polyethylene glycol (PEG) bypasses opsonisation and increases the "stealth" behaviour that leads to prolonged circulation time and enhanced transport of nanoscaffolds across the brain via endocytosis [258].

According to Fick's law of diffusion, permeability of any drug is directly proportional to the partition coefficient of membrane and the concentration gradient. The drug first crosses the phospholipidic membrane by passive transport from the donor cavity and then from the phospholipid membrane to the acceptor cavity. The gradual increase in concentration gradient during the incubation process due to penetration of large amount of drug from well into the donor-acceptor plate results in subsequent increase in Pe. As the incubation time increases, the drug permeability decreases due to a decrease in concentration gradient, however, an increased amount of drug is found in the phospholipid membrane due to the hydrogen bonding between the drug and the solvent. Once Pe reaches its maximum, backscattering phenomenon occurs and some of the drug returns from the acceptor opening to the phospholipid membrane. As a result, the Pe value gradually decreases [259].

PLGA nanocarriers can cross the BBB passively or through active endocytosis. Surface of PEG coated PLGA Nanoscaffolds have positive charge (+23mv) that electrostatically interact with negatively charged regions of the luminal surfaces, which helps nanoscaffolds to cross the BBB. The PEG-PLGA copolymer is widely used in pharmaceutical products and devices to modify the surface of the nanocarriers to further increase their ability to cross the BBB and deliver drugs into the brain [260].Upon intrathecal administration, nanoscaffolds move into the spinal canal, then via subarachnoid space reach the cerebrospinal fluid (CSF). After reaching CSF these nanocarriers are paracellularly transported across BBB via transcytosis [261]. Intrathecal route of administration provides an efficient route for delivery of drug to site of action by passing the blood brain barrier, infusing therapeutic agents into the cerebrospinal fluid. However, when same drug is given orally, very little amount is able to reach the brain region because of its inefficiency to cross BBB [157,262].

6.3.8 Ex-vivo study

6.3.8.1 Enzyme Kinetic study of Acetylcholinesterase (AChE), Butyrylcholinesterase (BUChE) and β-Secretase

The acetylcholinesterase and butylcholinestrase (AChE and BChE) enzyme kinetics were evaluated through this study using memantine-loaded nanoscaffolds at concentrations of 0, 2.5, 5, 10, and 20 μM as inhibitor and substrate concentrations of 10, 20, 30, 40 and 50 μM. The Lineweaver–Burk plot of AChE enzyme inhibition assay (Figure 28 a) showed a decrease in the Vmax values from 0.403 to 1.112 μM/min, and the Km value changed from 25.46 to 76.36 μM, indicating non-competitive mode of inhibition with a Ki of 7.74 μM^{-1}. The Lineweaver–Burk plot for BUChE (Figure 28 b) showed an increase in Vmax value from 1.073 to 3.355 μM/min alongwith an increase in Km value from 15.5 to 23.93 μM^{-1} indicating non-competitive mixed inhibition with a Ki of 6.53 μM^{-1}. The Lineweaver-Burk plot of β secretase (Figure 28 c) shows an increase in value of Vmax (1.080 to 1.166 μM/min) and Km from 66.93 to 203.710 μM^{-1} indicating non-competitive mixed inhibition with a Ki of 6.11 μM. The maximum inhibitory effect of memantine-loaded nanoscaffolds on AChE, BUChE, and β secretase in the brain was found to be 61.38%, 83.83%, and 75.43% respectively. The half maximally inhibitory concentration (IC_{50}) of memantine-loaded nanoscaffolds in brain acetylcholinesterase (AChE), butyrylcholinesterase (BUChE) and β secretase were 3.653±0.81 μM, 6.035±0.085μM, and 5.68±0.144 μM respectively. A higher inhibition was observed for butyrylcholinesterase and β secretase than acetylcholinesterase indicating probably towards retention of butyrylcholine, APP, and acetylcholine, in the brain that helps to preserve cognitive functions in the brain.

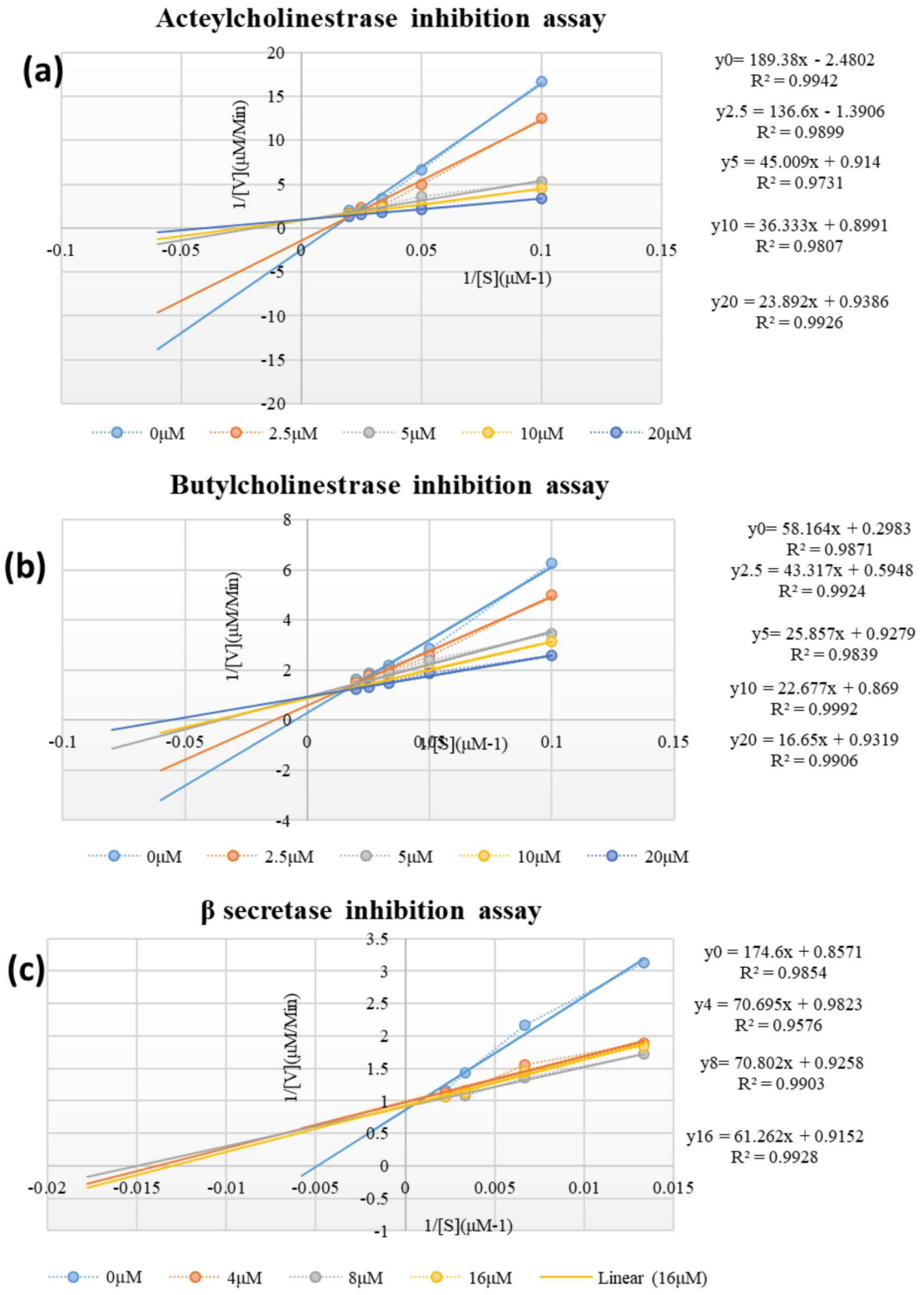

Figure 28: Lineweaver–Burk plots for (a) AChE, (b) BUChE and (c) β secretase inhibition over a range of substrate concentrations (10–50 µM) and (75-450 µm) from Brain homogenate samples in the presence of (0, 2.5, 5, 10, 20 µM) and (0, 4, 8, 16 µM) of memantine-loaded nanoscaffolds.

6.3.8.2 Enzyme Kinetic study against AChE, BChE and β secretase in Cortex and Hippocampus

The cholinesterase (AChE and BChE) enzyme kinetics was studied at increasing inhibitor concentrations of (PEG-MEM-PLGA) SANs at 0, 2.5, 5, and 10 μM and substrate concentrations of 10, 20, 30, 40 and 50 μM. The Lineweaver–Burk plot of AChE enzyme inhibition assay (Figure 29 (a)) showed a decrease in the Vmax value from 0.868 to 0.0425 μM/min, though the Km value remain unchanged at 47.261 μM, indicating non-competitive mode of inhibition with Ki value of 6.32 μM^{-1}.

The Lineweaver–Burk plot of for BUChE (Figure 29 (b)) showed a decrease in Vmax value from 0.192 to 0.0773 μM/min with an unchanged Km value of 51.40 μM^{-1} value indicating non-competitive inhibition with an increase in Ki value from 6.35 to 21.8 μM^{-1}.

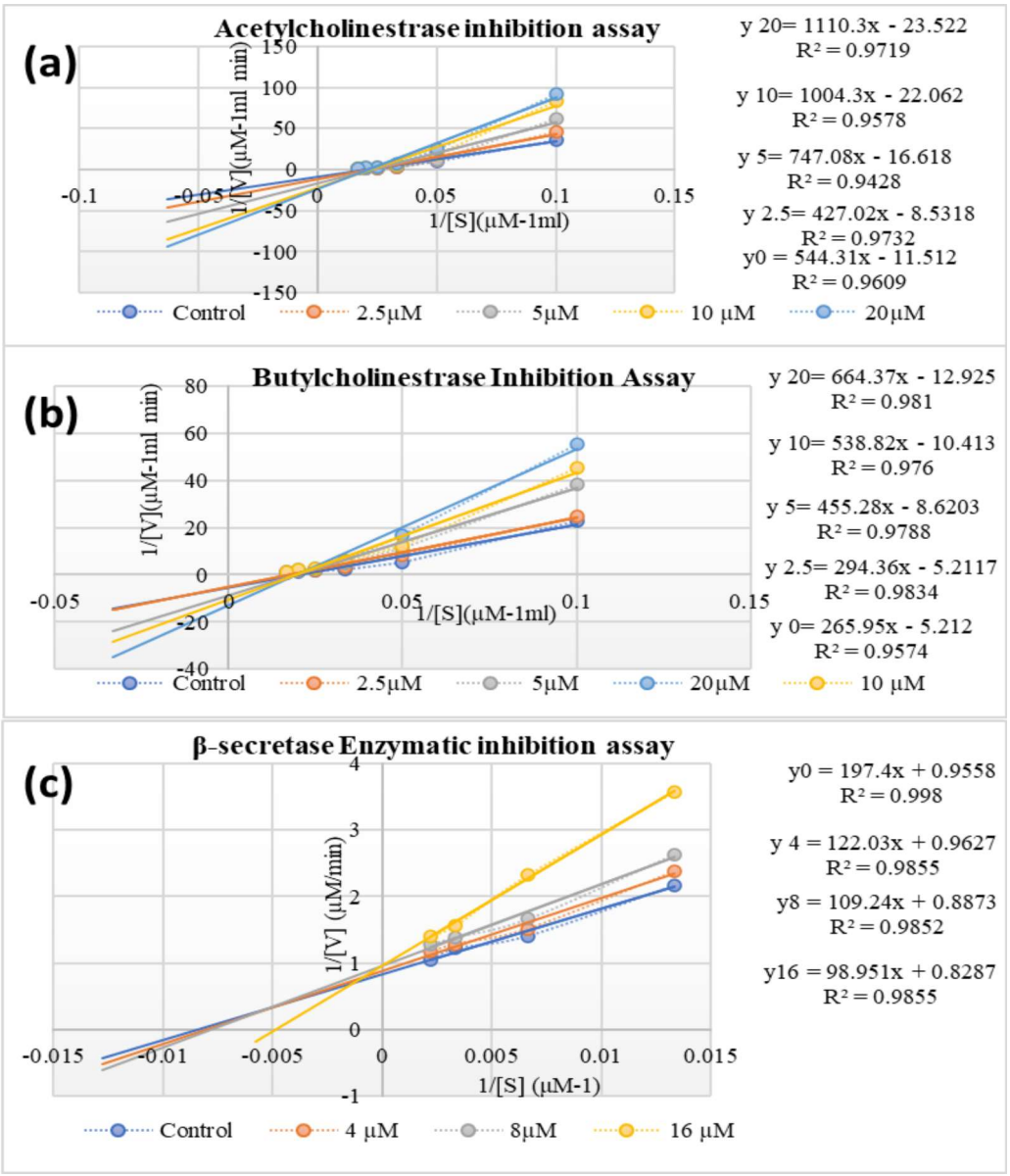

Figure 29: Lineweaver–Burk plots for (a) AChE, (b) BUChE and (c) β secretase inhibition over a range of substrate concentrations (10–50 µM) and (75-450 µm) from Brain homogenate samples in the presence of (0, 2.5, 5, 10, 20 µM) and (0, 4, 8, 16 µM) of memantine-loaded nanoscaffolds.

The enzyme kinetics of β-secretase was evaluated at increasing inhibitor concentrations of 0, 4, 8, and 16 µM, and substrate concentrations of 75, 150, 300, and 450 µM. The Lineweaver-Burk plot of (PEG-MEM-PLGA) SANs (Figure 29 (c)) showed increase in value of Vmax (1.046 to 1.206 µM/min) and Km from 2.0652 to 119.40 μM^{-1} indicating non-competitive mixed inhibition with increase in Ki value from 2.46 to 10.35µM.

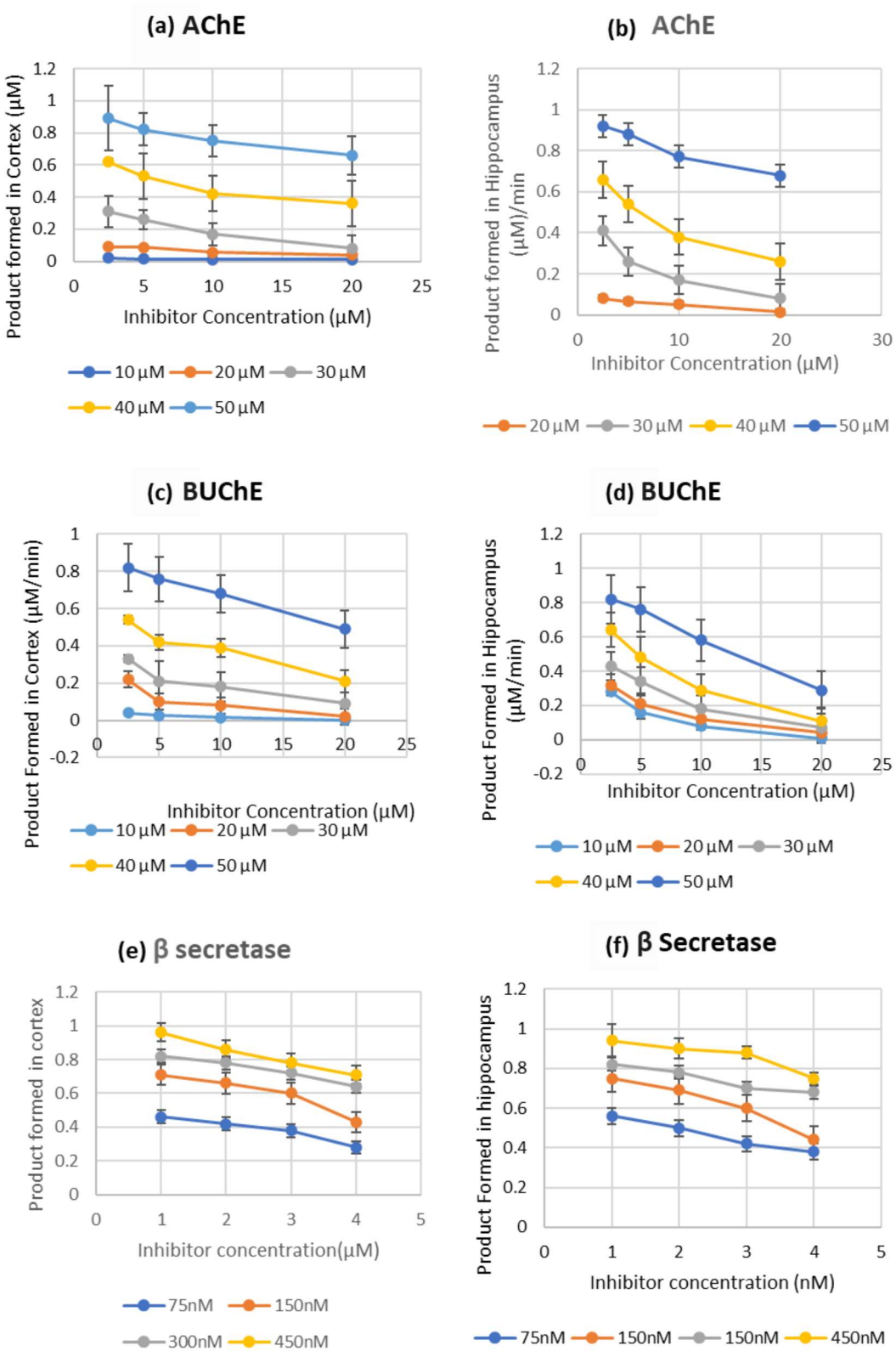

Figure 30: Effect of 0, 2.5, 5, 10, 20 µM (PEG-MEM-PLGA) SANs on AChE (fig. 8a and 8b) and BUChE (fig 6c and 6d). Fig 6e and 6f shows the effect of (PEG-MEM-PLGA) SANs on β secretase activity in mice cortex and hippocampus. Product formed was (Acetylcholine) upon 60 min of incubation.

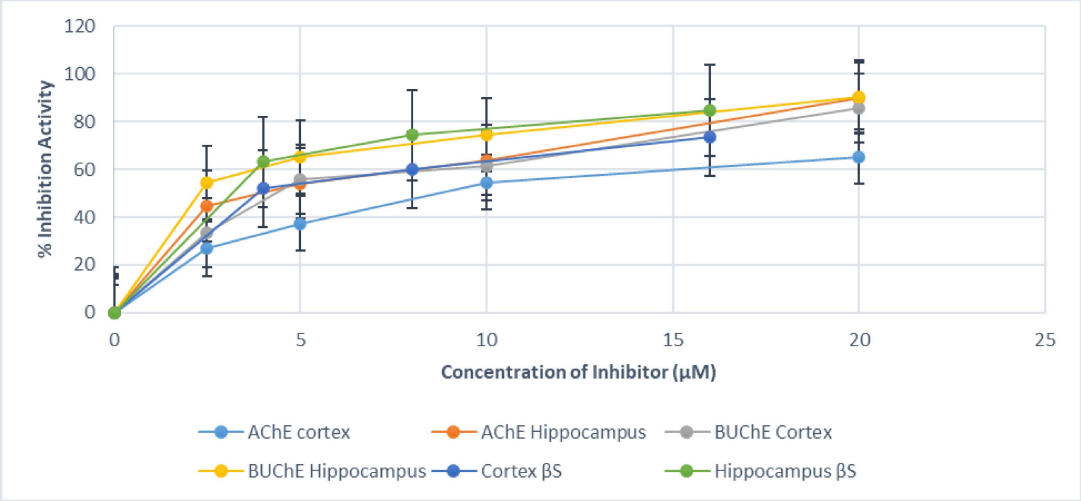

Figure 31: Inhibition activity of 0, 2.5, 5, 10, and 20 µM (PEG-MEM-PLGA) SANs on AChE, BUChE, and β secretase activity in mice cortex and hippocampus. Each value represents mean ± S.E.M. (n = 3). *p < 0.05.

Figure 30 (a-f) shows significant inhibition of AChE, BUChE and βsecretase activity by (PEG-MEM-PLGA) SANs in a dose-dependent manner after 60 min of incubation with the brain homogenate. Extent of inhibition of AChE, BUChE and β secretase was studied in terms on the basis of Acetylcholine produced at 60 min of incubation with varying range of inhibitor concentration of (PEG-MEM-PLGA) SANs as shown in figure 30 (a-f). The dose/effect association of AChE was determined with Pearson's coefficients as follows: $R^2 = 0.9127$ ($p < 0.001$) for cortex and $R^2 = 0.9139$ ($p < 0.001$) for hippocampus (Figure 30 (a-b)), while for BUChE $R^2 = 0.8952$ ($p < 0.001$) was observed for cortex and $R^2 = 0.9168$ ($p < 0.001$) for hippocampus (Figure 30 (c-d). The Pearson's coefficients of β secretase were R^2 0.8992 ($p < 0.001$) for cortex and $R^2 = 0.9198$ ($p < 0.001$) for hippocampus (Figure 30 (e-f)).

The inhibitory activity of AChE, BUChE and β secretase increased with a graded increase in inhibitor concentration (0, 2.5, 5, 10, 20 µM) (Figure 31). The maximum inhibitory effect of (PEG-MEM-PLGA) SANs on AChE, BUChE and β secretase for cortex homogenate was found to be 65.38 %, 85.83 % and 73.43 % respectively, whereas for Hippocampus it was 89.92%, 90.32% and 84.63% respectively. The half maximally inhibitory concentration (IC_{50}) of (PEG-MEM-PLGA) SANs for cortex and Hippocampus homogenate of acetylcholinesterase (AChE) was 8.653±0.81 µM and 6.64±0.73 µM respectively. The half maximally inhibitory concentration (IC_{50}) of (PEG-MEM-PLGA) SANs for cortex butyrylcholinesterase (BUChE) and Hippocampus BUChE were 4.15±0.15 µM and 3.035±0.085µM respectively (Table 9). The half maximally inhibitory concentration (IC_{50}) of (PEG-MEM-PLGA) SANs for cortex β secretase (βS) and Hippocampus βS were 3.68±0.144 µM and 2.90±0.10 µM respectively (Table 9). This study showed higher inhibition of hippocampus AChE, BUChE and β secretase

activity by (PEG-MEM-PLGA) SANs as compared to that of cortex region.

Table 9: Maximum inhibitory effect and IC_{50} value of (PEG-MEM-PLGA) SANs on AChE, BUChE and β secretase

Maximum inhibitory effect of (PEG-MEM-PLGA) SANs on AChE, BUChE and β secretase				
Enzymes	Brain cortex		Brain Hippocampus	
	Inhibitory effect (%)	IC_{50}	Inhibitory effect (%)	IC_{50}
AChE	65.38	8.653±0.81 µM	89.92	6.64±0.73 µM
BUChE	85.83	4.15±0.15 µM	90.32	3.035±0.085 µM
β secretase	73.43	3.68±0.144 µM	84.63	2.90 ±0.10 µM

6.3.9 Hemocompatibility study

The Hemocompatibility was determined to assess biocompatibility of nanocarriers. Different concentrations of MEMp, (MME-PLGA) SANs and (PEG-MEM-PLGA) SANs (2, 4, 6, 8, 10 and 12 mg/ml) were used. The percentage haemolysis increases with increase in concentration from 2 mg/ml to 12 mg/ml as shown by observed variation in intensity of red colour of blood in figure 32. (PEG-MEM-PLGA) SANs showed good hemocompatibility with 1.534 % haemolysis (low intensity red colour) as compared to pure Memantine drug (MEMp) and (MEM-PLGA) SANs indicating no rupture of RBC cells up to 12 mg/mL of (PEG-MEM-PLGA) SANs (Figure 32). According to ISO/TR 7406, the critical safe haemolytic ratio should be less than 5%, which indicates high compatibility whereas within 10% is compatible and, >20% is non-compatible with blood. As can be observed from figure 22, (PEG-MEM-PLGA) SANs at all tested concentrations exhibited insignificant haemolysis as compared to MEMp and (MEM-PLGA) SANs. Memantine-loaded PLGA self-assembled nanoscaffolds show higher hemocompatibility (7.187 % at 12 mg/ml) as compared to pure memantine drug (9.26 % at 12 mg/ml). PEG coated PLGA nanoscaffolds (PEG-MEM-PLGA) SANs were the most hemocompatible due the stealth characteristic provided by addition PEG to the PLGA nanoscaffolds. PEG hydrates the phospholipid membranes and stabilizes the RBC membrane and also minimizes surface interaction of the nanoscaffolds with opsonin, preventing macrophage uptake and clearance from the body [263,264].

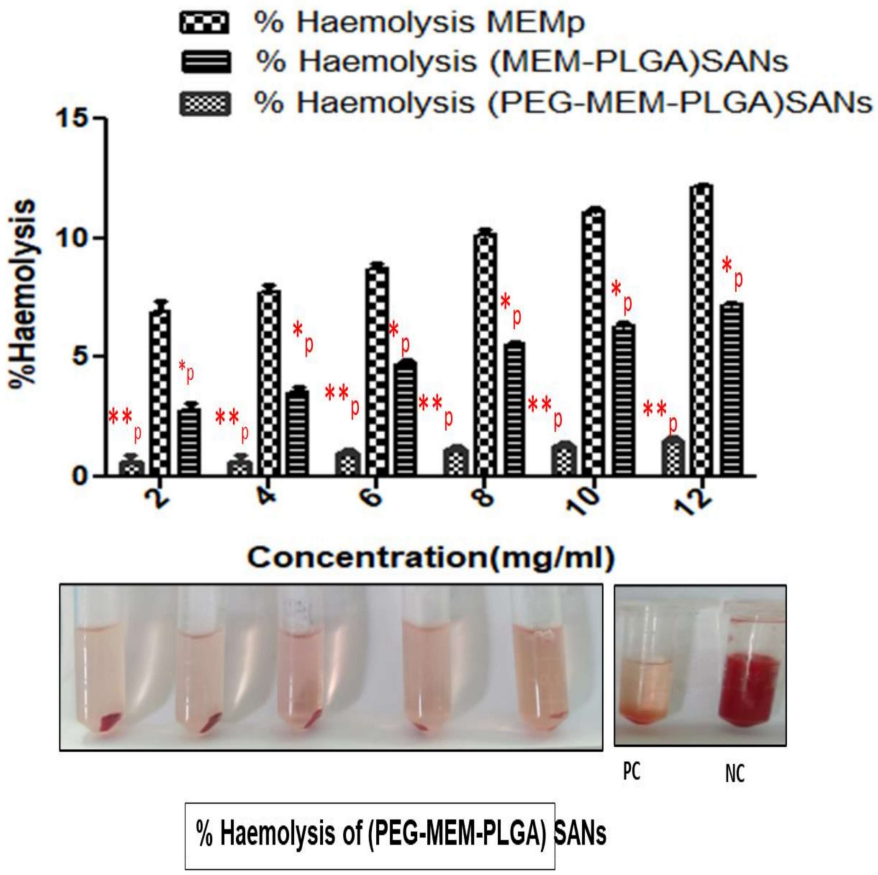

Figure 32: Hemocompatibility assay of 0, 2, 4, 6, 8, 10 and 12 mg/ml (PEG-MEM-PLGA) SANs in mice blood. Each value represents mean ± S.E.M. (n = 3). *p < 0.05. 20µl blood was added to saline water for negative control (0% hemolysis), whereas 20µl blood was added to the Triton X-100(1%v/v) for positive control (100% hemolysis).

6.3.10 Neurobehavioral Effects

6.3.10.1 Y-Maze Test

Increase in spontaneous alternation in behaviour in the Y-maze is used to determine short-term memory retention in animal models of amnesia. Therapeutic effect of equivalent doses of 10 mg/kg MEMp tablets, (MEM-PLGA) SAN, (PEG-MEM-PLGA) SAN, (PEG-MEM-PLGA) SANs-BMSc and Admenta were evaluated in mice. The circulation time of PEG coated SANs was improved due to stealth property as a result of PEG coating which reduced mononuclear phagocyte uptake, enhancing drug delivery at the target site alongwith the neuroregeneration due to the presence of BMSc in (PEG-MEM-PLGA) SANs-BMSc thereby contributing to enhanced cognitive behaviour and explorative activity (90.11±1.94 %) of group III animals as compared to all groups Animals administered with (PEG-MEM-PLGA) SANs showed a significant increase in novel arm entries in comparison to Admenta, Memantine (standard) and (MEM-PLGA) SANs treated groups which displayed neophobic character; novel arm entries

and % spontaneous alteration in behaviour of mice have been illustrated in table 10.

The group treated with PLGA nanoscaffolds showed 44% alteration in behaviour on 1st day which increased up to 89% on the 6th day of Y-maze study. This indicates the potential of PLGA nanoscaffolds in improving neuronal activity and brain health (Figure 33 (a)). Morris water maze study of mice treated with memantine loaded PLGA nanoscaffolds showed a significant improvement in neurobehavioral activity (***p<0.0001) as indicated by decrease in the time required for finding platform by travelling less distance as compared to disease control group (Figure 33 (b)).

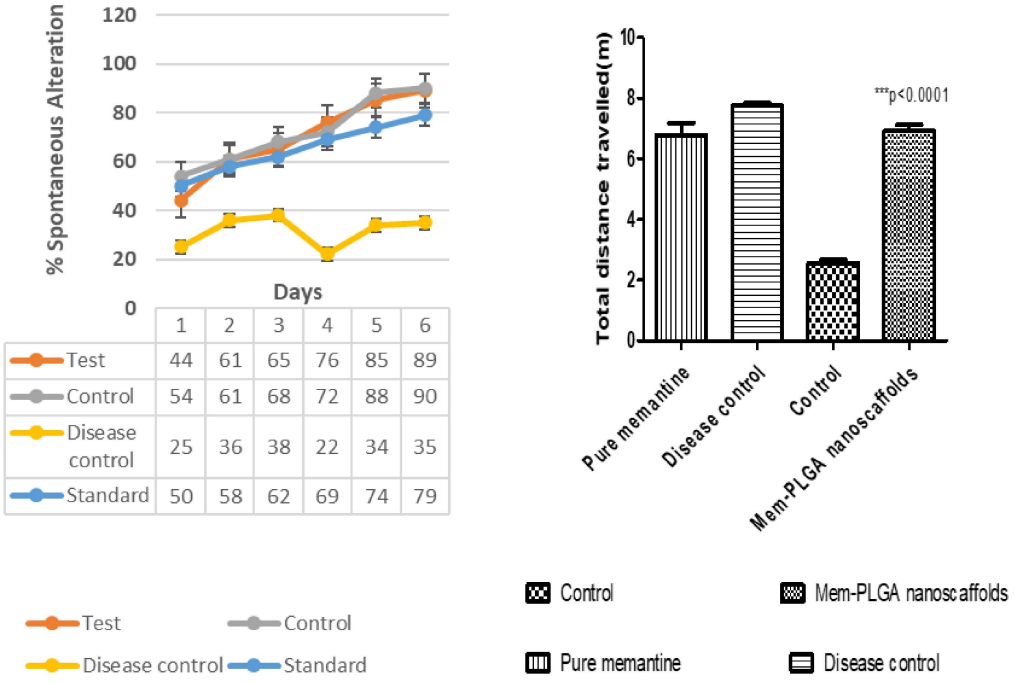

Figure 33: Neurobehavioral effect in Y-maze test on % spontaneous alteration and total distance travelled in morris water maze test.

Table 10: Animal groups showing % spontaneous alteration in behavior

Animal group	% Spontaneous Alteration	Indication
Group I- Normal Control	85.7± 2.83 %	Memory retention from the previous trial
Group II- (PEG-MEM-PLGA) SANs 10 mg/kg	77.2 ± 2.62%	Recovery of cognitive impairment
Group III- (PEG-MEM-PLGA) SANs- BMSc 10 mg/kg	90.11± 1.94 %	Enhanced cognitive behavior and display of high explorative activity
Group IV- Admenta 10 mg/kg	65.2 ± 2.26 %	Improved memory retention
Group V- Memantine standard (10 mg)	73 ± 0.31%	cognitive Recovery
Group VI- (MEM-PLGA) SANs	72.4 ± 0.49%	cognitive Recovery
Group VII- Disease control	33.3 ± 2.84 %	Cognitive impairment

Data was analysed using one-way ANOVA and post-hoc comparison tests were performed

using turkey's test which showed significant effect in cognitive enhancement among (PEG-MEM-PLGA) SANs and (PEG-MEM-PLGA) SANs-BMSc tre ated groups showing ***p <0.001, and **p <0.01 for Memantine (Standard) as compared to untreated diseased animal group (Group VII) (Figure 34 (b)). Other parameters of Y-maze such as total distance travelled, average speed and path efficiency observed during travelling of mice from one arm to the other were also determined by Any-Maze software and have been mentioned in table 11. Total distance travelled and time spent in Arm A, B and C were plotted as shown in Figure 34 (a). Maximum time was spent in Arm C by all the groups then arm B followed by arm A. Group I, II, III, IV, V and VI showed greater mobility as indicated by higher distance covered.

To understand the degree of impairment and to investigate therapeutic options scientists need tools, such as behavioral tests. the Morris maze assay detects AD-related impairment and hippocampal dysfunction in mice and humans. Morris water maze (MWM) studies include visible-target training, hidden-target learning, and probe trials. Search-to-platform area determines the degree of reliance on spatial versus non-spatial strategies and cued trials determine whether performance factors that are unrelated to place learning are present. Escape from water is relatively immune from activity or body mass differences, making it ideal for many experimental models. Therefore, MWM is proven to be a robust and reliable test that is strongly correlated with hippocampal synaptic plasticity and NMDA receptor function. Also, MWM performance has been linked to long-term potentiation (LTP) along with NMDA receptor function, making it a key technique in the investigation of hippocampal circuitry. In addition, it has shown that there is involvement of the entorhinal and perirhinal cortices, as well as involvement of the prefrontal cortex, the cingulate cortex, the neostriatum, and perhaps even the cerebellum to some extent [265].

However, Y Maze Spontaneous Alternation is a behavioral test for measuring the willingness of mice to explore new environments. Mice typically prefer to investigate a new arm of the maze rather than returning to one that was previously visited. The spontaneous alternation y-maze provides researchers with data on memory as well as exploratory activity of animals in a short time frame. Furthermore, the standard y-maze is flexible and can be adapted to measure spatial and object recognition, as well as novelty exploration using the y-maze. In this protocol, we described how the spontaneous alternation y-maze can be used to assess short-term spatial working memory. Also, the spontaneous y-maze measures spatial recognition memory at a rudimentary level using the natural exploratory behavior of animal model [266].

The contextual and cued fear conditioning test is one of the behavioral tests that assesses the ability of mice to learn and remember association between environmental cues and aversive experiences. In this test, mice are placed into a conditioning chamber and are given parings of a conditioned stimulus (an auditory cue) and an aversive unconditioned stimulus (an electric footshock). As such, translational research using appropriate and validated animal models and tests for olfactory memory may advance better diagnosis and treatment for neurodegenerative disorders. However, aversively established contextual fear memory manifests itself in robust freezing behavior, often lasting several weeks or months. Therefore, this approach is amenable to investigate the underlying neural circuitries by lesion or inactivation of specific brain regions or to test efficacy of substances that disrupt either the ability to acquire the association or to retrieve memories [267]. In contrast, investigation of memory enhancement using this technique is time intensive since the non-treated control group naturally forgets the learned association only weeks after acquisition. Pharmacological interventions have been used to overcome this time span by disrupting memory at any time point, however, limiting it a mechanistic model of reversal of impairments instead of studying memory enhancement.

In addition, the social transmission of food preference (STFP) test is used in animals to evaluate the innate ability to learn about food safety from their conspecifics. Underlying select-reject decision, processes involve assessment of the sensory characteristics of the food and an animal must be able to review and ingrate different features (i.e., taste and odor) [268]. Analyzing necessary conditions resulting in this preference, showed that direct subject – demonstrator exposure (eaten or dusted with a food) is enough to boost the observer's preference. However, purely smelling nor eating a food are not sufficient to induce this type of preference. Therefore, in this study MWM study and Y-maze studies were preferred to explore hippocampus circuit function, NMDA receptor function, long term potentiation, short-term spatial working memory and spatial recognition memory in natural condition without any aversive circumstances.

Table 11: Y-maze parameters analysis by using Any-Maze software

Parameter Studied	Group I	Group II	Group III	Group IV	Group V	Group VI	Group VII
Total distance travelled (m)	31.2±0.002	15.297±0.003	23.356±0.012	22.23±0.142	18.5±0.023	22.235±0.03	12.64±0.11
Average speed (m/s)	0.347±0.021	0.477±0.02	0.26±0.002	0.247±0.003	0.206±0.112	0.247± 0.013	0.14±0.04
Path efficiency	0.016±0.065	0.071±0.012	0.024±0.001	0.024±0.002	0.014±0.03	0.024±0.001	0.052±0.002
Time in the Starting Arm C zone (s)	58.2±0.012	26.2±0.112	29.6±0.33	65.7±0.01	71.6±0.02	65.7±0.04	81.4±0.22
Average speed (m/s)	0.364±0.204	0.505±0.003	0.253±0.04	0.266±0.131	0.191±0.01	0.266±0.02	0.133±0.01
Distance travelled (m)	21.2±0.5	13.2±0.03	17.628±0.121	17.48±0.231	13.7±0.03	1.52±0.11	10.8±0.02
Longest visit to the Starting Arm C zone (s)	11.7±0.44	18.8±0.02	18.1±0.03	39.9±0.55	40.9±0.23	1.7±0.054	41.9±0.12
Time in the Arm B zone (s)	13.3±0.02	1.7±0.01	8.2±0.32	3.8±0.12	1.3 ±0.01	3.8±0.01	4±0.22
Latency to first entry to the Arm B zone (s)	6.5± 0.14	10.5± 0.22	12.3±0.02	61.3±0.02	59.6±0.02	61.3±0.33	35.2±0.11
Average speed (m/s)	0.43±0.02	0.807±0.23	0.318±0.11	0.502±0.210	0.338±0.01	0.502±0.33	0.164±0.01
Distance travelled (m)	5.73±0.03	1.411±0.12	2.597±0.054	1.885±0.004	0.34±0.001	1.348±0.02	0.652±0.34
Longest visit to the Arm B zone (s)	7.9±0.04	1.7±0.02	3.3±0.03	1.6±0.05	1.3±0.04	1 7.2±0.23	4±0.02
Average duration of visit to the Arm B zone (s)	1.9±0.01	1.7±0.02	2±0.04	1.3±0.05	1.3±0.001	1.3±0.403	4±0.002
Path efficiency to first entry to the Arm B zone	0.528±0.002	0.121±0.012	0.483±0.03	0.069±0.002	0.087±0.003	0.069±0.112	0.123±0.001
Latency to first entry to the Arm A zone (s)	6.5 ±0.02	5.1±0.01	17.2±0.001	39.9±0.003	40.9±0.001	62.9±0.22	45±0.33
Average duration of visit to the Arm A zone (s)	2.7±0.04	2.1±0.02	3±0.043	0.7±0.004	3.2±0.343	0.7±0.012	3.1±0.003
Path efficiency to first entry to the Arm A zone	0.291±0.02	0.414±0.02	0.169±0.004	0.274±0.01	0.914±003	0.274±0.01	0.128±0.003
Average speed (m/s)	0.23±0.06	0.163 ±0.03	0.25±0.004	0.718±0.006	0.197±0.015	0.718±0.003	0.273±0.02
Distance travelled (m)	3.71±0.003	0.675±0.012	3.004±0.002	1.52±0.004	3.14±0.005	1.52±0.002	0.857±0.012
Longest visit to the Arm A (s)	6.1±0.014	3.2±0.011	6.2±0.012	1.7±0.002	12.1±0.001	1.7±0.002	3.1±0.023
Path efficiency to first entry to the center position zone	0.345±0.005	0.643±0.001	0.089±0.003	0.067±0.002	1.105±0.023	0.067±0.001	0.258±0.013
Latency to first entry to the centre position zone (s)	16.9±0.001	7.3±0.002	30.1±0.004	62.9±0.012	42.8±0.123	62.9±3.3	20.3±0.22
Average speed (m/s)	0.234±0.34	0.622±0.004	0.7±0.02	6.1±0.003	1.105±0.1	0.073±0.001	0.229±0.34
Distance travelled (m)	0.539±0.02	1.819±0.004	0.127±0.132	1.348±0.004	1.269±0.002	1.348±0.01	0.331±0.002
Longest visit to the center zone (s)	1.9±0.003	0.5±0.001	0.1±0.002	17.2±0.004	0.8±0.05	17.2±0.02	1.4±0.002

* All data represented in form of mean ±SD (n=3)

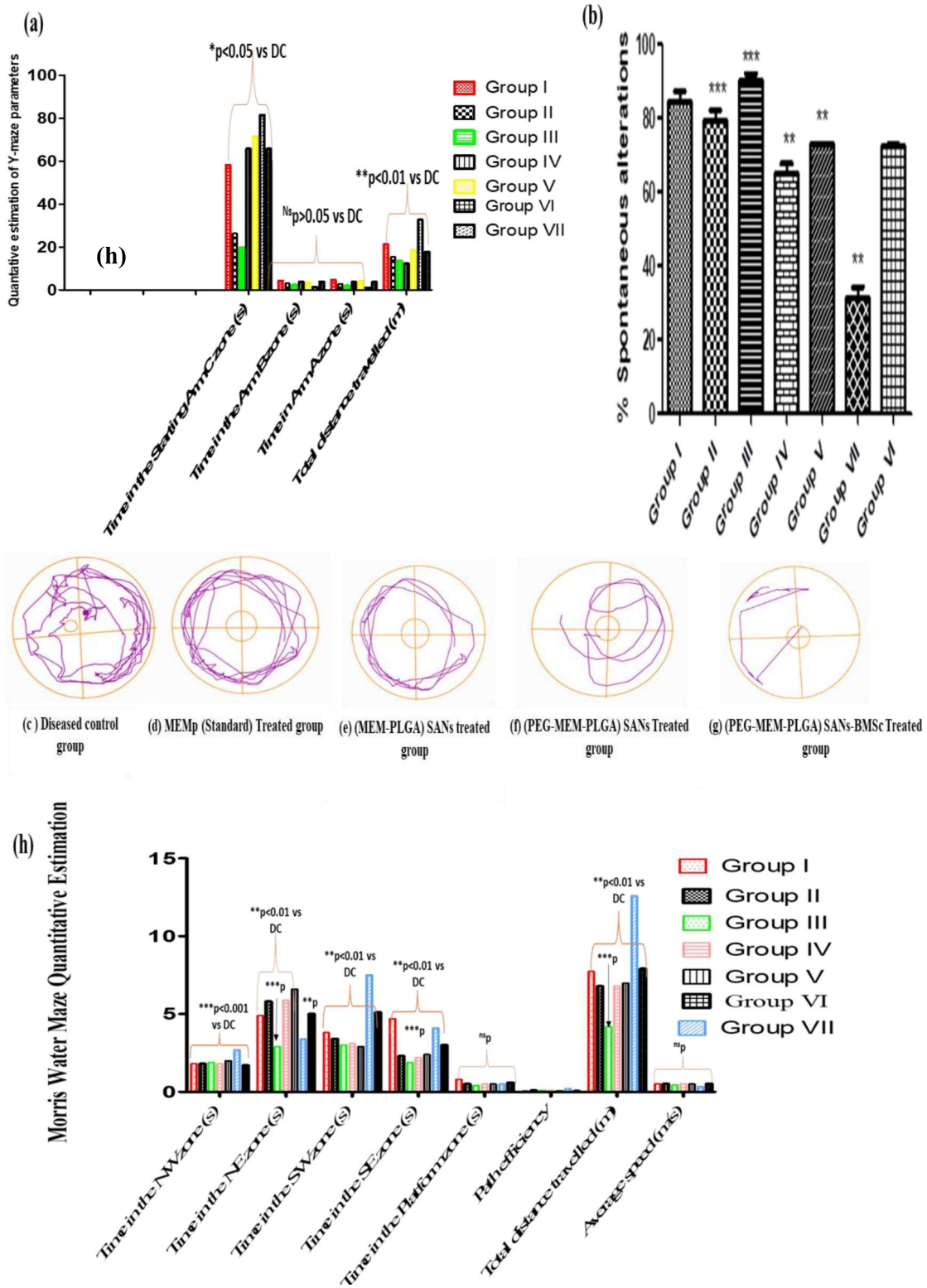

Figure 34: (a) Y-maze parameter analysis of Time spent in Arm C, B, A and total distance travelled; and (b) Spontaneous alteration in behavior by animal groups; each value represents mean ± S.E.M. (n = 3). *p < 0.05; (c-g) trajectories covered by (c) diseased control (DC), (d) MEMp (Standard), (e) (MEM-PLGA)SANs, (f) (PEG-MEM-PLGA)SANs and (g) (PEG-MEM-PLGA)SANs-BMSc treated group; (h) Morris water maze analysis of

time spent in quadrants NW, NE, SW, SE and platform, total distance travelled, average speed, path efficiency.

6.3.10.2 Morris Water Maze Test

The Morris Water Maze is widely used for spatial learning studies in the animals by evaluating performance measures of animals in the Morris Water Maze: escape latency, time spent in quadrants, average speed, and time taken to reach the platform by using Any-Maze software as shown in table 12.

Table 12: Morris water maze (MWM) test parameters analysis by using Any-Maze software

Parameter Studied	Group I	Group II	Group III	Group IV	Group V	Group VI	Group VII
Total distance travelled (m)	7.73±0.01	6.782±0.4	4.198±0.05	6.81±0.002	6.991±0.03	7.918±0.002	2.592±0.001
Average speed (m/s)	0.509±0.043	0.509±0.054	0.431±0.001	0.521±0.002	0.504±0.004	0.535±0.01	0.339±0.013
Path efficiency	0.052±0.04	0.081±0.001	0.097±0.002	0.082±0.01	0.077±0.004	0.051±0.002	0.21±0.02
Number of entries to the NW zone	3±0.001	3±0.24	2±0.004	3±0.005	3±0.014	3±0.012	1±0.002
Time in the NW zone (s)	1.8±0.004	1.8±0.02	1.9±0.001	1.8±0.002	2±0.001	1.7±0.003	0.7±0.01
Distance travelled in the NW zone (m)	1.713±0.023	1.74±0.013	0.828±0.003	1.717±0.001	1.62±0.002	1.574±0.004	0.313±0.012
Latency to first entry to the NW zone (s)	3.6±0.03	2.1±0.001	0	2±0.003	2.9±0.001	3.4±0.12	1.5±0.11
Average speed in the NW zone (m/s)	0.973±0.004	0.958±0.005	0.427±0.003	0.938±0.001	0.814±0.002	0.908±0.014	0.458±0.015
Longest visit to the NW zone (s)	0.7±0.06	0.7±0.012	1.3±0.003	0.7±0.001	0.8±0.002	0.7±0.01	0.7±0.01
Average duration of visit to the NW zone (s)	0.6±0.004	0.6±0.002	1±0.01	0.6±0.002	0.7±0.14	0.6±0.02	0.7±0.002
Path efficiency to first entry to the NW zone	0.334±0.11	0.928±0.056	0.894±0.04	0.927±0.023	0.83±0.001	0.333±0.004	0.988±0.002
Number of entries to the NE zone	4±0.02	4±0.002	2±0.004	4±0.001	4±0.012	4±0.001	2±0.002
Time in the NE zone (s)	4.9±0.03	5.8±0.002	2.9±0.001	5.9±0.003	6.6±0.004	5.0±0.001	3.4±0.005
Distance travelled in the NE zone (m)	2.731±0.2	2.123±0.06	1.251±0.004	2.397±0.001	2.516±0.113	2.811±0.006	1.08±0.014
Latency to first entry to the NE zone (s)	2.6±0.114	0	2.4±0.113	0	0	2.4±0.431	0
Average speed in the NE zone (m/s)	0.552±0.007	0.363±0.004	0.432±0.006	0.405±0.002	0.382±0.002	0.567±0.001	0.321±0.012
Longest visit to the NE zone (s)	1.9±0.13	2.1±0.032	1.8±0.002	2±0.004	2.9±0.006	1.8±0.001	1.9±0.01
Average duration of visit to the NE zone (s)	1.2±0.011	1.5±0.113	1.4±0.01	1.5±0.002	1.6±0.002	1.2±0.004	1.7±0.001
Path efficiency to first entry to the NE zone	0.679±0.001	0.414±0.004	0.043±0.004	0.312±0.003	0.238±0.01	0.663±0.06	0.142±0.04
Number of entries to the SW zone	3±0.014	3±0.005	2±0.006	3±0.001	3±0.001	4±0.002	1±0.002
Time in the SW zone (s)	3.8±0.01	3.4±0.002	3±0.003	3.1±0.04	2.9±0.034	5.1±0.65	2.5±0.134
Distance travelled in the SW zone (m)	1.174±0.09	1.153±0.04	0.758±0.002	1.154±0.002	1.068±0.01	1.370±0.05	0.549±0.112

Parameter Studied	Group I	Group II	Group III	Group IV	Group V	Group VI	Group VII
Latency to first entry to the SW zone (s)	4.3±0.01	2.7±0.004	1.3±0.002	2.7±0.02	3.6±0.004	00	5.1±0.02
Average speed in the SW zone (m/s)	0.31±0.04	0.344±0.001	0.256±0.04	0.372±0.003	0.368±0.12	0.266±0.11	0.217±0.45
Longest visit to the SW zone (s)	3±0.002	2.6±0.002	2.6±0.001	2.4±0.05	2.3±0.64	2.8±0.002	2.5±0.004
Average duration of visit to the SW zone (s)	1.3±0.001	1.1±0.004	1.5±0.132	1±0.007	1±0.006	1.3±0.003	2.5±0.002
Path efficiency to first entry to the SW zone	0.005±0.002	0.48±0.002	0.914±0.001	0.478±0.132	0.403±0.144	0.326±0.544	0.229±0.123
Number of entries to the SE zone	4±0.111	3±0.332	4±0.001	3±0.002	3±0.123	4±0.112	1±0.121
Time in the SE zone (s)	4.7±0.001	2.3±0.132	1.9±0.112	2.2±0.104	2.4±0.03	3±0.003	1.1±0.112
Distance travelled in the SE zone (m)	2.112±0.004	1.765±0.002	1.361±0.01	1.542±0.03	1.787±0.121	2.164±0.113	0.651±0.113
Latency to first entry to the SE zone (s)	0	3.2±1.345	1.6±0.001	3.2±0.234	3.9±0.343	1.5±0.003	4±0.455
Average speed in the SE zone (m/s)	0.45±0.001	0.763±0.321	0.704±0.112	0.697±0.002	0.745±0.01	0.729±0.002	0.603±0.303
Longest visit to the SE zone (s)	2.6±0.01	1.1±0.233	1.1±0.001	1.1±0.113	1.1±0.443	1.1±0.123	1.1±0.234
Average duration of visit to the SE zone (s)	1.2±0.001	0.8±0.01	1±0.02	0.7±0.004	0.8±0.007	0.7±0.001	1.1±0.02
Path efficiency to first entry to the SE zone	0.125±0.01	0.233±0.02	0.518±0.002	0.233±0.045	0.153±0.02	0.926±0.001	0.284±0.001
Number of entries to the Platform zone	1±0.1	1±0.001	1±0.002	1±0.03	1±0.002	1±0.02	1±0.002
Time in the Platform zone (s)	0.8±0.002	0.5±0.001	0.4±0.113	0.5±0.103	0.5±0.112	0.6±0.001	0.5±0.002
Average duration of visit to the Platform zone (s)	0.8±0.003	0.5±0.001	0.4±0.011	0.5±0.006	0.5±0.0123	0.6±0.112	0.5±0.004xe4

*All data has been represented as mean ±SD (n=3)

Morris water maze test revealed a significant effect of Memantine loaded nanocarriers, the obtained result like time spent, distance travelled, average speed and path efficiency in Northwest, Northeast, Southwest, Southeast and platforms zones were statistically analysed by two-way ANOVA (Bonferreni test) and bar graph were plotted as shown in figure 34 (h). The animal group I (4.272, **p< 0.01), group II (3.484, *p< 0.05), group III (3.658, **p< 0.01), group IV (3.507, *p< 0.05) and group V (3.076, *p< 0.05) showed significant effect in comparison with group VII (disease control) ((t value and p value for each group have been mentioned in bracket), and obtained F value and p-value for the experiment was 4.171 and 0.0043 (**p<0.05)). This analysis indicates that groups II and III exhibited higher escape latency patterns (the time for the animal to find the platform and escape the maze) representative of improved cognitive behaviour. Group III animals treated with (PEG-MEM-PLGA) SANs-BMSc showed good memory retention in the morris-maze study by reaching the platform in short span of time which indicates the potential of self-assembled nanoscaffolds in the recovery and regeneration of nerve cells.

6.4 Pharmacokinetic and Biodistribution study

6.4.1 HPLC Study

High performance Liquid chromatography is used as an important analytical tool for the quantification and characterization of drugs in serum and plasma. In the present study, the analysis was carried out in serum at 240 nm at column temperature of 25±2 °C, using sample injection volume of 20 µL, maintaining isocratic flow rate of 1.0 mL.min-1, and a run time of 5 minutes for detection of memantine as active ingredient in nanoscaffolds via HPLC coupled with UV-Visible detector (Shimadzu, Columbia, MD, USA). The mobile phase, composed by Acetonitrile: water 85:15 (v/v) provided a symmetric peak for memantine with low retention time. The peak was detected at 2.3 min (Figure 36), which can very suitable for routine analyses. A linear relationship between the peak area and the memantine concentration from 5 to 1000 μg/mL was observed (Figure 37 (a)) with the linear equation: y= 1478.4x+ 91456 with regression coefficient of 0.9964, where y is the peak area and x is concentration at μg/mL.

Pure Memantine drug elutes at 2.372 min and that from memantine-loaded nanoscaffolds elutes at 2.27 min in serum as shown in figure 36 (a) and figure 36 (b) respectively. T A minor shift in retention time is generally due changes in the tissue matrix (serum, brain, liver and kidney). The drug was observed at 2.300 min and 2.325 min respectively in memantine drug and memantine-loaded nanoscaffolds in brain tissue homogenates is (Figure 36 (c) and 36 (d)). In order to understand the biodistribution pattern of Memantine, memantine in liver and kidney

tissue homogenates was also estimated which was respectively obtained at 2.308 min and 2.317 min (Figure 36 (e) and 36 (f)).

The oral administration of memantine hydrochloride tablets (Admenta) undergoes metabolism, with the majority (57-82%) of an administered dose excreted unchanged in the urine; the remainder is converted primarily to three polar metabolites: the N-gludantan conjugate at 1.82 min, 6-hydroxy memantine at 2.4 min, and 1-nitroso-deaminated memantine at 2.52 min and memantine at 2.28 min as illustrated in figure 35 [269,270]. The intrathecal administration of (PEG-MEM-PLGA)SANs showed single of peak memantine in plasma which represents the absence of metabolites in plasma (Figure 36 (b)). This indicates that intrathecal administration prevents the metabolism of memantine and hence improves the bioavailability of memantine in systemic circulation.

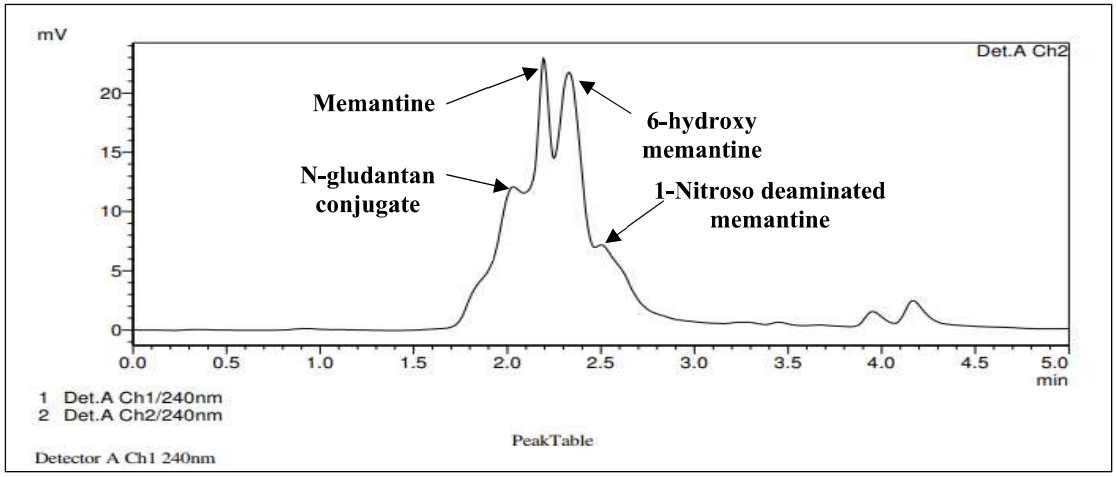

Figure 35: Chromatogram of Memantine hydrochloride tablet (Admenta).

Memantine was not administered intravenously because of its serious adverse effects. According to the published reports, when Memantine hydrochloride was intravenously administered in doses of 0.01, 0.1 and 1 mg/kg over 10 min, providing subtherapeutic, clinically-relevant and supratherapeutic concentrations, respectively, with increase in dose from low to high there is increase in the mean blood pressure and left ventricular contraction and enhanced the atrioventricular nodal conduction, resulting in increase of sympathectomy output from the central nervous system [271]. However, some reported studies show that memantine may not induce repolarization delay (prolonged Q-T interval and abnormal U waves in electrocardiogram) indicating lack of risk for inducing torsade de pointes cardiac arrest but in combination with other drug like donepezil it can cause QT prolongation and arrythmias [272]. However, some research studies have shown prolongation administration of memantine

intravenously may cause prolonged QT and excessive QT prolongation carries a risk of sudden cardiac death due to polymorphic tachycardia, also known as Torse de Pointes. Torsades de Pointes is a type of polymorphic ventricular tachycardia characterized by a gradual change in amplitude and twisting of the QRS complexes around an isoelectric line on the electrocardiogram [273]. Because of these reasons, memantine was not used for intravenous administration.

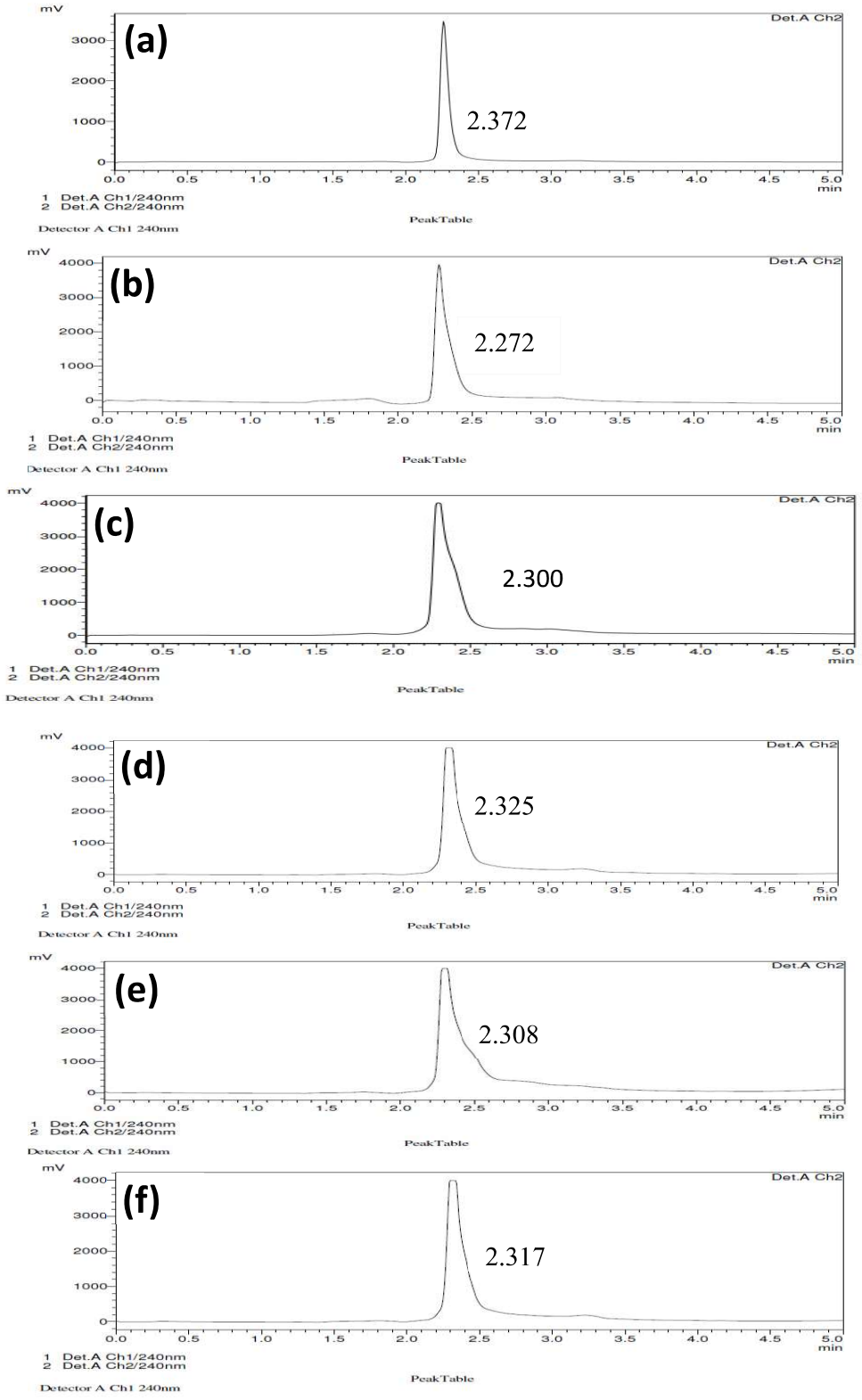

Figure 36: Reverse Phase-High Performance Liquid Chromatography (RP HPLC) Chromatogram of memantine on administration of (a) pure memantine drug (in serum) (b) PEGylated memantine loaded PLGA nanoscaffolds *(*in serum) (c) memantine drug (in brain tissue homogenates) (d) PEGylated memantine loaded PLGA nanoscaffolds *(*in brain tissue homogenates) (e) memantine loaded nanoscaffolds (in liver tissue homogenates) (f) memantine loaded nanoscaffolds (in kidney tissue homogenates).

6.4.1.1 Pharmacokinetic studies

This study was used to evaluate the improvement in the bioavailability of memantine alongwith control delivery of the same. The pharmacokinetic parameters were calculated by non-compartmental analysis using Kinetica 2000 software. The pharmacokinetic parameters, AUCtotal, tmax, Cmax, MRT, Ke, C_L, V_D, and $t_{1/2}$ were calculated for (PEG-MEM-PLGA) SANs and compared with (MEM-PLGA)SANs, MEMp, and Admenta. The chromatogram of blank (plasma) and standard memantine obtained using HPLC have been illustrated in table 13.

Table 13: Pharmacokinetic Parameters of (PEG-MEM-PLGA) SANs, MEM-PLGA) SANs, MEMp, and Admenta

Pharmacokinetic Parameters	(PEG-MEM-PLGA)SANs	(MEM-PLGA)SANs	MEMp	Admenta
Cmax (ug/ml)	9.5336±0.132	6.7861±0.211	6.38244±1.22	6.3529±0.54
Tmax (h)	35±1.2	24±0.914	8±1.1	12±1.2
V_d (L/kg)	12.12±6.76	7.17±4.55	2.05±5.22	8.81±4.11
Clearance(ml/min)	0.250±0.54	0.72165±0.33	2.9088±0.56	0.94995±0.37
AUCtotal(ug/uL*h)	0.85922±0.12	0.63095±0.101	0.057297±0.041	0.1366±0.011
Ke(1/h)	0.00743±0.001	0.05699±0.002	0.0290±0.001	0.04423±0.001
t1/2 (h)	56.16±1.42	41.34±1.32	20.61±2.01	30.56±1.91
MRT(h)	39.200±2.22	28.0493±3.32	12.46±4.11	17.31±1.21
R^2	0.924665±0.11	0.5024±0.032	0.7973±0.44	0.836835±0.32

The plasma calibration curve of memantine was prepared in the range of 1–1000µg/ml, as shown in figure 37 (a). The retention time of memantine in plasma and brain tissue homogenates was obtained at 2.273 min and 2.300 min with peak area of 48378707 and 47243457 respectively However, the retention time of memantine drug eluted from Pegylated memantine loaded PLGA nanoscaffolds in brain tissue homogenates, liver tissue homogenates and in kidney tissue homogenates is 2.325 min, 2.308 min and 2.317 min with peak area of 559648, 685576 and 242645 respectively. Various pharmacokinetics parameters such as C_{max}, T_{max}, AUC(total), K_{el}, $T_{1/2}$, Vd, and Cl were calculated using plasma concentration versus time profile have been shown in table 13. The obtained mean residence time (MRT) of (PEG-MEM-PLGA)SANs (39.2 h) is higher than (MEM-PLGA)SANs (28.04 h), MEMp (12.46 h) and marketed memantine tablet (Admenta) (17.31 h). Eventually, clearance and elimination rate constant of the (PEG-MEM-PLGA) SANs is lower than (MEM-PLGA) SANs, MEMp and Admenta which shows the presence of drug in the body for a longer period. Volume of distribution of (PEG-MEM-PLGA) SANs (12.12±6.76 L/kg) was higher as compared to (MEM-PLGA) SANs, MEMp and Admenta which indicates higher distribution of drug in

extravascular compartments of the body. Whereas MEMp and Admenta showed low Vd which has a propensity to remain in the plasma and not being distributed to other body parts [274]. Cmax and AUC (total) of drug for (PEG-MEM-PLGA)SANs were found to be significantly higher (9.53 μg/ml and 0.659 μg/ml*h, ***$p < 0.001$) than the (MEM-PLGA)SANs (6.78 μg/ml and 0.23 μg/ml*h), MEMp (6.38 μg/ml and 0.057 μg/ml*h) and Admenta (6.35 μg/ml and 0.136 μg/ml*h), which indicates prolonged and sustained-release effect. The relative bioavailability of (PEG-MEM-PLGA) SANs was found to be 2.26 and that of (MEM-PLGA) SANs was 1.69 as compared to Admenta. The improved bioavailability could be attributed to site specific delivery by intrathecal route of administration, and surface functionalization with PEG [275]. Upon oral administration, Cmax and tmax are dependent on the extent, and the rate of drug absorption and the disposition profile of the drug. Cmax of MEMp, (MEM-PLGA) SANs and Admenta comes nearly similar because equivalent dose of these formulation has been used and all the route involve absorption across the biological membrane However, (PEG-PLGA-MEM)SANs showed higher Cmax as compared to MEMp, Admenta and (MEM-PLGA)SANs due to higher rate of absorption and penetration across blood brain barrier.

In pharmacokinetic studies the half-life of memantine (MEMp) was 20 h which is significantly higher as compared to previous reports. Half-life is the time required for the concentration of a drug in blood or plasma to reduce to half of its initial value. This outcome is due to greater volume of distribution and less elimination or clearance of drug because Half-life is dependent on both clearance and volume of distribution. An increased volume of distribution will prolong the half-life and lead to a longer dosage interval [276]. Plasma profile of memantine showed an initial rapid decline, followed by a slower decline at later time points. The first phase or rapid decline is assumed to be primarily due to distribution, while the later phase of decline is slower and assumed to be primarily due to elimination [277]. Herein, an optimized fabrication approach has been used for the preparation of (PEG-MEM-PLGA)SANs loaded with memantine for Intrathecal administration for improving the residence time and other pharmacokinetic property of memantine. $T_{1/2}$ of (PEG-MEM-PLGA) SANs found higher due to release of encapsulated drug from the polymeric matrix of PLGA in controlled manner within body. Also, surface modification of PLGA nanoscaffolds with PEG can further enhance nanocarriers long-circulating properties which is responsible for increase in $T_{1/2}$ value of (PEG-MEM-PLGA) SANs. These nanocarriers contributed to increased blood residence time of memantine fulfilling their role as long-circulating sustained-release drug delivery systems.

The Tmax of (PEG-MEM-PLGA) SANs was found to be higher *i.e* 35 h and showed better pharmacodynamic effect as compared to MEMp, Admenta and (MEM-PLGA)SANs. Tmax is often related to the length of a drug's half-life ($t½$), drugs with short half-lives tend to peak and eliminate quickly, often requiring more frequent dosing to maintain a drug within its clinically effective therapeutic range. "The relative bioavailability of (PEG-MEM-PLGA) SANs was 50 % higher as compared to MEMp. Similarly, (PEG-MEM-PLGA) SANs showed maximal distribution in the brain followed by liver and kidney due to considerably longer residence time in systemic circulation. Furthermore, the improved therapeutic effects and pharmacodynamic properties of encapsulated drug showed neophobic behaviour which indicate recovery of the hippocampus circuit function, NMDA receptor function, long term potentiation, short-term spatial working memory and spatial recognition memory which further helps in memory preservation.

PEGylation helps to improve the pharmacokinetic behaviour of therapeutic drugs. PEGylation influences the circulation life-span, tissue distribution pattern, and elimination pathway of the parent drug/particle. Hydrophilicity of PEGs incorporated into the layer of nanoscaffolds creates a protective shield around itself that protects particles from being phagocytosed by natural particle eliminating mechanisms, mainly organs of reticuloendothelial system (RES). (PEG-MEM-PLGA)SANs (56.16±1.42 h) showed greater elimination half-life as compared to (MEM-PLGA)SANs (41.34±1.32h), MEMp (20.61±2.01 h) and Admenta (30.56±1.91 h) which represents higher retention of drug in body for prolonged period [278]. This surface modification resulted in 2.8 fold increase in plasma half-life of nanoscaffolds over the parent particle (MEMp) [279]. Hydrophilic coating with PEG sterically stabilizes PLGA nanoparticles and reduces opsonisation and phagocytosis and uptake by neutrophilic granulocytes *in vivo*. PEGylation changes the physical and chemical properties of the molecule, such as its conformation, electrostatic binding, and hydrophobicity, and results in an improvement in the pharmacokinetic behaviour of the drug. In general, PEGylation improves drug solubility and decreases immunogenicity. PEGylation also increases drug stability and the retention time of the conjugates in blood; and reduces proteolysis and renal excretion, thereby allowing a reduced dosing frequency [280].

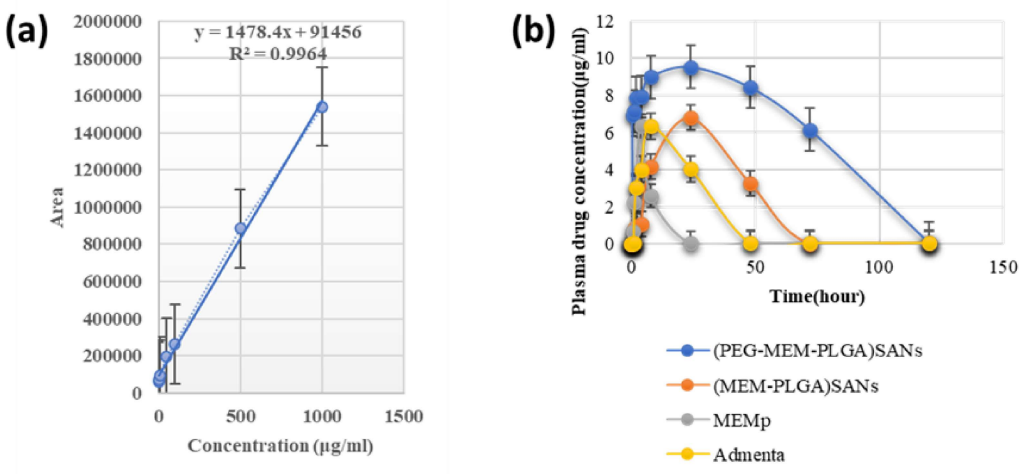

Figure 37: (a) Plasma calibration curve of memantine (1–1000 µg/ml) (b) Comparative Plasma drug concentration profile of (PEG-MEM-PLGA)SANs, (MEM-PLGA)SANs, MEMp and Admenta.

The rationale behind using Admenta and pure drug memantine in this study is to evaluate the improved therapeutic efficacy of (PEG-MEM-PLGA)SANs and whether it exhibits better in-vitro and in vivo properties, pharmacokinetic and pharmacodynamic activity as compared to Admenta and memantine. Admenta is an FDA approved formulation and it has been used as a reference for comparing the therapeutic efficacy of our formulated SANs. As there are no marketed nanocarriers for memantine, so have used pure drug suspension of memantine to compare the dispersion type properties of the drug with our nanocarriers.

Admenta is single unit dosage form (available as 5mg, 7mg, 10mg and 14 mg tablets) whereas (PEG-MEM-PLGA) SANs is multiunit dosage form intended for use in form of powder which provides an immense benefit over single unit dosage form including the flexibility of choosing potential route of administration.

6.4.1.2 Biodistribution study

After intrathecal injection of memantine-loaded nanoscaffolds, marketed formulation, and pure memantine drug, homogenates of organs from the drug/formulation treated mice administered with (PEG-MEM-PLGA) SANs (MEM-PLGA)SANs, MEMp and Admenta were analysed using the chromatographic method and distribution of memantine was assessed (Figure 38 (a-g)). Concentration of memantine in each organ (µg/g of tissue) was quantified as shown in table 14. Memantine was found in brain, indicating its permeation of memantine across blood–brain barrier (BBB). (PEG-MEM-PLGA) SANs accumulated in the brain followed by liver and kidney whereas (MEM-PLGA)SANs was maximally quantified in kidney followed by brain and liver may be due to uptake of memantine via mononuclear phagocyte system which is mainly found in the liver and kidneys [281,282]. Distribution of memantine in brain upon administration of (PEG-MEM-PLGA) SANs might be due to stealth behaviour of PEG which

imparts stability against opsonisation of nanoscaffolds and accumulation in mononuclear phagocyte system and reticuloendothelial uptake [122,283].

Memantine does not cross the blood-brain barrier when administered through oral route. However, direct delivery of the drugs in the cerebral spinal fluid (CSF) surrounding the spinal cord and brain results in distribution of drug into spinal cord and brain tissue. It has reported that bolus injection into the CSF results in better distribution in the CNS than oral route of administration. Distribution kinetics from the CSF into CNS tissues is rapid with a distribution half-life of less than 1 h that is likely due to the combination of uptake into CNS tissues and transfer to systemic circulation [284,285]. Similar to drug kinetics in plasma following systemic dosing, the CSF concentrations of drug exhibit multiphasic kinetics with a long terminal half-life at very low concentrations in CSF that appear to be in equilibrium with central nervous system tissues [286]. PEGylated PLGA nanoscaffolds are generally cleared slowly both in urine and faeces due to increase in molecular weight of the carrier attached with and hence the dominant elimination route shifts from renal to hepatic pathway. This in turn, leads to considerably longer residence time in systemic circulation and therefore in whole body as represented by the obtained pharmacokinetic data (table 13).

Table 14: Biodistribution study 30 min and 72 hours post administration of (PEG-MEM-PLGA) SANs, (MEM-PLGA) SANs, MEMp and Admenta

Organ	30 minutes				72 hour			
	(PEG-MEM-PLGA)SANs (µg/g)	**(MEM-PLGA)SANs (µg/g)**	**MEMp (µg/g)**	**Admenta (µg/g)**	**(PEG-MEM-PLGA)SANs (µg/g)**	**(MEM-PLGA) SANs (µg/g)**	**MEMp (µg/g)**	**Admenta (µg/g)**
Brain	0.0238± 0.22	0.00271± 0.20	0.00007± 0.40	0.00269± 0.12	2.995± 1.99	1.781± 0.44	0.238± 0.32	0.465± 0.50
Liver	0.0136± 0.68	0.0236± 0.40	0.023± 0.22	0.0207± 0.32	1.067± 0.50	0.6230± 0.32	0.223± 0.61	0.121± 0.32
Kidney	0.0162± 0.20	0.00185± 0.46	0.023± 0.33	0.0207± 0.45	0.994± 0.86	0.2230± 0.65	0.994± 0.07	0.128± 0.34

The intrathecal route of administration facilitates movement of drug across the blood-brain barrier and can be found in the brain within a short span of time. After 30 minutes of dosing the concentration of (PEG-MEM-PLGA) SANs increases being maximum at 72 h, after which it starts declining and remains in brain up to 120 h. The concentration of drug from (PEG-MEM-PLGA) SANs (2.995±1.99 µg/g) was approximately 1.7 times higher than that obtained from (MEM-PLGA) SANs (1.781±0.44 µg/g) in the brain after 72 h of similar dose exposure (10 mg intrathecally) (Figure 38 (a) and (d)). However, the concentration of drug released from (PEG-MEM-PLGA) SANs was negligible in the liver and kidney but 72 h post-dosing the

concentration increased up to 120 h (Figure 38 (e) and (f)). Memantine from pure drug suspension (MEMp) and marketed memantine tablet (Admenta) accumulated mainly in kidney and liver after 30 minutes of dosing. Meanwhile the memantine from pure drug suspension (MEMp) and marketed memantine tablet (Admenta) were minimally distributed in brain because of inability to cross blood-brain barrier.

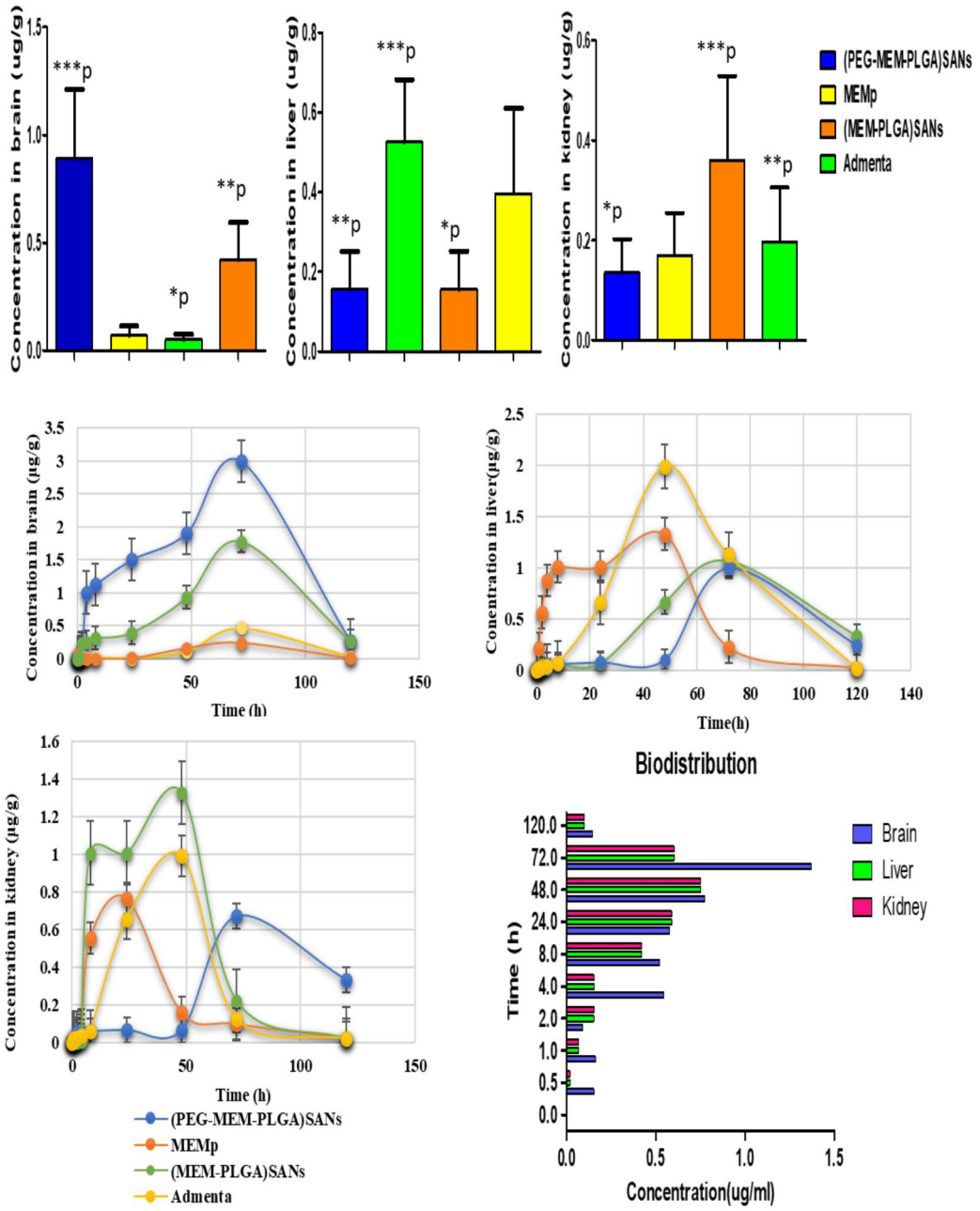

Figure 38: Concentration of Memantine released from (PEG-MEM-PLGA) SANs, (MEM-PLGA) SANs, MEMp and Admenta in brain, liver and kidney. **(g)** Comparative biodistribution pattern of drug from (PEG-MEM-PLGA) SANs in brain, liver and kidney; Each value represents mean ± S.E.M. (n = 3). P value represents significance by showing *p < 0.05, **p<0.01, ***p<0.001 as compared to standard group (Memantine pure drug suspension 10mg/kg).

Comparative biodistribution analysis of (PEG-MEM-PLGA) SANs in brain, liver and kidney showed higher availability of drug in brain as compared to liver and kidney (Figure 36 (g))

The recovery rate (RR) was calculated using the ratio between the slopes of the memantine calibration curves in biological matrix to that in phosphate buffer. The results are shown in table 15. The regression equations presented satisfactory correlation coefficients: 0.993 in serum, 0.998 in the brain, 0.991 in the liver, and 0.934 in kidney.

Table 15: Recovery of memantine in serum, brain, liver and kidney

Organ	Correlation coefficient	Recovery Rate (RR%)
Serum	0.993	85.2
Brain	0.998	91.2
Liver	0.991	89.8
Kidney	0.934	64.2

6.4.1.3 Pharmacodynamic study

Biochemical study

The following biochemical parameters were determined in the serum of mice using a UV/Vis spectrophotometer (Shimadzu, Kyoto, Japan) [287]. The concentrations of Aspartate aminotransferase (AST), Alkaline phosphatase (ALP), Bilirubin total, Bilirubin direct, Serum potassium, Serum calcium, Serum phosphorus, Serum uric acid, Serum sodium, Serum cholesterol and Blood urea were analysed. Aspartate aminotransferase (AST), Alkaline phosphatase (ALP), Serum sodium, Blood urea, and Serum cholesterol showed elevation in diseased conditions and a decrease was observed following treatment with (PEG-MEM-PLGA) SANs, (MEM-PLGA)SANs. In contrast, the elevated levels of Aspartate aminotransferase (AST), Alkaline phosphatase (ALP), Serum sodium, Blood urea, and Serum cholesterol were found in mice serum for groups treated with MEMp and Admenta. Meanwhile nonsignificant effect of treatment was noticed on the concentration of Serum potassium, Serum calcium, Serum phosphorus, Serum uric acid, Bilirubin total, and Bilirubin direct in diseased, control, and treatment groups. Biochemical indices have significance in monitoring clinical symptoms produced in diseased and toxicological conditions. In the past several years, serum aminotransferases analyses have become a standard measure of hepatotoxicity because of the significance of these enzymes [288]. Normally, these enzymes are present in the liver and other tissues where they function in energy metabolism involving the transamination of amino acids. However, in cases of cellular and neural damage, the AST and ALT could leak out into the general circulation leading to an elevated level [289,290].

The level of ALT, AST, and bilirubin total, blood urea, uric acid, serum sodium, serum potassium, and serum cholesterol spiked to 49.0±0.41 IU/Lt, 54.2±0.61 IU/Lt, 12.4±0.02 mg/dl, 132.6±3.06 mg/dl, 11±1.25 mg/dl, 149.4±0.65 mEq/L, 6.8± 0.33 mEq/L and 132±9.5 mg/dl in

diseased condition as compared to control group (32.11± 0.75 IU/Lt, 30.5±1.36 IU/Lt, 1.2±0.08 mg/dl, 30.2±0.02 mg/dl, 2.2±1.41 mg/dl, 20.5±1.02 mEq/L, 123.4±1.01 mEq/L and 2.5±0.02 mg/dl (Figure 39 and Table 16). Whereas the serum globulin level of diseased group 0.6±0.02 decreased as compared to control group 1.2±0.06 indicating destructive effect on globulin protein. Liver function indicator enzymes ALT, AST, and bilirubin total in serum of mice administered with (PEG-MEM-PLGA)SANs (37.0±6.40 IU/Lt, 34.7±5.56 IU/Lt, and 1.7±0.05 mg/dl) were lower than those given (MEM-PLGA)SANs (39.2±1.37 IU/Lt, 39.8±1.79 IU/Lt and 2.46±0.09 mg/dl) and both were approximate similar to the non-treated control group (32.11±0.75 IU/Lt, 30.5±1.36 IU/Lt and 1.2±0.08 mg/dl) which indicates the safety of (PEG-MEM-PLGA)SANs and (MEM-PLGA)SANs. Kidney function indicators blood Urea and uric acid evaluated in (MEM-PLGA) SANs (34.80±0.05 mg/dl and 5.2±1.67 mg/dl) and (PEG-MEM-PLGA) SANs (30.5±0.08 mg/dl and 2.6±0.80 mg/dl) were found to be similar to the control group (30.2±0.02 mg/dl and 2.2±1.41 mg/dl); respectively which indicates no renal toxicity with the treatment. Similarly, the serum cholesterol, serum sodium, and serum potassium of (MEM-PLGA) SANs (24.4±6.89 mg/dl, 115.2±1.07 mEq/L and 2.8±0.22 mEq/L) and (PEG-MEM-PLGA) SANs (21.0±0.48 mg/dl, 119.5±0.80 mEq/L and 2.3±0.22 mEq/L) were found to be similar to control group (20.5±1.02 mg/dl, 123.4±1.01 mEq/L and 2.5±0.02 mEq/L). The serum globulin level of (MEM-PLGA) SANs and (PEG-MEM-PLGA) SANs (2.2±0.18 gm/dl and 1.8±0.20 gm/dl) are slightly higher than control group (1.2±0.06 gm/dl) which could be because of the protection of proteins from the destruction due to AD.

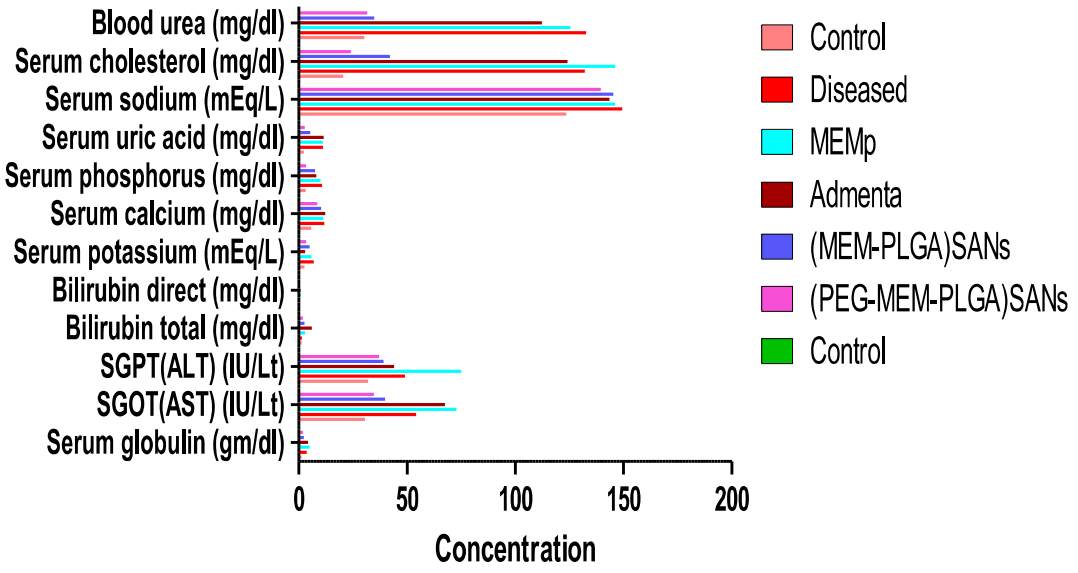

Figure 39: Estimation of Biochemical Parameters.

Table 16: Biochemical parameters of Control, Diseased, MEMp, Admenta, (MEM-PLGA)SANs and (PEG-MEM-PLGA)SANs

Parameters	Control	Diseased	MEMp	Admenta	(MEM-PLGA) SANs	(PEG-MEM-PLGA) SANs	Control
Serum globulin (gm/dl)	1.2±0.06	0.6±0.02	4.8±0.004	4.2±0.002	2.2±0.012	1.8±0.02	1.5-3.5
SGOT(AST) (IU/Lt)	30.5±1.36	54.2±0.61	72.7±0.33	67.4±0.42	39.8±1.79	34.7±5.56	0-40
SGPT(ALT) (IU/Lt)	32.11±0.75	49.0±0.41	75.0±0.22	44.1±0.43	39.2±1.37	37.0±6.40	10-40
Bilirubin total (mg/dl)	1.2±0.08	12.4±0.02	2.81±0.41	5.9±0.42	2.46±0.66	1.7±0.05	0.1-10
Bilirubin direct (mg/dl)	0.1±0.14	0.4±0.34	0.9±0.113	0.7±0.43	0.3±0.21	0.1±0.41	<0.2
Serum potassium (mEq/L)	2.5±0.02	6.8±0.33	5.7±0.23	4.8±0.12	2.8±0.22	2.3±0.22	1.5-3.5
Serum calcium (mg/dl)	5.6±0.21	11.7±0.24	11.3±0.42	12.2±0.51	10.2±0.61	8.5±0.22	8.5-10.5
Serum phosphorus (mg/dl)	3.12±0.11	10.7±0.54	9.9±0.21	8.1±0.42	7.4±0.11	3.3±0.61	2.5-4.5
Serum uric acid (mg/dl)	2.2±1.41	11±1.25	10.9±0.02	11.4±0.03	5.2±0.06	2.6±0.09	2-7
Serum sodium (mEq/L)	123.4±1.01	149.4±0.65	146±0.45	143.5±0.66	115.2±1.07	119.5±0.80	132-145
Serum cholesterol (mg/dl)	20.5±1.02	132±9.5	146±4.56	124±4.87	24±6.89	21.0±0.48	13-45
Blood urea (mg/dl)	30.2±0.02	132.6±7.4	125.4±3.2	112.4±4.1	34.80±6.2	31.50±4.1	13-453.6

6.5 Histological study

6.5.1 Histological studies

In the control group, the brain tissue exhibited a normal neuronal architecture without any pathological abnormalities. The brain tissue obtained from diseased mice showed severe accumulation of β amyloid plaque which is responsible for neurodegeneration and amnesia. Diseased mice administered with 10mg memantine loaded PLGA nanoscaffolds intrathecally showed a reduction in the accumulation of β amyloid plaque compared to the disease control group illustrated in figure 40 (a-c).

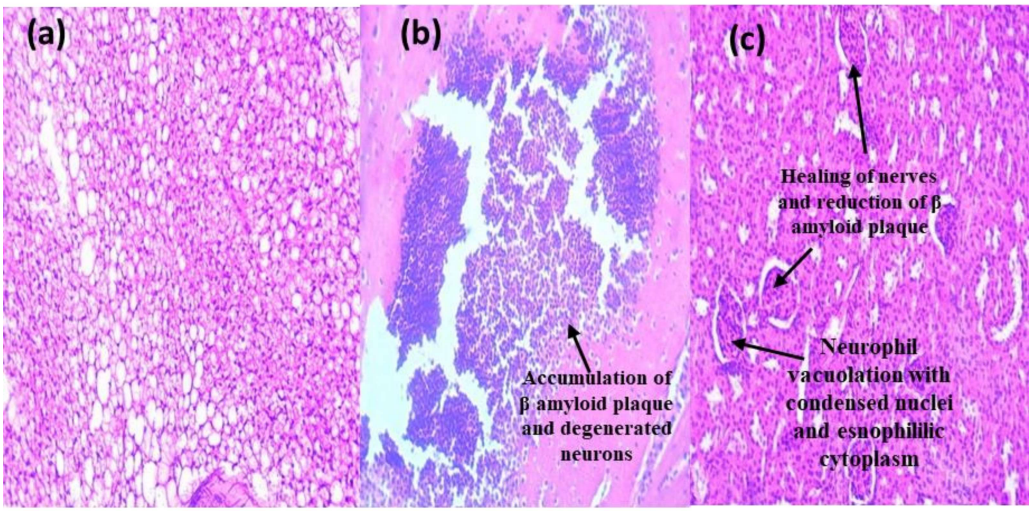

Figure 40: Cross-section of brain taken from (a) control group (b) diseased mice (c) treated animals (with PLGA nanoscaffolds)

The microscopy of the tissue sections was performed using a Nikon OptiPhot microscope and Ni-kon Digital Sight camera using NIS-Elements software. Brightfield microscopy under the visible light spectra was used to view whole tissue section images under 40X bright field magnification. Hematoxylin stain was used to enhance the detection of degenerating neurons showing eosinophilic (degenerating) neurons within the pyramidal layer of the hippocampus of a mice. The combination of hematoxylin and eosin stains is one of the most widely used staining techniques in histology of brain tissues. Hematoxylin imparts a blue color to the basophilic tissue elements including nuclear chromatin, degenerated neurons while eosin gives various shades of red color to acidophilic tissue components such as collagen, cytosol, musculature and erythrocytes [291].

Figure 40 (a) showed a normal pattern of distribution of neurons and figure 40 (b) shows the classic monomorphic pattern of dark neurons within the pyramidal layer of the hippocampus. It also shows dark neurons that are bilaterally arranged within two major midbrain nuclei of brain with an intense accumulation of amyloid β protein and neurodegenerative neurons in diseased animal and figure 40 (c) shows recovery of neurons following 6 week of treatment with memantine-loaded nanoscaffolds. Figure 40 (c) also shows a classic appearance of eosinophilic (degenerating) Purkinje neurons with condensed nuclei and bright eosinophilic cytoplasm characterized by neutrophil vacuolation.

It showed appearance of eosinophilic (degenerating) Purkinje neurons with condensed nuclei and bright eosinophilic cytoplasm. In addition, there is vacuolation within the overlying molecular layer suggesting concurrent swelling/degeneration of Purkinje neuron dendrites. It is characterized by a heterogeneous pattern, including shrunken eosinophilic neurons with

either pyknotic or karyorrhectic nuclei, neuron swelling and vacuolation (long arrow), and an active-appearing microglial cell. Figure 41 (e), (f) and (g) showed recovery of neurons following 3rd, 6th and 9th week of treatment with (PEG-MEM-PLGA) SANs. The section in figure 39 (f) also shows neutrophil vacuolation. Figure 39 (k) and 39 (l) represent recovery of degenerated neurons after 6 week and 9 weeks of treatment with (PEG-MEM-PLGA) SANs.

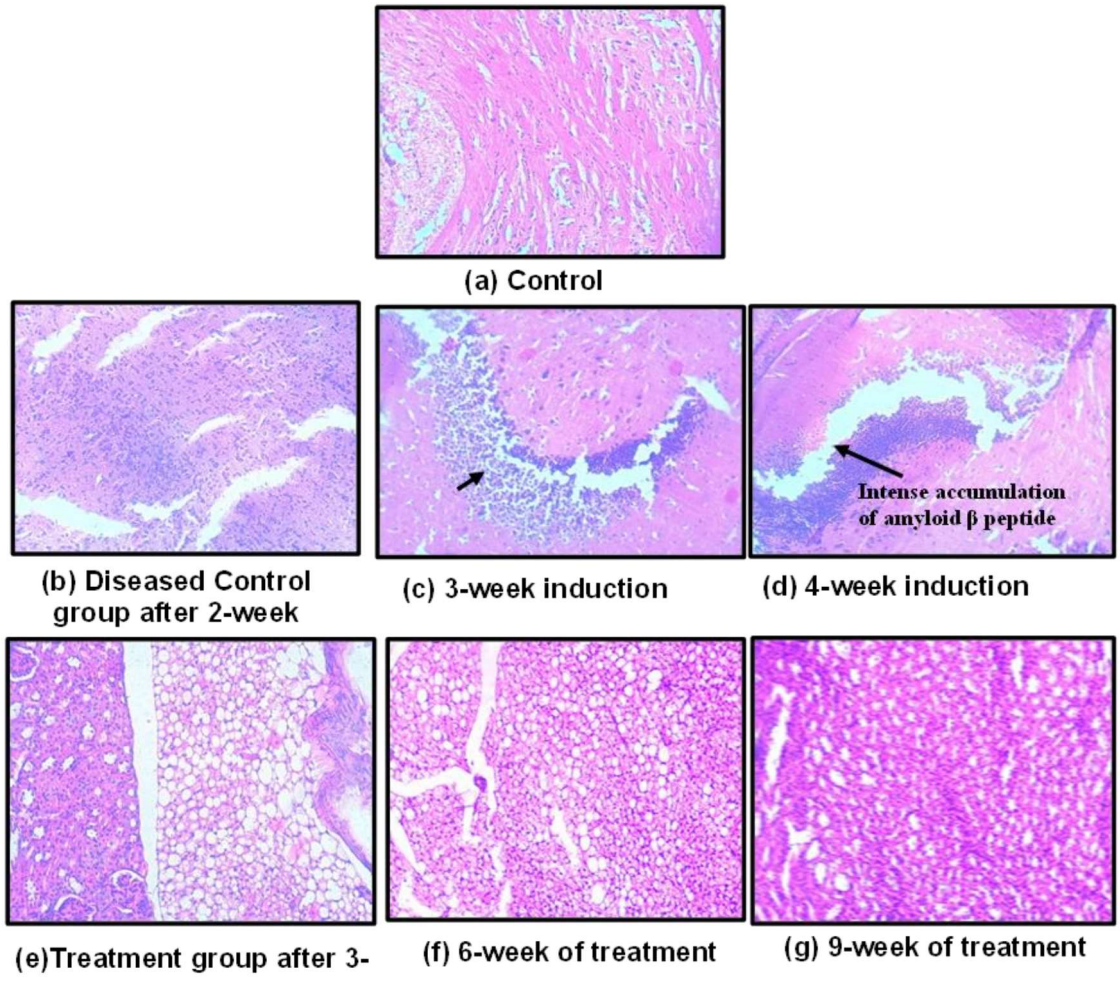

Figure 41: Cross-section of brain taken from Alzheimer's disease induced mice and recovery of neurons and neuroregeneration after 1, 6 and 9 week of treatment after treatment with (PEG-MEM-PLGA) SANs.

6.6 Estimation of pro-inflammatory cytokines

Neurodegeneration and plaque-associated microglia result in cerebral ischemia influenced by inflammatory processes which lead to release of IL-1β, IL-6, IL-10 and TNF-α in brain tissue of AD mice. Elevated levels of IL-1β (196.83±0.898pg/ml), IL-6 (204.28±0.5pg/ml), IL-10 (119.24±1.91pg/ml and TNF-α (185.57±6.4 pg/ml) in brain tissue homogenates of scopolamine-induced AD mice model compared to normal control group (IL-

1β:16.42±2.6pg/ml, IL-6: 14.23±1.6pg/ml IL-10: 11.55±18.32pg/ml and TNF- α: 1.155±0.68 pg/ml) were observed. The overexpression of TNF- α in mice brain tissue activates NFκB- that leads to Aβ-induced neuronal apoptosis and neurodegeneration [292]. IL-1β is generally produced after inflammation that is specifically associated with the induction of COX-2 in the CNS [293]. Furthermore, the activated perpetuated microglia contribute in the subsequent release of IL-1β, neuroinflammatory reactions and progression of neuronal and vascular degeneration. A reduction in IL-1β, IL-6, IL-10 and most prominently reduction in TNF-α was noticed in AD induced animal group treated with MEMp (IL-1β: 65.24±6.87pg/ml, IL-6: 58.07±3.86pg/ml, IL-10: 61.8±2.97pg/ml and TNF-α: 23.45±0.165 pg/ml), marketed (Admenta) (IL-1β: 45.76±4.7pg/ml, IL-6: 41.68±1.6pg/ml, IL-10: 54.62±3.9pg/ml and TNF-α: 11.200±0.15pg/ml) and memantine loaded nanoscaffolds (IL-1β: 38.04±4.2pg/ml, IL-6: 23.36±2.9pg/ml, IL-10: 18.68±9.97pg/ml and TNF-α: 1.2±0.06pg/ml) treated group as compared to the diseased group. Decreased in levels of IL-1β, IL-6, IL-10 and TNF-α were noticed after treatment with MEMp, marketed (Admenta) and memantine-loaded nanoscaffolds in scopolamine-induced AD mice. Memantine-loaded nanoscaffolds showed efficient reduction IL-1β, IL-6, IL-10 and TNF-α in brain due to stimulation of protective mechanism. In addition, the reduction of cytokines was observed primarily involved in the maintenance of blood-brain barrier (BBB) integrity and regulation of signaling of neurons in cerebral ischemia by regulating Janus kinase/STAT pathway and NFκB pathways (Figure 42). Regulation in level of IL-6 upon treatment of AD-induced mice with memantine-loaded nanoscaffolds was observed leading to decrease in pro-inflammatory cytokines, including tumor necrosis factor-α and IL-10. The proposed therapy can be used in potential therapeutic management of AD in clinical practice.

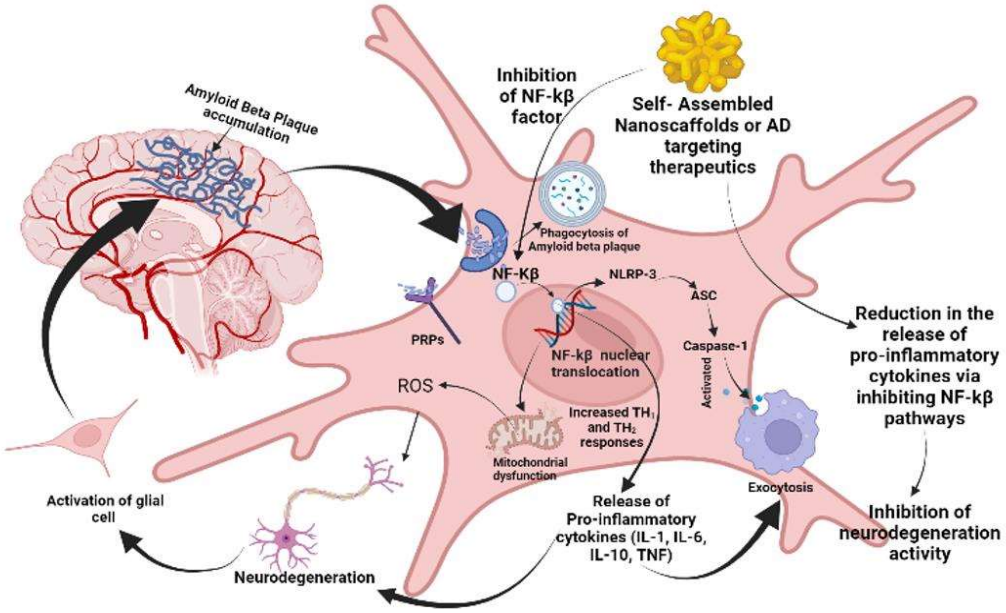

Figure 42: Pathways of neurodegeneration in microglial cell, and release of pro-inflammatory cytokines in Alzheimer's disease.

6.6.1 Expression of pro-inflammatory cytokines in serum, cerebral, hepatic and renal tissues

Despite modest changes in Aβ pathology, pro-inflammatory and microglial responses were found to be in the brain following treatment of AD mice. The elevated expression of serum proinflammatory cytokines (IL-1β, IL-6, IL-10 and TNF-α) is primarily due to stimulation of blood circulating monocytes at the site of neuroinflammation and in systemic circulation (Figure 43 (a)). IL-1β (296.83±0.898 pg/ml) was visible in cerebral tissue followed by IL-6 concentration (274.28±0.5 pg/ml) and TNF-α (185.57±6.4 pg/ml) with minimal concentration of IL- 10 (139.24±1.91 pg/ml) was observed (Figure 43 (b)). Meanwhile, high level of TNF-α (245.885 ± 0.85 pg/ml) was noticed in liver tissue homogenates of scopolamine induced AD group compared to normal control group (3.375 ± 0.085 pg/ml) (Figure 43 (c)). Although direct evidence of the role of TNF-α in AD has not been found but the enhanced TNF-α might be due to stimulation of NF-κB signalling cascades [294]. Several studies have reported elevation of IL-1β and IL-6 levels in serum and brain of AD patients generally due to formation of diffused plaques during early stage of AD [294,295]. This study has revealed the potential of nanoscaffolds and nanoscaffolds grafted with stem cells on the alteration of proinflammatory cytokines in different organ of body that can be used for diagnosis and treatment of AD (PEG-MEM-PLGA)-BMSc SANs showed 20-fold reduction in serum IL-1β whereas, (PEG-MEM-PLGA) SANs, (MEM-PLGA) SANs, MEMp and marketed (Admenta) showed 13-fold, 9-fold, 15-fold and 2-fold reduction IL-1β level in serum. Similarly, (PEG-MEM-PLGA) SANs and

(PEG-MEM-PLGA)-BMSc SANs respectively showed 9-fold and 12-fold reduction in levels of IL-6 in serum, whereas no reduction in expression of IL-6 was obtained in cerebral, hepatic and renal tissue of AD induced mice. [296]. Meanwhile, high level of IL-6 (274.6 ± 1.22 pg/ml) was found in hepatic tissue of healthy mice as IL-6 is also inherently expressed in hepatic cells. Recent studies have revealed that HSF differentially regulates IL-6 production in hepatocytes and HSF expresses a variety of innate immune receptors which interact with pathogen or damage-associated molecular patterns, and can produce cell-autonomous innate immune responses that may result in host defence or immunopathology [294]. However, it has been observed that IL-6 and IL-10 are produced due to modulation in NF-kB and STAT3 signalling, which indicates initiation of neurodegeneration, and prolonged IL-6 and IL-10 secretion can actively suppress T-cell responses by inhibiting the lipopolysaccharide- (LPS-) induced production of several inflammatory mediators in microglia. This protective response further prevents damage of neurons and helps to restore neuronal function [297].

The animal groups, standard, marketed and treatment groups T1, T2 and T3 showed highly significant effect on reduction of IL-1β (***$p< 0.001$) in serum, cerebral, hepatic and renal tissues as compared to diseased group. Standard, T1, T2 and T3 showed significant effect on reduction of IL-6 and TNF-α in serum (***$p< 0.01$), and IL-10(**$p<0.01$), and marketed group showed significant reduction of IL-1β (**$p<0.01$), IL-6 (*$p<0.05$), IL-10 (**$p<0.01$) and TNF-α (***$p<0.001$) in serum as compared to diseased control group. Standard, marketed, T1, T2 and T3 showed significant reduction in IL- 1β (***$p<0.001$). However, T1 and T2 group showed non-significant reduction of IL-6 in cerebral tissue as compared to diseased group. Standard, marketed, T1, T2 and T3 showed non-significant reduction of IL-6 in hepatic and renal tissue ($^{ns}P>0.05$), and showed significant reduction of IL-10 in hepatic (**$P<0.01$) and renal tissue (*$p<0.05$) (Figure 35). Following treatment with standard, marketed, T1, T2 and T3 significant reduction in IL-1β, IL-10 and TNF-α in serum and cerebral tissue was observed that showed the therapeutic effect of formulation in reducing pro-inflammatory cytokines mediated neuroinflammation. However, Group T1 and T2 showed non-significant effect on reduction of IL-6 in cerebral tissue indicating neuroprotective homeostasis stimulated via prolonged neuroinflammation mediated neurodegeneration [298]. Standard, marketed, T1, T2 and T3 showed nonsignificant reduction in concentration of IL-6 in hepatic and renal tissue which indicates the protective mechanism on cerebral, hepatic and renal tissues [295,299].

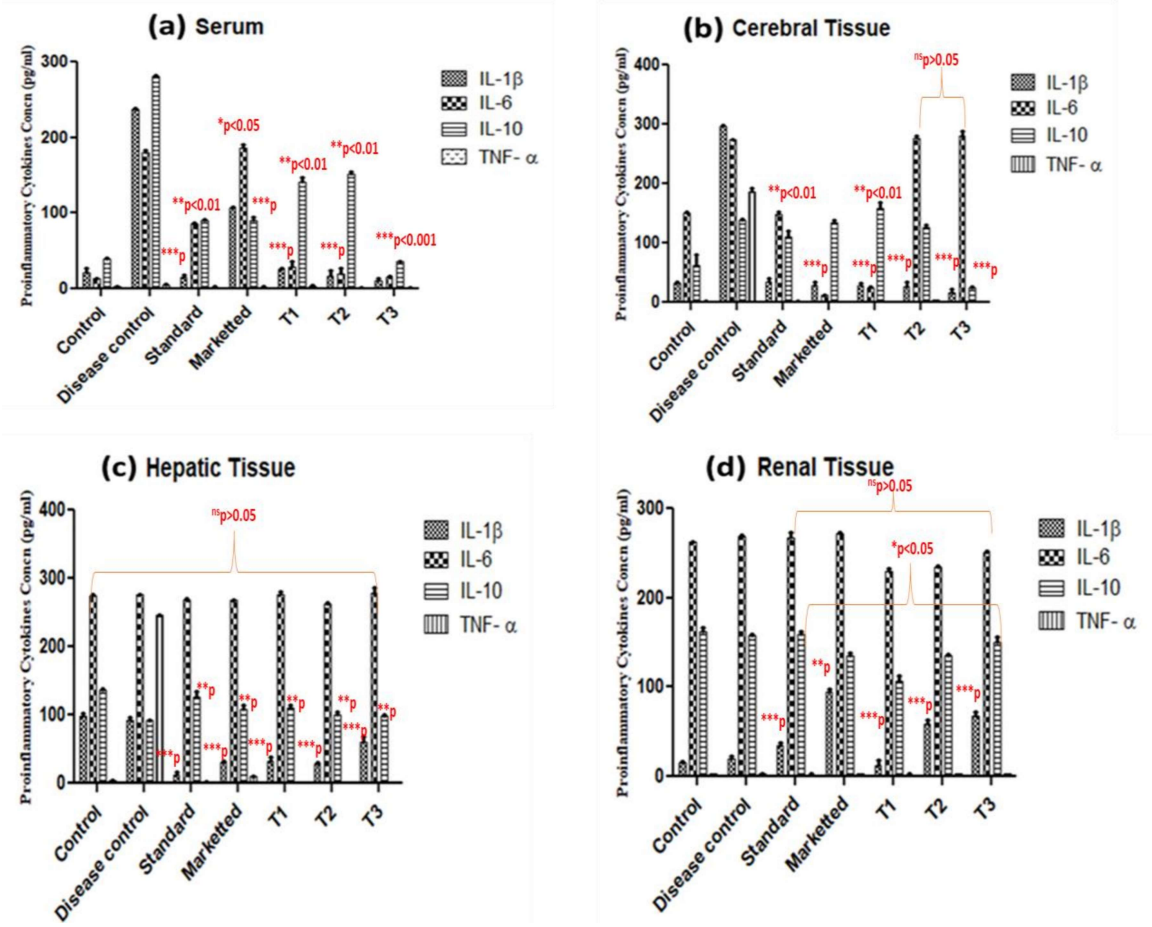

Figure 43: Expression of pro-inflammatory cytokines IL-1β, IL-6, IL-10 and TNF-α in MEMp, Marketed, T1-(MEM-PLGA) SANs, T2-(PEG-MEM-PLGA) SANs and T3-(PEG-MEM-PLGA)-BMSc SANs in (a) serum, (b) cerebral tissue, (c) hepatic tissue and (d) renal tissues of treatment groups of scopolamine induced AD model. vs. control and disease control (untreated cells) group. Data has been represented as Mean ± SEM, (n = 3).

In summary, we can understand that the decrease in level of IL-1β, IL-10 and TNF-α and elevated level of IL-6 were noticed after treatment with (PEG-MEM-PLGA) SANs and (PEG-MEM-PLGA)-BMSc SANs in scopolamine induced AD mice. The release of IL-6 during treatment of AD in induced mice with MEMp, (MEM-PLGA) SANs, (PEG-MEM-PLGA) SANs, (PEG-MEM-PLGA)-BMSc SANs, leads to downregulation of a number of pro-inflammatory cytokines, including tumour necrosis factor-α and IL-10. Therefore, modulation in IL-6 could provide potential therapeutic management of AD in clinical practice [295,299]. In addition, some studies have also shown that IL-6 contributes to stem cell regeneration that is responsible for neuronal stem cell expansion (induced pluripotent stem cells (iPSCs)) within a short time window) and regulation of neuronal outgrowth by following JAK-STAT signalling pathways [298]. Moreover, an increased level of TNF-α in AD mice might be responsible for the imbalance of excitation and inhibition phenomena occurring during neuronal signal conduction leading to loss of memory functions. However, (PEG-MEM-PLGA) SANs and

(PEG-MEM-PLGA)-BMSc SANs also showed almost 3-fold and 4-fold reduction in TNF-α in serum, cerebral, hepatic and renal tissue in AD induced mice which indicates the recovery of neurons. Overall, (PEG-MEM-PLGA)-BMSc SANs showed greater reduction in of pro-inflammatory cytokines as compared to (PEG-MEM-PLGA) SANs, (MEM-PLGA) SANs, MEMp and marketed (Admenta) in serum, cerebral, hepatic and renal tissue.

The concentration of pro-inflammatory cytokines quantified across various treatment groups have been presented in table 17.IL-1β, IL-6, IL-10 and TNF-α are prominently expressed in brain which indicates regulatory effects of cytokines in neuroinflammation and neurodegeneration in AD. Reduction in pro-inflammatory cytokines facilitates regulation of neuroinflammation and thus prevents degeneration of neurons.

Table 17: Estimated pro-inflammatory cytokines concentration in serum, cerebral, hepatic and renal tissue

Pro-inflammatory cytokines concentration in serum (pg/ml)				
	IL-1β	**IL-6**	**IL-10**	**TNF-α**
Control	20.87±6.03	13.35±0.26	39.26±1.44	2.88±0.255
Disease Control	237.29±0.805	180.74±2.1	280.66±0.98	4.98±1.02
Standard	15.71±3.14	85.14±1.67	89.62±1.43	2.215±0.305
Marketed	106.91±1.35	186.97±3.5	90.485±4.56	1.85±1.285
T1	25.15±1.57	28.37±6.03	140.86±7.09	3.72±0.505
T2	17.48±6.9	20.03±6.68	152.33±2.56	1.385±0.241
T3	10.98±2.71	15.02±1.67	36.32±0.33	1.035±1.425
Pro-inflammatory cytokines concentration in cerebral Tissue (pg/ml)				
	IL-1β	**IL-6**	**IL-10**	**TNF-α**
Control	31.42±2.6	149.74±1.66	61.55±18.32	1.455±0.68
Disease Control	296.83±0.898	274.28±0.5	139.24±1.91	185.57±6.4
Standard	35.24±8.87	148.07±4.86	110.8±9.97	2.475±0.465
Marketed	27.76±4.7	11.68±1.6	134.62±3.9	1.200±0.15
T1	28.04±4.2	23.36±2.9	158.68±9.97	1.2±0.06
T2	26.34±6.1	277.12±3.34	127.27±3.76	3.815±0.125
T3	17.24±5.7	280.96±7.73	23.39±3.55	2.91±0.01
Pro-inflammatory cytokines concentration in hepatic Tissue (pg/ml)				
	IL-1β	**IL-6**	**IL-10**	**TNF-α**
Control	98.5±4.1	274.6±1.22	136.62±1.27	3.375±0.085
Disease Control	93.33±2.6	275.45±1.28	91.62±1.45	245.885±0.85
Standard	13.07±3.8	268.77±1.02	125.65±9.35	3.08±0.2
Marketed	29.65±2.9	267.94±0.82	109.21±5.09	10.845±0.335
T1	32.390±5.7	277.95±9.18	110.44±3.38	3.3±0.015
T2	28.29±2.4	262.1±1.67	99.925±4.57	2.98±0.01
T3	61.280±6.1	277.95±9.180	98.97±1.62	3.21±0.032
Pro-inflammatory cytokines concentration in renal Tissue (pg/ml)				
	IL-1β	**IL-6**	**IL-10**	**TNF-α**
Control	14.56±1.8	262.1±1.01	161.8±4.68	3.81±0.05
Disease Control	20.41±2.2	268.83±1.67	158.06±0.84	3.48±0.17
Standard	34.58±3.4	267.165±6.615	159.64±3.05	2.34±0.85
Marketed	94.15±4.1	271.26±2.01	135.24±2.59	3.405±0.025
T1	11.63±6.4	230.27±2.51	107.21±5.62	2.005±0.605
T2	58.74±5.2	234.38±1.14	135±2.11	3.335±0.075
T3	67.77±4.8	250.41±1.26	150.32±5.73	2.9±0.045

*All the data are report as mean ± SD (n=3)

6.6.2 Involvement of cytokines in AD

The cerebral vasculature of Alzheimer's disease exhibits a destructive pathology in which Aβ

deposition, neuronal inflammation and release of inflammatory mediators occurs. In the present study, low level of pro-inflammatory cytokines IL-1β, IL-10 and TNF-α were detected in serum, cerebral tissue, hepatic tissue in healthy mice, and these levels were further found enhanced in mice on the induction of AD which indicates the contributory role of cytokines in pathophysiology of AD. Various studies have suggested that low levels of IL-1β are expressed in healthy central nervous system and its expression increases in CNS due to stimulation of microglial cells in neurodegenerative disorders. The contributing role of IL-1β in pathogenesis of AD were evident by the increased levels of IL-1β in serum (237.29±0.805 pg/ml) and cerebral (296.83±0.898 pg/ml) tissue. Being a pleiotropic cytokine IL-6 initially caused neurodegeneration Also, IL-6 facilitates nervous tissue survival and mitigates inflammatory responses promoting the resolution of inflammatory cascades that are important for the brain integrity and serves as a therapeutic or potential biomarker during neuroregeneration [300]. Meanwhile, release of IL-10 leads to an inflammatory state that promotes chronic neurodegeneration and prolonged IL-10 production which actively suppresses T helper cell responses alongwith host immune response. Microglial activation and upregulation of TNF-α expression is a common feature of several neurodegenerative disorders. Furthermore, TNF-α can potentiate glutamate-mediated cytotoxicity by inhibiting glutamate transport across astrocytes by triggering the surface expression of Ca^{+2} permeable-AMPA receptors and NMDA receptors, while decreasing inhibitory $GABA_A$ receptors on neurons. Thus, the net effect of TNF-α might be responsible for the imbalance of excitation and inhibition phenomena occurring during neuronal signal conduction that can be responsible for memory deficit. Therefore, modulation in TNF-α signalling may represent a valuable target for the therapeutic intervention in AD [301,302].

6.6.3 Therapeutic effect of Memantine and nanoscaffolds on inflammation in AD

The combined drug therapy with stem cell within a nanoscaffold matrix potentiates the effect of drug and showed marked recovery in brain health. This nanoscaffolds have been designed for, site-specific delivery via intrathecal route of administration which eliminates the risk of hepatic and renal toxicity along with shortening of dosage regimen and improves patient compliance simultaneously. The therapy with memantine-loaded nanoscaffold via the intrathecal route helps to reduce the complication involved in AD by improving its BBB penetration, improved drug release, retention of drug within brain, and improving cerebral microvasculature, neuronal regrowth, and maintaining neuron signalling. In spite of contributing role of proinflammatory cytokines therapeutic activity of memantine and memantine loaded nanoscaffolds is an important aspect for maintaining mental health.

Memantine is an N-methyl-D-aspartate (NMDA) receptor antagonists which provides protection against neuroinflammation and neuronal death accompanied by suppression of proliferation and activation of microglial cells and regulation of inflammatory cytokines in AD. In the present study, memantine-loaded PEG-coated self-assembled nanostructures (PEG-MEM-PLGA) SANs have been developed for penetration and delivery of drug across the BBB for prolonged action in Alzheimer's disease. Potential activity of memantine and memantine incorporated nanoscaffolds showed significant effect on reduction of TNF-α, IL-1β, IL-6, IL-10 and thus contributes in reduction of neuroinflammation. Additionally, figure 44 (a) significant ($p^{***} < 0.001$) effect of MEMp, (MEM-PLGA) SANs, (PEG-MEM-PLGA) SANs and (PEG-MEM-PLGA)-BMSc on reduction in the levels of insoluble amyloid-β, hyperphosphorylated tau was observed via decrease in IL-1β concentration which leads to inhibition of NF-κB activity to restore cognition. Thus, diseased (dementia) group showed an increase of this cytokine as compared to the control group ($p < 0.01$), and this increase was reversed by treatment with memantine and its memantine loaded nanoscaffolds ($p < 0.001$). (MEM-PLGA) SANs has shown reduction in enhanced IL-1β level of AD mice from 237.29±0.805 pg/ml to 25.15±1.57 pg/ml in serum, 296.83±0.898 pg/ml to 28.04 ± 4.2 pg/ml in cerebral tissue, 93.33 ± 2.6 pg/ml to 32.39 ± 5.7 in hepatic tissue, and 20.41±2.2 pg/ml to 11.63 ± 6.4 pg/ml in renal tissue. However, (PEG-MEM-PLGA) SANs and (PEG-MEM-PLGA)-BMSc SANs treated animal group has shown prominent reduction in IL-1β level from 25.15 ± 1.57 pg/ml to 17.48±6.9 pg/ml in serum, 28.04 ± 4.2 pg/ml to 26.34±6.1 pg/ml in cerebral tissue, 93.33 ± 2.6 pg/ml to 28.29±2.4 pg/ml in hepatic tissue as compared to (MEM-PLGA) SANs. (PEG-MEM-PLGA)-BMSc has shown the potential in reduction of neuroinflammatory response via regulating proinflammatory cytokines levels mostly in serum and cerebral tissue. (PEG-MEM-PLGA)-BMSc SANs reduces IL-1β in serum from 237.29±0.805 pg/ml to 10.98±2.71 pg/ml and cerebral tissue from 296.83±0.898 pg/ml to17.24±5.7 pg/ml. (PEG-MEM-PLGA)-BMSc SANs showed 20-fold, 17-fold and 1.5-fold most reduction in IL-1β level in serum, cerebral and hepatic tissue respectively which indicates the maximized therapeutic effect in brain and blood with less distribution in other organs because BMSc facilitates neuronal recovery by regeneration confined at brain that helps in treatment of AD most effectively by incorporating in nanoscaffolds loaded with memantine.

Figure 44 (b) represents nonsignificant effect of IL-6 in cerebral, hepatic and renal tissue in AD mice treated with MEMp, (MEM-PLGA) SANs, (PEG-MEM-PLGA) SANs, (PEG-MEM-PLGA)-BMSc SANs. Significant reduction in IL-6 serum level from 180.74±2.1pg/ml to 85.14±1.67 pg/ml, 28.37±6.03 pg/ml, 20.03±6.68 pg/ml and 15.02±1.67 pg/ml was obtained

after administration of MEMp, (MEM-PLGA) SANs, (PEG-MEM-PLGA) SANs, (PEG-MEM-PLGA)-BMSc SANs respectively. The reduction of serum IL-6 concentration is mostly due to regulation of pro-inflammatory cytokines after administration of MEMp, (MEM-PLGA) SANs, (PEG-MEM-PLGA) SANs, (PEG-MEM-PLGA)-BMSc SANs. (PEG-MEM-PLGA)-BMSc SANs has shown 10-fold, 5-fold and 3-fold greater reduction in serum IL-6 level as compared with MEMp, (MEM-PLGA) SANs, (PEG-MEM-PLGA) SANs. Furthermore, it was obtained that the level of IL-6 in cerebral tissue of mice treated with (PEG-MEM-PLGA) SANs (277.12±3.34 pg/ml) and (PEG-MEM-PLGA)-BMSc SANs (280.96±7.73 pg/ml) was found elevated even after following the treatment protocol which indicates the contributory role in AD and higher than that of standard group treated with MEMp ((148.07±4.86 pg/ml) indicating the neuroregenerative capacity of nanoscaffolds containing bone marrow stem cells. The elevated IL-6 level indicates the neurodegenerative condition in AD mice initially without treatment and later neuroprotective behaviour of IL-6 were noticed after following treatment protocol with (PEG-MEM-PLGA) SANs and (PEG-MEM-PLGA)-BMSc SANs. The exerted neuroprotective behaviour is mainly due to prolonged neurodegeneration augmented the hippocampal levels of phosphorylated signal transducer, activator of transcription-3 (p-STAT3) and anti-apoptotic protein while diminished nuclear factor-kappaB (NF-κB) and caspase-3 (casp-3) expression. These outcomes promotes the protective effect of neurodegeneration, memory deficits and AD-like pathological condition probably via modulating NF-kB and STAT3 signalling mediated by modulating N-methyl-D-aspartate (NMDA) receptors [303,304].

The IL-10 concentration in cerebral tissue and serum found diminished in animals subjected to administration of MEMp, (MEM-PLGA) SANs, (PEG-MEM-PLGA) SANs, (PEG-MEM-PLGA)-BMSc SANs. IL-10 concentration was significantly reduced in serum from 280.66±0.98 pg/ml to 36.32±0.33 pg/ml, and cerebral tissue from 139.24±1.91 pg/ml to 23.39±3.55 pg/ml in AD induced animal group treated with (PEG-MEM-PLGA)-BMSc SANs which showed 4-fold and 5-fold more potent than standard, marketed, (MEM-PLGA) SANs and (PEG-MEM-PLGA) SANs respectively. (MEM-PLGA) SANs, (PEG-MEM-PLGA) SANs and (PEG-MEM-PLGA)-BMSc SANs treated group also showed slight increase in hepatic tissue IL-10 level as compared to AD mice. Similarly, IL-10 level in renal tissue was found to be slightly reduced in AD induced animal groups treated with marketed formulation (Admenta) (135.24±2.59 pg/ml), (MEM-PLGA) SANs (107.21±5.62pg/ml, (PEG-MEM-PLGA) SANs (135±2.1 pg/ml) and (PEG-MEM-PLGA)-BMSc SANs (150.32±5.73 pg/ml compared to untreated AD mice (158.06±0.84pg/ml) (Table 17) (Figure 44 (c)). The finding indicates the contributory role of IL-10 predominately in serum and cerebral tissue whereas hepatic tissue

and renal tissue were not involved in the pathogenesis of AD and regulation of proinflammatory cytokines in the therapeutic management of AD. The observed neurodegenerative effect is primarily due to non-competitive NMDA receptor antagonist activity of memantine that is responsible for attenuation of B cell receptor (BCR) and Toll-like receptor 4 (TLR4) for mediating B-cell signalling and can affect the production of IL-10 [305].

The results revealed that TNF-α were predominately expressed in cerebral and hepatic cells after induction of AD whereas TNF-α found lesser expressed in serum and renal tissue as compared to IL-1β, IL-6, IL-10. The TNF-α concentration were found significantly increased in cerebral and hepatic tissue of AD induced mice as compared to normal healthy mice which was reduced after administration of MEMp, marketed (Admenta), (MEM-PLGA) SANs, (PEG-MEM-PLGA) SANs and (PEG-MEM-PLGA)-BMSc SANs. (PEG-MEM-PLGA)-BMSc SANs showed almost 14-fold and 15-fold greater reduction in cerebral and hepatic TNF-α level as compared to MEMp, marketed (Admenta), (MEM-PLGA) SANs, (PEG-MEM-PLGA) SANs. TNF-α level in renal tissue varied non-significantly amongst the groups (Table 17) (Figure 44 (d)). In addition, the incorporation of bone marrow stem cell therapy fastens the recovery of neurons and nanoscaffolds provides an environment for growth and regeneration of neurons. Furthermore, (PEG-MEM-PLGA)-BMSc incorporated with bone marrow stem cell stimulate regeneration of neurons facilitating improvement in cognitive function in AD.

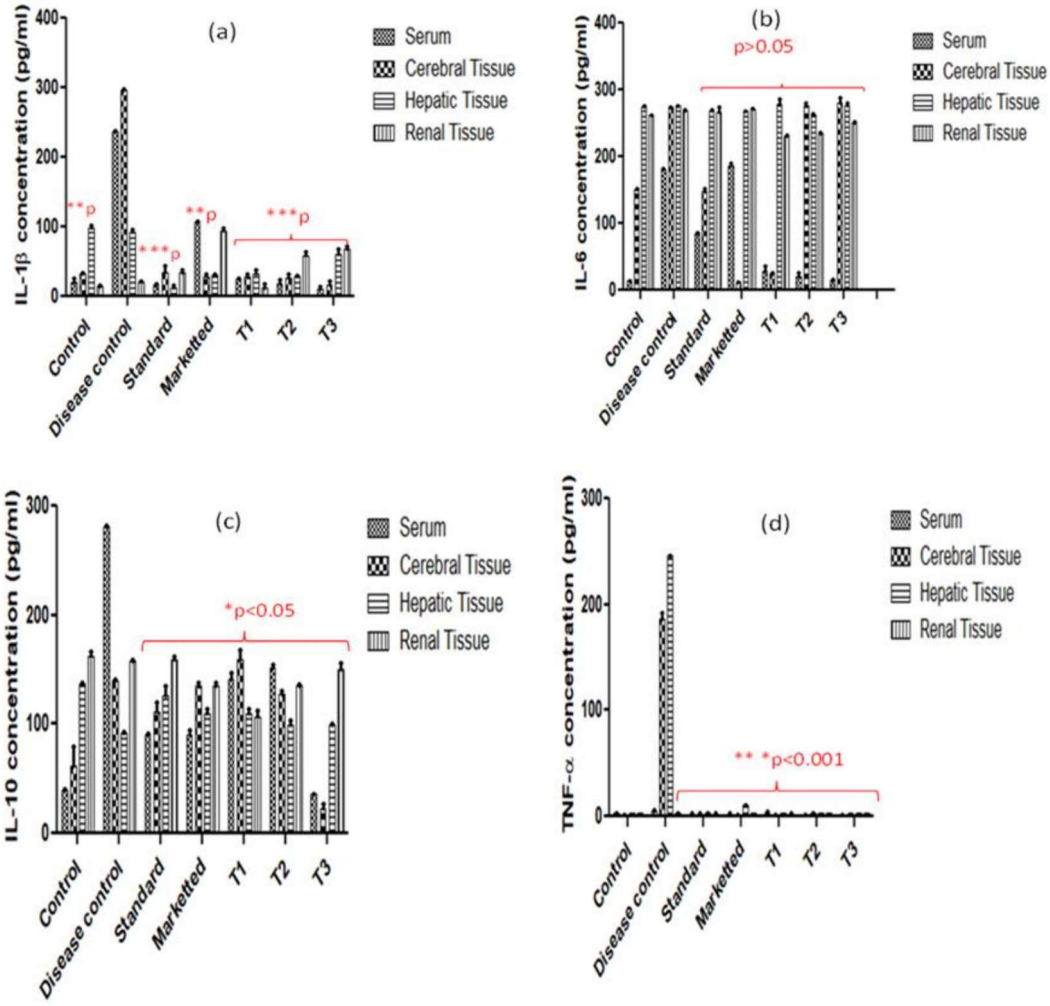

Figure 44: Effect of MEMp, Marketed, (MEM-PLGA) SANs, (PEG-MEM-PLGA) SANs and (PEG-MEM-PLGA)-BMSc SANs on pro-inflammatory cytokines (a) IL-1β (b) IL-6 (c) IL-10 and (d) TNF-α observed in serum, cerebral, hepatic and renal tissues of treatment groups of scopolamine induced AD model vs. control and disease control (untreated cells) group and Data are represented as Mean ± SEM, (n = 3).

The outcomes of the study of estimation of pro-inflammatory cytokines in serum, cerebral, hepatic and renal has revealed that the level of IL-1β, IL-6, IL-10 and TNF-α cytokines were mostly affected by nanocarriers in serum, cerebral tissue of scopolamine induced amnesia model of mice. The rationale behind examining the expression of pro-inflammatory cytokines is to identify the effect of treatment, inflammation and oxidative stress in hepatic and renal tissues following the treatment, because it becomes necessary to evaluate the potential effect of nanocarriers in Alzheimer's disease without harming other major metabolizing organs like liver and kidney. Also, Alzheimer's disease patients are mostly prone to the liver and kidney damage, and higher level of cytokines can worsen the situation of memory impairment.

In addition, according to our study the pattern of expression of pro-inflammatory cytokines are obtained in different manner like, TNF-α concentration were found to be significantly increased

in cerebral and hepatic tissue of AD induced mice as compared to normal healthy mice which was reduced after administration of MEMp, marketed (Admenta), (MEM-PLGA) SANs, (PEG-MEM-PLGA) SANs and (PEG-MEM-PLGA)-BMSc SANs. (PEG-MEM-PLGA)-BMSc SANs showed almost 14-fold and 15-fold greater reduction in cerebral and hepatic TNF-α level as compared to MEMp, marketed (Admenta), (MEM-PLGA) SANs, (PEG-MEM-PLGA) SANs. TNF-α level in renal tissue varied non-significantly amongst the groups because TNF-α were predominately expressed in cerebral and hepatic cells after induction of AD.

IL-10 is predominately expressed in serum and cerebral tissue because attenuation of B cell receptor (BCR) and Toll-like receptor 4 (TLR4) for mediating B-cell signalling and can affect the production of IL-10 in serum and cerebral tissue whereas pro-inflammatory cytokines IL-10 of hepatic tissue and renal tissue were not involved in the pathogenesis of AD [305].

However, reduction of pro-inflammatory cytokines IL-6 after administration of MEMp, (MEM-PLGA) SANs, (PEG-MEM-PLGA) SANs, (PEG-MEM-PLGA)-BMSc SANs were mostly obtained in serum. Whereas no reduction in expression of IL-6 was obtained in cerebral, hepatic and renal tissue of AD induced mice after administration of MEMp, (MEM-PLGA) SANs, (PEG-MEM-PLGA) SANs, (PEG-MEM-PLGA)-BMSc SANs Because, IL-6 contributes to stem cell regeneration that is responsible for neuronal stem cell expansion (induced pluripotent stem cells (iPSCs)) within a short time window) and regulation of neuronal outgrowth by following JAK-STAT signalling pathways [298].

6.6.4 Statistical Analysis

The absorbance (Abs) obtained in the Microtiter wells was subtracted by blank Abs to obtain original absorbance of cytokines and by using interpolation method, concentration of pro-inflammatory cytokines was determined. The statistical analysis was performed and the results were interpreted by the interpolation method using GraphPad prism software (version 5). Data has been presented as mean$\pm$ standard deviation. Statistical analysis has been performed using two-way ANOVA followed by Bonferroni post-hoc test for comparison among the groups and P value ($p<0.05$) was regarded as significant.